CFD INVESTIGATION OF CROSS FLOW OVER TUBE BANKS

TEH WEI YUAN

A report submitted
in fulfillment of the requirements for the degree of
Bachelor of Mechanical Engineering

Faculty of Mechanical Engineering

UNIVERSITI TEKNIKAL MALAYSIA MELAKA

2019

DECLARATION

I solemnly declare that this project report entitled "CFD Investigation of Cross Flow over Tube Banks" is the outcome of my own work except as cited in references during the course of my study under the supervision of Dr. Fatimah Al-Zahrah Binti Mohd Sa'at.

Signature : ....

Name of author : ……..

Date : ……..

APPROVAL

I hereby declare that I have read this project report and in my opinion this report is sufficient in terms of scope and quality for the award of the degree of Bachelor of Mechanical Engineering.

Signature : ....

Name of supervisor : ……..

Date : …...

DEDICATION

I humbly dedicate this project report to my beloved families who always have my back and show unceasing support to me. They have made the fruition of my efforts possible. I also dedicate this project report to the field of research. The contents of this project report should be helpful for future researches and studies. Last but not least, I dedicate this work to the Almighty God, the creator and curator of immeasurable wisdom and knowledge who made everything possible.

ABSTRACT

Heat exchangers are devices that facilitate the exchange of heat between two fluids that are at different temperatures while keeping them from mixing. Heat transfer in a conventional heat exchanger usually involves convection in each fluid and conduction through the wall separating the two fluids. Tube banks are usually found within a heat exchanger and circular tube bundle is one of the simplest geometries that is widely used. However, in the recent years, thermoacoustic heat engine has been receiving increased attention. Thermoacoustic engines are devices which use high-amplitude sound wave to pump heat from one place to another. The main difference between conventional heat exchanger and thermoacoustic heat engine is that one uses one-directional steady flow and the other one uses unsteady oscillatory flow. The main purpose of this project is to gain insight into the characteristics of heat transfer and fluid flow of cross flows over tube banks for both steady and oscillatory flows. All flows are investigated under similar operating condition. Two-dimensional numerical CFD model is conducted using finite volume discretization to evaluate the performance of these systems. The effect of cross flows on temperature, velocity, enthalpy (heat flux), and pressure drop are all investigated. Effect of cross flows over tube banks on fluid flow characteristic and heat transfer performance has been investigated. Numerical simulation has been conducted on a design model of circular tube banks with staggered arrangement using commercial CFD package, Ansys Fluent 16.0. Constant variable is the material, in which air will be flowing over tube banks while the tube is made of aluminium. The flow velocity of air is standardized which implies that Reynold number is constant. The manipulating variables are steady flow and transient oscillatory flow. Mesh independence study has been conducted by increasing the number of element. Best grid is the one with 19170 elements. Oscillatory flow model is a wave function and is ran for 7 cycles for stabilization of variables. The results are validated with theoretical results and consistency is achieved. It is found that steady flow with higher Re has better heat transfer performance compared to those with low Re. Oscillatory flow with higher drive ratio has better heat transfer performance. Steady flow has better heat transfer performance compared to oscillatory flow at identical Re. However this statement is inconclusive and more works are required to substantiate it. Recommendation for future work is to develop appropriate correlation or equation to compute heat transfer coefficient for oscillatory cross flow over tube banks.

ABSTRAK

Penukar haba adalah peranti yang memfasilitasi pertukaran haba antara dua cecair yang berada pada suhu yang berbeza sambil mengekalkannya daripada pencampuran. Pemindahan haba dalam penukar haba konvensional biasanya melibatkan perolakan dalam setiap bendalir dan konduksi melalui dinding yang memisahkan kedua-dua cecair. Bank-bank tiub biasanya dijumpai dalam penukar haba dan berkas tiub adalah salah satu geometri paling mudah yang digunakan secara meluas. Walau bagaimanapun, pada tahun-tahun kebelakangan ini, enjin panas thermoacoustik telah menerima perhatian yang semakin meningkat. Enjin thermoacoustik adalah peranti yang menggunakan gelombang bunyi amplitud tinggi untuk mengepam haba dari satu tempat ke tempat lain. Perbezaan utama antara penukar haba konvensional dan enjin haba thermoacoustik adalah bahawa yang konvensional menggunakan aliran mantap satu arah manakala thermoacoustik menggunakan aliran ayunan yang berubah dengan masa. Tujuan utama projek ini adalah untuk mendapatkan gambaran tentang ciri-ciri pemindahan haba dan aliran bendalir aliran bersilang ke atas bank tiub untuk kedua-dua aliran yang stabil dan berayun. Semua aliran disiasat di bawah keadaan operasi yang sama. Model CFD berangka dua dimensi dijalankan menggunakan kaedah pemecahan isipadu jumlah terhingga untuk menilai prestasi sistem-sistem tersebut. Kesan aliran bersilang pada suhu, halaju, entalpi (fluks haba), dan kejatuhan tekanan semua disiasat. Kesan aliran rentas ke atas bank tiub pada ciri aliran cecair dan prestasi pemindahan haba telah disiasat. Simulasi berangka telah dilakukan pada model reka bentuk bank tiub bulat dengan susunan berperingkat menggunakan pakej CFD komersil, Ansys Fluent 16.0. Pemboleh ubah malar adalah bahan, di mana udara akan mengalir ke bank-bank tiub sementara tiub tersebut terbuat dari aluminium. Halaju aliran udara diseragamkan yang menunjukkan bahawa bilangan Reynold adalah malar. Pemboleh ubah manipulasi adalah aliran mantap dan aliran ayunan. Kajian kebebasan bergerak telah dilakukan dengan meningkatkan jumlah elemen. Grid terbaik adalah yang mempunyai 19170 elemen. Model aliran ayunan adalah fungsi gelombang dan telah berlari untuk 7 kitaran untuk penstabilan pembolehubah. Hasil kajian telah disahkan dengan keputusan teoritis dan konsistensi telah dicapai. Hasil kajian menunjukkan aliran mantap dengan Re yang lebih tinggi mempunyai prestasi pemindahan haba yang lebih baik berbanding dengan Re yang rendah. Aliran ayunan dengan nisbah pemacu yang lebih tinggi mempunyai prestasi pemindahan haba yang lebih baik. Aliran mantap mempunyai prestasi pemindahan haba yang lebih baik berbanding aliran ayunan dengan Re yang sama. Bagaimanapun kenyataan ini tidak dapat disimpulkan dan lebih banyak kerja diperlukan untuk membuktikannya. Cadangan untuk kerja masa depan adalah untuk membangunkan korelasi atau persamaan yang sesuai untuk mengira pekali perpindahan haba untuk aliran silang ayunan ke atas tiub bank.

ACKNOWLEDGEMENTS

First and foremost, I would like to take this opportunity to express my deepest gratitude to my supervisor, Dr. Fatimah Al-Zahrah Binti Mohd Sa'at from the Faculty of Mechanical Engineering, Universiti Teknikal Malaysia Melaka (UTeM) for her undivided supervision, guidance, support and encouragement towards the completion of this project report.

I would also like to convey my recognition to the second reviewer, Dr. Mohamad Shukri Bin Zakaria, also from the Faculty of Mechanical Engineering, UTeM, for his time and patience to evaluate my progress and project report.

Last but not least, I thank all my friend and my beloved families for their continual support and heart-warming motivation that push towards the fruition of this project report.

TABLE OF CONTENTS

				PAGE
DECLARATION				
APPROVAL				
DEDICATION				
ABSTRACT				**i**
ABSTRAK				**ii**
ACKNOWLEDGEMENTS				**iii**
TABLE OF CONTENTS				**iv – vi**
LIST OF TABLES				**vii – viii**
LIST OF FIGURES				**ix – x**
LIST OF APPENDICES				**xi**
LIST OF ABBREVIATIONS				**xii**
LIST OF SYMBOLS				**xiii – xiv**
CHAPTER				
1.	**INTRODUCTION**			1
	1.1	Background		1 – 2
	1.2	Problem statement		2 – 3
	1.3	Objective		3
	1.4	Scope of project		4
2.	**LITERATURE REVIEW**			5
	2.0	Introduction		5
	2.1	Heat transfer		5 – 6
		2.1.1.	Conduction	6 – 8
		2.1.2	Convection	8 – 10
	2.2	Fluid mechanics		10
		2.2.1	Fluid	10 – 11
		2.2.2	No-slip condition	11 – 12
		2.2.3	Classification of fluid flows	13
			2.2.3.1 Viscous versus inviscid region of flow	13
			2.2.3.2 Internal versus external flow	13
			2.2.3.3 Compressible versus incompressible flow	13 – 14
			2.2.3.4 Laminar versus turbulent flow	14 – 15
			2.2.3.5 Natural (unforced) versus forced flow	15
			2.2.3.6 Steady versus unsteady flow	15 – 16
			2.2.3.7 Cross flow	16 – 17
			2.2.3.8 Oscillatory flow	17 – 19
		2.2.4	Properties of fluid	20
			2.2.4.1 Continuum	20
			2.2.4.2 Viscosity	20 – 22
		2.2.5	Governing equations	23
			2.2.5.1 Navier-Stokes equations	23
			2.2.5.2 Continuity equation	23 – 24
			2.2.5.3 Bernoulli's equation	24 – 25
			2.2.5.4 Womersley number	25 – 26
		2.2.6	Friction and pressure drag	26 – 27

		2.2.7 Flow separation	27 – 28
	2.3	Principles behind cross flow over tube banks	28
		2.3.1 Heat transfer and equations	28
		2.3.1.1 Convection heat transfer coefficient	28 – 29
		2.3.1.2 Nusselt number	29
		2.3.1.3 Prandtl number	30
		2.3.1.4 Reynolds number	31
		2.3.1.5 Rayleigh number	31 – 32
		2.3.1.6 Grashof number	32
		2.3.2 Flow across cylinders	33 – 36
		2.3.2.1 Effect of surface roughness	36
		2.3.3 Heat transfer coefficient for horizontal cylinders	36 – 39
		2.3.4 Flow across tube banks	39 – 40
		2.3.4.1 Configurations of tube banks	40 – 43
		2.3.4.2 Nature of flow across tube banks	43 – 46
		2.3.4.3 Pressure drop in tube banks	46 – 48
		2.3.4.4 Brief introduction to heat exchangers	48 – 50
	2.4	Numerical simulation	51
		2.4.1 Computational Fluid Dynamics (CFD)	51 – 52
		2.4.2 CFD methodology	52
		2.4.3 Mesh generation	52 – 54
		2.4.4 Discretization methods	54 – 55
		2.4.5 Pressure-velocity coupling	55 – 56
		2.4.6 Turbulence models	56
		2.4.7 Flow patterns and flow visualization	57
		2.4.7.1 Plots of fluid flow data	57 – 59
3.	**METHODOLOGY**		60
	3.0	Introduction	60
	3.1	Overall project planning	60
		3.1.1 Overall project planning flow chart	61
	3.2	Research methodology	62
		3.2.1 Literature review	63
		3.2.2 CFD model development	63 – 64
		3.2.3 Definition of domain and geometry	64
		3.2.4 Selection of discretization method and set up of mesh	65 – 66
		3.2.5 Definition of boundary and fluid condition	66
		3.2.5.1 Setup for steady flow model	66 – 68
		3.2.5.2 Setup for oscillatory flow model	68 – 71
		3.2.5.3 Heat transfer rate and pressure drop	71 – 72
		3.2.6 Solving and visualization	72 – 73
	3.3	Grid test	74
		3.3.1 Mesh quality	74
		3.3.2 Grid independency test	75
		3.3.2.1 Grid test for steady flow model	75 – 77
		3.3.2.2 Grid test for oscillatory flow model	77 – 78
		3.3.3 Grid selection	78 – 79
4.	**RESULT AND DISCUSSION**		80
	4.1	Validation of results	80

	4.1.1.	Validation of steady flow's result	80 – 82
	4.1.2	Validation of oscillatory flow's result	82 – 85
4.2	Fluid flow characteristics – vector & vorticity		85
	4.2.1	Steady flow – vector & vorticity	85 – 86
	4.2.2	Oscillatory flow – vector & vorticity	87 – 91
4.3	Temperature, velocity, pressure contours		91
	4.3.1	Contour plots for steady flow model	91 – 93
	4.3.2	Contour plots for oscillatory flow model	94 – 97
4.4	Heat transfer coefficient		97 – 99
4.5	Discussion		99 – 102

5. CONCLUSION & RECOMMENDATIONS FOR FUTURE WORK 103

REFERENCES 104 – 111
APPENDICES 112 – 120

LIST OF TABLES

TABLE	TITLE	PAGE
2.1	Thermal conductivities of materials at room temperature	7
2.2	Typical values of convection heat transfer coefficient	9
2.3	Type of flows and Reynolds number for pipes and flat plate	15
2.4	Dynamic viscosity of fluids at 1atm and 20 °C	22
2.5	Typical ranges of Prandtl numbers for common fluids	30
2.6	Empirical correlations for the average Nusselt number for flow across cylinders	39
2.7	Nusselt number correlations for cross flow over tube banks	44
2.8	Correction factor of $N_L < 16$, $Re_D > 1000$	45
3.1	Description of tube banks	64
3.2	Mesh sizing options	66
3.3	Boundary conditions for steady flow model	66
3.4	Physical properties of materials used in steady flow model	67 – 68
3.5	Air velocity corresponding to Reynolds number	68
3.6	Boundary conditions for oscillatory flow model	70
3.7	Physical properties of materials used in oscillatory flow model	70
3.8	Mesh quality of grid	74
3.9	Grid test for steady flow model	75
4.1	Vector plot for steady flow model	85
4.2	Vorticity contour for steady flow model	86

4.3	Vector plot for oscillatory flow model	89
4.4	Vorticity contour for oscillatory flow model	90
4.5	Temperature contour for steady flow model	91
4.6	Velocity contour for steady flow model	92
4.7	Pressure contour for steady flow model	93
4.8	Temperature contour for oscillatory flow model	94
4.9	Velocity contour for oscillatory flow model	95
4.10	Pressure contour for oscillatory flow model	96
4.11	Nusselt number for steady flow model	97
4.12	Nusselt number for oscillatory flow model	97

LIST OF FIGURES

FIGURE	TITLE	PAGE
2.1	Conduction of heat through a wall with thickness *Δx* and area *A*	7
2.2	Variation of thermal conductivity of materials with temperature	8
2.3	Deformation of rubber due to shear force	11
2.4	Evolution of velocity gradient due to no-slip condition	12
2.5	Laminar, transitional, and turbulent flows over a flat plate	14
2.6(a)	Both fluids unmixed	16
2.6(b)	One fluid mixed, one fluid unmixed	16
2.7	Velocity profiles of oscillatory flow at different Womersley number	18
2.8	Shear stress is proportional to velocity gradient	21
2.9	Viscosities of liquids and gases against temperature	22
2.10	Flow separation and wake region	27
2.11	Regimes of fluid flow across cylinder	34
2.12	Examples of fluid flow over cylinder	35
2.13	Average drag coefficient for flow over smooth cylinder and sphere	36
2.14	Variation of local heat transfer coefficient along the circumference of cylinder	37
2.15(a)	In-line configuration of tube bank	40
2.15(b)	Staggered configuration of tube bank	40
2.16	Friction factor *f* and correction factor *X* for staggered tube banks	48
2.17	Mesh topology	53
2.18(a)	Standard profile plot	58

2.18(b)	Profile plot with arrows	58
2.19	Vector plot	58
2.20(a)	Filled color contour plot	59
2.20(b)	Contour plot with pressure values	59
3.1	Overall project planning flow chart	61
3.2	Research methodology flow chart	62
3.3	Design of staggered tube banks	63
3.4	Named selections for the surface of the model	64
3.5	Default meshing	65
3.6	Mesh around tube walls	65
3.7	Graph of convergence for temperature	76
3.8	Graph of convergence for velocity and pressure	76
3.9	Graph of oscillating velocity for DR 1.2%	77
3.10	Graph of oscillating pressure for DR 1.2%	78
4.1	Nu versus Re for numerical-experimental validation	80
4.2	Eu versus Re for numerical-experimental validation	81
4.3	Comparison between theoretical and simulation oscillating pressure for DR 0.3%	83
4.4	Comparison between theoretical and simulation oscillating velocity for DR 0.3%	83
4.5	Comparison between theoretical and simulation oscillating pressure for DR 1.2%	84
4.6	Comparison between theoretical and simulation oscillating velocity for DR 1.2%	84
4.7	Velocity profile for DR 0.3%	87
4.8	Velocity profile for DR 1.2%	88
4.9	Nu versus Re for steady and oscillatory flow models	98
4.10	Nusselt number development for steady flow model	101
4.11	Nusselt number development for oscillatory flow model	101

LIST OF APPENDICES

APPENDIX	TITLE	PAGE
A	Grid no.2, No of elements: 1181, Relevance centre: fine, smoothing: high, number of division: 30, behaviour: hard	110
B	Grid no. 3, No of elements: 4713, Relevance centre: fine, smoothing: high, number of division: 30, behaviour: hard, face refinement: 1	111
C	Grid no. 4, No of elements: 10600, Relevance centre: fine, smoothing: high, number of division: 30, behaviour: hard, face refinement: 2	112
D	Grid no. 5, No of elements: 14841, Relevance centre: fine, smoothing: high, number of division: 30, behaviour: hard, face refinement: 2	113
E	Grid no. 6, No of elements: 19170, Relevance centre: fine, smoothing: high, number of division: 50, behaviour: hard, face refinement: 2	114
F	Grid no. 7, No of elements: 49675, Relevance centre: fine, smoothing: high, number of division: 50, behaviour: hard, face refinement: 2, inflation at tube_wall edges: smooth transition, 10 layers, 1.2 growth rate	115
G	Grid no. 8, No of elements: 86892, Relevance centre: fine, smoothing: high, number of division: 50, behaviour: hard, face refinement: 3, inflation at tube_wall edges: smooth transition, 10 layers, 1.2 growth rate	116
H	Gantt chart for FYP I	117
I	Gantt chart for FYP II	118

LIST OF ABBEREVATIONS

CFD	Computational Fluid Dynamics
DR	Drive ratio
Re	Reynolds number
Ma	Mach number
Pr	Prandtl number
Nu	Nusselt number
Eu	Euler number
Ra	Rayleigh number
Gr	Grashof number
S_L	Longitudinal pitch
S_D	Diagonal pitch
S_T	Transverse pitch
RANS	Reynolds-averaged Navier-Stokes
LES	Large eddy simulation
DES	Detached eddy simulation
DNS	Direct numerical simulation
CAD	Computer aided design

LIST OF SYMBOL

$\dot{Q}$	=	Rate of heat transfer
k	=	Thermal conductivity / Wave number
A	=	Area
h	=	Convection heat transfer coefficient
T	=	Temperature
ε	=	Effectiveness of heat exchanger
E	=	Power
P	=	Pressure
$\dot{V}$	=	Volume flow rate
ρ	=	Density
m	=	Mass
V	=	Volume
g	=	Gravitational acceleration
τ	=	Shear stress
γ_s	=	Specific weight
μ	=	Dynamic viscosity
F	=	Correction factor
α	=	Womersley number / Thermal diffusivity
L	=	Length
D	=	Diameter

v	=	Kinematic viscosity
ω	=	Angular frequency
U	=	Velocity / Overall heat transfer coefficient
C_p	=	Specific heat
f	=	Friction factor / Frequency
$\dot{m}$	=	Mass flow rate
Δx	=	Thickness
t	=	Time period
c	=	Speed of sound
θ	=	Phase difference
λ	=	Wavelength
m'	=	Mass flux

CHAPTER 1

INTRODUCTION

1.1 Background

Heat exchangers are instruments that speed up the transfer of thermal energy between two fluids with distinct temperatures while keeping them unmixed (Cengel and Ghajar, 2015). They are used in a wide range of applications such as power production, air-conditioning, chemical processing etc. It works based on the principles of convection (in each fluid) and conduction (between the walls separating the two fluids) mainly. Selection of appropriate heat exchangers is crucial as there are various types of heat transfer applications and each type requires dissimilar hardware, equipment, and configurations.

In order to achieve large heat transfer surface over unit volume, compact heat exchanger is designed specifically. Cross flow is usually found in this kind of heat exchanger, where the two fluids move perpendicular to each other. It is further classified as mixed and unmixed flow. The dissimilarity between mixed and unmixed cross flow is that the fluid is free to move in transverse direction for mixed cross flow while there are plate fins which force the fluid to flow through a particular interfin spacing and prevent it from moving in the transverse direction (like parallel to the tubes) for unmixed cross flow.

Tube bank is the most common type of configuration found in compact heat exchanger. The tubes in a tube bank are usually arranged either in-line or staggered in the direction of flow. Flow through the tubes can be analyzed by considering flow through a single tube, and multiplying the results by number of tubes. However, this is not the case for flow over the tubes because the tubes will affect the flow pattern and turbulence level downstream, and thus heat transfer to or from them.

Thermoacoustic engine is a device that works in similar way like a heat exchanger. Instead of using fan or pump to drive the fluid forward, it works by using acoustic power to pump heat from a low-temperature sink to a high temperature sink. One of the uniqueness in a thermoacoustic engine is that it doesn't consist of moving parts therefore it's relatively cheap to produce. Oscillatory flow mode is often found in a thermoacoustic engine because it employs acoustic power which is power transmitted by sound wave. Oscillatory flow is a very interesting topic and there isn't enough research done on it especially for tube banks.

In this project, steady and oscillatory cross flow over tube banks will be studied using Computational Fluid Dynamics (CFD) software such as Ansys Fluent. Using CFD will make the analysis much easier by performing numerical simulation and eliminating the need of experimenting without compromising the accuracy and integrity of results.

The heat transfer characteristics for cross flows over tube banks are of important practical interest (Bhutta et al., 2012), which also represents an idealization of many other industrially important processes (Mandhani et al., 2002). Therefore, it is very important to study the characteristics of fluid flow and heat transfer of cross flows over tube banks, which could lead to a better design of heat exchanger (Kim, 2013).

1.2 Problem statement

The thermodynamics performances like heat transfer are exceptionally significant when designing or selecting the right heat exchanger. One of the criteria is the flow of fluids over the tube banks. There are many kinds of flows over the tube banks, however, only steady one-directional and oscillatory cross flows are focused in this study. In simple terms, steady one directional cross flow implies that the fluids only flow in one direction (transverse motion is acceptable). While on the other hand, oscillatory cross flow works almost like the flow mentioned before, however, it flows in oscillatory manners which mean it changes the direction over time (reverse motion included). For instance, the oscillatory flow cases can be found if the tube bank is placed in situation like ocean flow, blood flow, and thermoacoustic engine.

The fluid dynamics and heat transfer across the tube banks is well-established particularly for a steady one-directional flow. The problem is that after reviewing several literatures regarding the subject matter, it is apparent that the research done on oscillatory cross flow over tube bank is limited and scarce. It is profound that the research on tube banks for now couldn't fully represent the whole ideal situation in which the flows could be more than just one-directional.

Therefore in this project, the one-directional cross flow over the tube banks will be studied, simulated and set as benchmark. For further analysis, oscillatory cross flow over the tube banks will be compared with the aforementioned case.

1.3 Objective

The objectives of this project are as follow:

1. To use CFD to model cross flow over tube banks.
2. To compare fluid flow characteristics between steady one-directional and oscillatory cross flows.
3. To compare heat transfer characteristics between steady one-directional and oscillatory cross flows.

1.4 Scope of project

The scopes of this project are:

1. Only CFD simulation method is used for this project. Experiment method is out of consideration.
2. Only focus on cross flow over tube bank instead of the whole performance of tube bundles with shell side as in a shell-and-tube heat exchangers.
3. CFD analysis will be conducted in 2D instead of 3D.
4. CFD simulation will focus on steady one directional and oscillatory cross flow.
5. Only consider the tube banks with base surfaces (no fins).
6. Only focus on the fluid which flows over tube banks instead of the fluid inside the tubes.

CHAPTER 2

LITERATURE REVIEW

2.0 Introduction

This chapter will discuss in details on the data and information of research topic which is CFD investigation of cross flow over tube banks. To be specific, some of the related terms and researches such as heat transfer modes and their characteristics, numerical simulation, fluid mechanics, tube bank configurations, flow criteria, etc. will be discussed elaborately. Research gap about cross flows over tube banks will be investigated.

2.1 Heat transfer

According to Cengel and Cimbala (2014), heat transfer is the discipline of thermal engineering that deals with determination of the rate of energy that can be transferred between physical systems to another as an outcome of temperature difference. Fundamental principle of heat transfer is the existence of temperature difference. It acts as a driving force for heat transfer just like potential difference is the driving force for electricity. Besides, the magnitude of temperature gradient influences the rate of heat transfer in specific direction, usually from higher temperature to low temperature according to second law of thermodynamics. The larger the temperature gradient, the higher the rate of heat transfer. However as the time goes, thermal equilibrium is achieved and the temperatures are uniform due to the gradual decay of temperature difference without external source of energy.

There are a few fundamental modes for the heat to be transferred, and they are conduction, convection, and radiation. Presence of temperature difference is a requirement for all modes mentioned.

2.1.1 Conduction

Conduction is the transfer of internal energy from particles with more energy to the adjacent particles with less energy of a substance as a result of interactions between the particles via direct contact. Conduction can take place not only in solids as everyone perceived, but in liquids, and gases as well.

In solids, conduction is due to the combination of collisions and vibrations of the molecules in a lattice and the energy transport by free electrons. While in liquids and gases, it is due to the collisions and diffusion of the molecules during their random motion. The rate of heat conduction relies on the temperature difference, material, thickness of the medium. Figure 2.1 shows an illustration of conductive heat transfer through a plane wall.

Fourier's law of heat conduction is defined as in Eq. (2.1):

$$\dot{Q} = -kA\frac{dT}{dx} \tag{2.1}$$

where $\dot{Q}$ is rate of heat conduction (SI units: W), k is thermal conductivity of material (SI units: W/m·K), A is heat transfer area (SI units: m^2), dT/dx is temperature gradient (SI units: K/m).

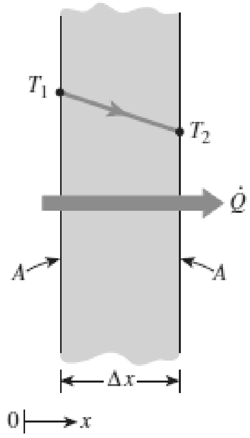

Figure 2.1: Conduction of heat through a wall with thickness *Δx* and area *A* (Cengel and Ghajar, 2015)

Thermal conductivity, *k* is an indicator of a material's capability to conduct heat. The higher the value, the better the material is as a heat conductor. Insulator is a term used for material that is weak in conducting heat. Values of thermal conductivity for selected materials are as shown in Table 2.1.

Table 2.1: Thermal conductivities of materials at room temperature (Cengel and Ghajar, 2015)

Material	**Thermal conductivity, *k* (W/m·K)**
Diamond	2300
Gold	317
Aluminium	237
Water	0.607
Air	0.026

The thermal conductivity of a metal is usually higher than its alloy. Small amount of foreign molecules in a pure metal can have tremendous effect on the thermal conductivity. Besides, temperature also plays an important role in determining the thermal conductivity of a material. Figure 2.2 shows the variation of thermal conductivity of materials with temperature.

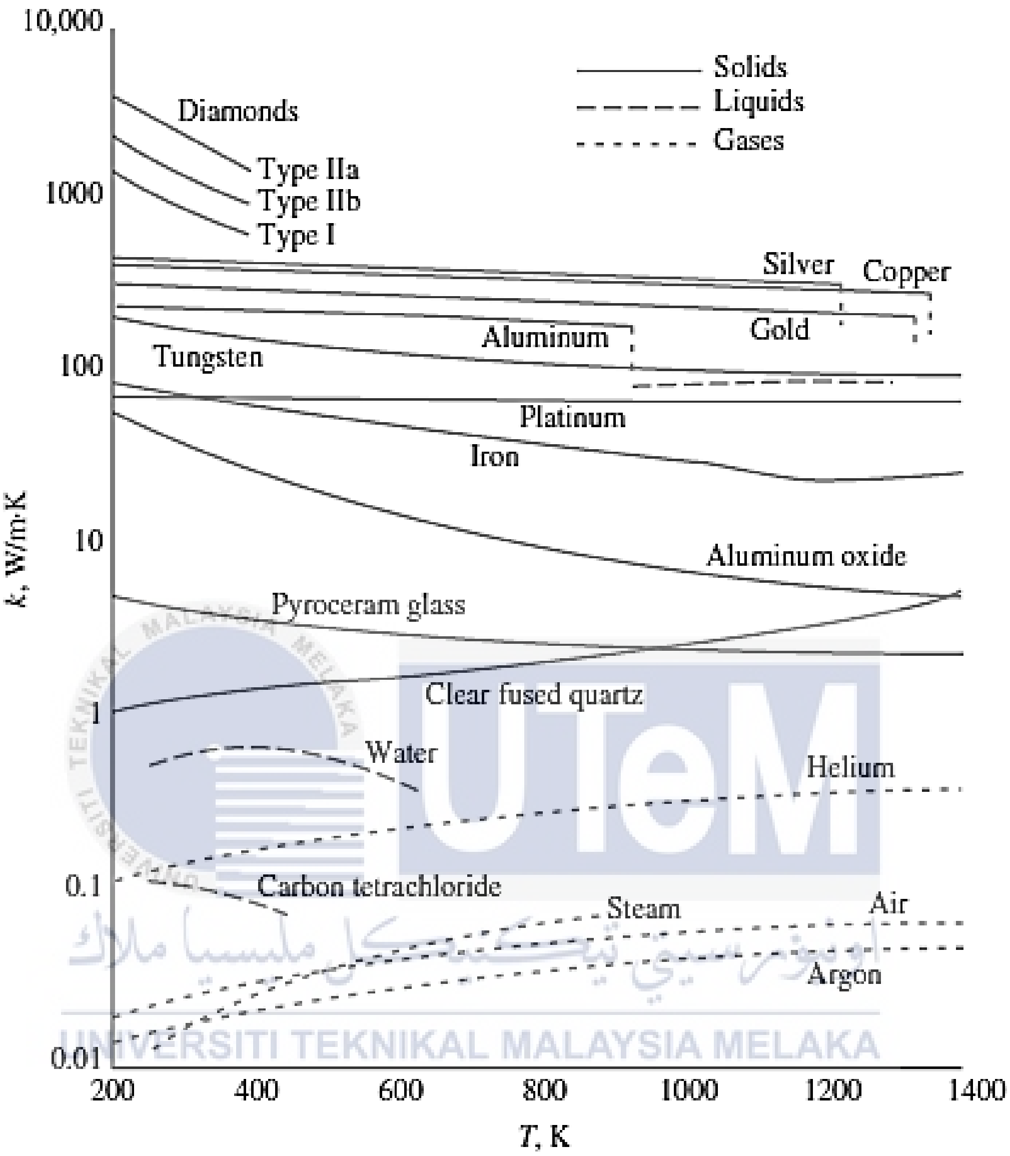

Figure 2.2: Variation of thermal conductivity of materials with temperature (Cengel and Ghajar, 2015)

2.1.2 Convection

Convection is a mode of energy transfer between solid surface and the adjacent liquid or gas that is in motion. The faster the fluid motion, the greater the convection heat transfer. In the absence of any bulk fluid motion, heat transfer between a solid surface and adjacent fluid is by pure conduction. The presence of bulk motion of the fluid enhances the heat transfer between solid surface and the fluid, but it also complicates the determination of heat transfer rate. There are 3 types of convection in general:

1. Forced convection – fluid is forced to flow over surface by outer energy source such as pump, fan, etc.
2. Natural convection – flow caused by natural factor such as buoyancy forces that are induced by density differences because of temperature fluctuation, in which warmer and lighter fluid rises while cooler and denser fluid falls.
3. Boiling and condensation – flow in which the fluid motion is induced during the change of phase process, for example: upwards movement of water vapour.

Newton's law of cooling states that rate of convection heat transfer is proportional to the temperature difference. It is defined in Eq. (2.2) as:

$$\dot{Q} = hA(T_s - T_\infty) \tag{2.2}$$

where $\dot{Q}$ is rate of heat convection (SI units: W), h is convection heat transfer coefficient (SI units: W/m^2·K), A is heat transfer area (SI units: m^2), T_s is surface temperature (SI units: K), T_∞ is temperature of fluid sufficiently far from surface (SI units: K). Values of convective heat transfer coefficient for selected materials are shown in Table 2.2.

Table 2.2: Typical values of convection heat transfer coefficient (Cengel and Ghajar, 2015)

Type of convection	**Convection heat transfer coefficient, *h* (W/m^2·K)**
Free convection of gases	2 – 25
Free convection of liquids	10 – 1000
Forced convection of gases	25 – 250
Forced convection of gases	50 – 20000
Boiling and condensation	2500 – 100000

Note that convection heat transfer coefficient is not an intrinsic property of the fluid, it is determined via experiment whose value depends on all the variables affecting the convection like fluid velocity, properties of fluid, nature of fluid motion, surface geometry, etc.

2.2 Fluid mechanics

Mechanics is the area of physical science that deals with both stationary and moving bodies under the influence of forces or displacement, and the succeeding effects of the mentioned bodies to their respective environment. One of the classical sub-disciplines under mechanics is fluid mechanics. It is defined as the branch of science concerned with the behaviour of fluid in motion (fluid dynamics) and fluids at rest (fluid statics), and the interaction with solids or other fluids at the boundaries.

2.2.1 Fluid

According to Cengel and Cimbala (2014), matter on earth exists in three fundamental phases, they are solid, liquid, and gas. Fluid is any kind of substance that is in liquid and gas phases. One of the most distinctive traits that set apart a solid and a fluid is the capacity to resist an applied shear stress. In the case of fluids, it has zero shear modulus, which mean it cannot resist any shear force applied to it. Thus, fluid will keep deforming until it reaches a constant strain rate, whereas solid will stop deforming at a specific strain angle. Figure 2.3 shows an illustration of deformation of rubber (a solid) due to shear stress.

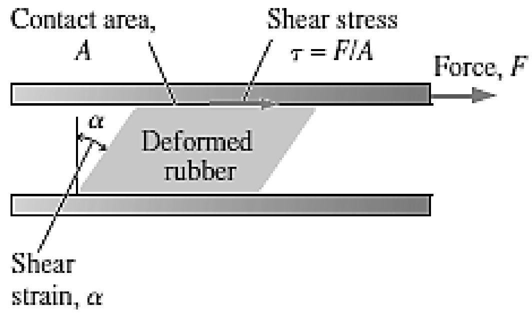

Figure 2.3: Deformation of rubber due to shear force (Cengel and Cimbala, 2014)

Fluids also display the ability to flow and takes the shape of container it is in. Due to the reason that liquid molecules can move relative to each other but strong cohesive force between molecules caused the volume to be persistent relatively, the fluid will form a free surface in a container under the influence of gravity and it will re-establish a new one once the constraints are subtracted or tilted and a shear is formed. Contrarily, a gas will keep expanding until it came into contact with the walls of a container, and diffuses throughout the entire available space. This is because the gas molecules are widely spaced, and the cohesive force between them are miniscule. Thus free surface is out of the question for gas.

2.2.2 No-slip condition

No-slip condition is a condition for viscous fluids in which the fluid will have zero velocity (stick to the surface) relative to the surface of a solid. In details, if the fluid came into contact with a stationary wall, the relative velocity of the fluid to the surface of the wall will be zero. However, if the wall is somehow moving, the fluid will possess the same velocity but the relative velocity of the fluid to the wall is still zero (Day, 1990). An evolution of velocity profile due to no-slip condition near a solid surface of a wall is illustrated in Figure 2.4.

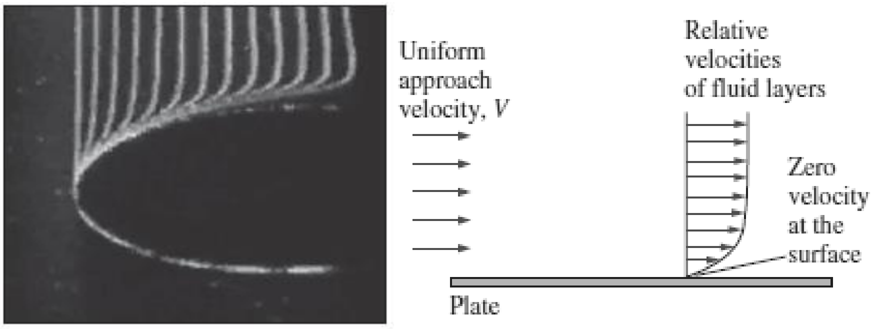

Figure 2.4: Evolution of velocity gradient due to no-slip condition (Cengel and Cimbala, 2014)

It is clear that the development for the velocity profile is caused by no-slip condition. A boundary layer is the layer of fluid in the close proximity of surface in contact where the viscous effect is notable. Prabhakara and Deshpande (2004) claimed that even turbulent flows which have a large velocity gradient near a wall have to satisfy the no-slip condition at every instant. They also claimed that although there is slipping in molecular scale but the effect is very small and only take place in length scale of the order of mean free path. Shu et al. (2017) claimed that no-slip condition is not always true especially under extreme circumstances such as very low pressure. Some stray fluid molecules in contact with a surface will bounce down the surface even though the continuum approximation is preserved. Besides, according to Gerritsma and Bochev (2016), a well-established conundrum is the formulation of least-squares finite element methods (LSFEMs) in order to solve Stokes equation with no-slip boundary condition. Existing LSFEMs that yield exactly divergence free velocities require non-standard boundary conditions (Bochev and Gunzburger, 2009), while methods that admit the no-slip condition satisfy the incompressibility equation only approximately.

2.2.3 Classification of fluid flows

2.2.3.1 Viscous versus inviscid region of flow

Friction force is formed between two fluid layers that are moving relative to each other. Viscosity is the measure of the internal stickiness of such fluids. For liquid, viscosity is caused by cohesive forces between the molecules while for gas, by collisions between the molecules. All fluids flow with viscosity in effect no matter how small since there is no fluid with zero viscosity. Fluid flows can generally be divided into two types of flow region.

1. Viscous flow region – flows in which the frictional effect is significant.
2. Inviscid flow region – viscous forces are negligibly small compared to inertial/pressure forces.

2.2.3.2 Internal versus external flow

Fluid can flow in two different conditions, internal flow and external flow. Description on both flows are shown below.

1. Internal flow – flows in which the fluid is completely bounded by solid surfaces, like flow in pipe or duct. Under the influence of viscous effect throughout the flow field.
2. External flow – flows in which the fluid is unbounded over solid surfaces, like flow over a plate, sphere, etc. Viscous effects are limited to boundary layers near solid surfaces and to wake regions downstream of bodies.

2.2.3.3 Compressible versus incompressible flow

Fluid flow can also be treated as a compressible flow or incompressible flow. Description on both of the flows are shown below.

1. Compressible flow – flow in which the variation of density of fluid is massive, like gases at supersonic speed.

2. Incompressible flow – flow in which the variation of density of fluid is negligible, like fluids at low speed. Ma $\leq$ 0.3.

2.2.3.4 Laminar versus turbulent flow

As fluid flows over or inside a structure, the flow behaves in a different way depending on the strength of the force on the flow. In general, fluid flow can be divided into two types of flow; laminar and turbulent flow.

1. Laminar flow – highly ordered fluid motion characterized by smooth layers of fluid.
2. Turbulent flow – highly disordered fluid motion (typically occurs at high velocity) characterized by velocity fluctuations.
3. Transitional – flow that alternates between laminar and turbulent.

Figure 2.5 shows the flow visualizations of laminar, transitional, and turbulent flows over a flat plate.

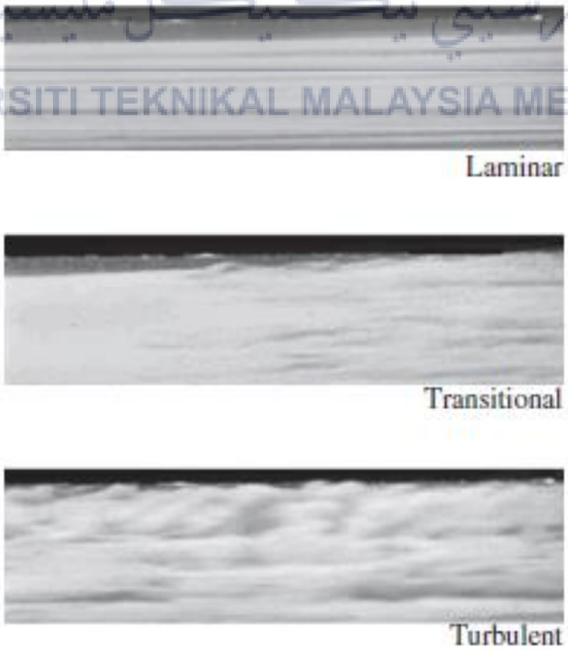

Figure 2.5: Laminar, transitional, and turbulent flows over a flat plate (Cengel and Cimbala, 2014)

Reynolds number, Re is the key parameter for the determination of flow regime in pipes or flat plate. Table 2.3 shows the range of Reynolds number for the classifications of flow for pipes and flat plate.

Table 2.3: Type of flows and Reynolds number for pipes and flat plate

Type of flows	**Pipes**	**Flat Plate**
Laminar flow	$Re \leq 2300$	$Re \leq 1 \times 10^5$
Transitional flow	$2300 \leq Re \leq 4000$	$Re_{cr} = 5 \times 10^5$
Turbulent flow	$Re \geq 4000$	$Re \geq 3 \times 10^6$

2.2.3.5 Natural (unforced) versus forced flow

In general, fluid can flow due to two different driving forces. The first driving force is known as forced flow. This is a situation where fluid is forced to flow via the use of external means such as a fan or pump. In the absence of external devices, fluid can still flow especially when there is enough temperature difference that can create significant buoyancy effect due to the change in density with temperature. This second condition is known as natural flow condition. Further description on both natural and forced flows are shown below.

1. Natural flow –flow caused by natural factor such as buoyancy effect, where warmer and lighter fluid rises while cooler and denser fluid falls.
2. Forced flow – fluid that is forced to flow by peripheral devices such as a fan or a pump.

2.3.3.6 Steady versus unsteady flow

Fluid flow can also be categorized under two different conditions of flow; steady and unsteady conditions.

1. Steady flow – flow with unchanging of properties, such as velocity, temperature, etc. at a point with time.

2. Unsteady flow – also known as transient flow, opposite of steady flow, implies flow with change of properties at a point with time.

3. Uniform flow – flow with unchanging with location over a specified region.

According to Cengel and Cimbala (2014), most devices used in industry such as heat exchangers, boilers, condensers, turbines and compressors are classified as steady-flow devices. This is because they operate for long periods of time under the same condition. They also mentioned that although the flow field near the rotating blades of a turbomachine is unsteady, but if only overall flow field is considered rather than specific localities, it is still seen as steady-flow devices.

2.3.3.7 Cross flow

Cross flow is a flow configuration when two fluids flow perpendicular to each other. This flow configuration can be usually found in compact heat exchangers. Unmixed and mixed flows are the further classification of the cross flow situation. This is as illustrated in Figure 2.6.

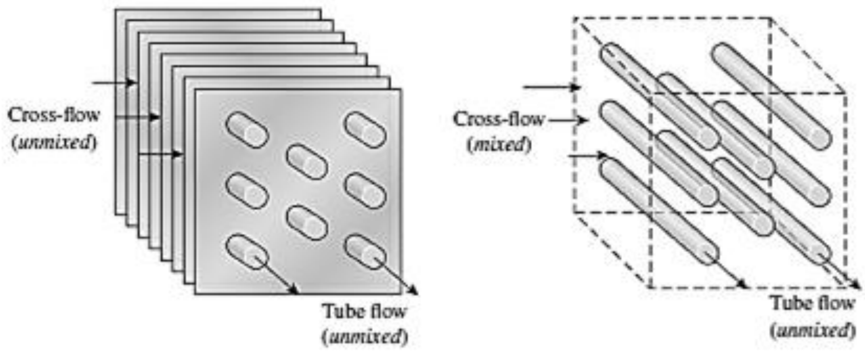

Figure 2.6(a): Both fluids unmixed

Figure 2.6(b): One fluid mixed, one fluid unmixed

(Cengel and Ghajar, 2015)

Cross flow is said to be unmixed like in Figure 2.6(a) since the plate fins prevent it from mixing by forcing them to flow through a set interfin spacing. On the other hand, cross flow in Figure 2.6(b) is said to be mixed since the fluid is free to mix around within confinement.

2.2.3.8 Oscillatory flow

According to Schoenmaker (2017), oscillatory flow is a manifestation of transient free surface flow subjected to gravitational forces. Understanding the physics of oscillating flow is an interest for industrial and biological processes and it brings a lot of benefit to it. For example, vascular diseases associated to disturbances of local flow condition in cardiovascular system ca be tackled if we understand how oscillatory flow of blood in blood vessel. Besides, knowledge of oscillatory flow can be applied in inkjet printer for quick switching while printing. Oscillatory flow is usually associated to wave motion and the velocity shape profile is governed by wave equation and Womersley number.

According to Feldmann and Wagner (2012), the shape of velocity profile of an oscillatory flow can be parabolic, M-profile shape, or flat profile with the increase of frequency. This is as illustrated in Figure 2.7. Momentum of the fluid determine the shape of velocity profiles. They found that the flow is slowed down earlier due to formation of boundary layer, thus it react with the wall faster and earlier to the pressure gradient and forming the shapes aforementioned at a range of frequency.

There are 4 types of flow patterns which can be found in cross flow over tube banks, and they are:

1. Steady, laminar flow
2. Disturbed laminar flow (small perturbations appear in the cycle’s acceleration part).

3. Intermittently turbulent flow (laminar flow for acceleration part, partly turbulent flow for deceleration part).
4. Turbulent flow (turbulent flow is in every part of the cycle)

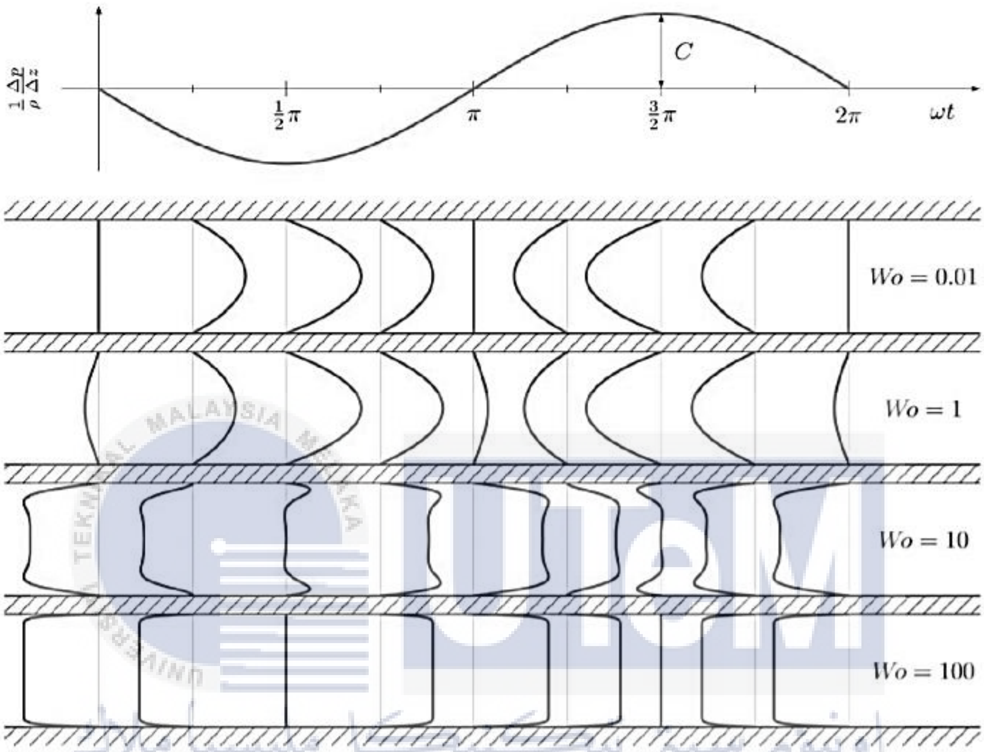

Figure 2.7: Velocity profiles of oscillatory flow at different Womersley number (Schoenmaker, 2017)

According to Swift (1988), thermoacoustic engine is a device that can produce or make use of acoustic power. Heat exchanger is a key elements within a thermoacoustic engine. This is because the engine uses high-amplitude sound waves to pump heat over a heating/cooling element in order to achieve certain purposes. There are two kinds of thermoacoustic engine:

1. Prime mover mode – Acoustic power can be generated then converted to electrical energy when the heat move from one place to another.

2. Heat pump mode – Acoustic power is used to cool down/heat up the reservoir with sound waves.

There are also two very important components found in a thermoacoustic engines mentioned before. They are used to aid in production and absorption of sound waves. The thermoacoustic engine will not be able to work correctly without them.

1. Stack – function by standing waves
2. Regenerator – function by travelling waves

Oscillatory cross flow over tube banks is beneficial to the future design of a thermoacoustic engine such as heat exchanger for better efficiency in pumping power, fluid flow and heat transfer characteristic.

Acoustic power is the quantity of power needed to drive an oscillatory flow through a component. It is defined in Eq. (2.3) as a velocity-driving force related to electric power.

$$E = \int_0^T p\dot{V}\,dt \tag{2.3}$$

where E is acoustic power (SI units: W), T is period (SI units: s), p = pressure (SI units: Pa), $\dot{V}$ is volume flow rate (SI units: m^3/s).

According to smith and swift (2003), due to viscous forces, increase in displacement amplitude and decrease in Reynolds number especially when the oscillatory flow is transitioning from laminar to turbulent through rounded exit with sudden area change will amplify the dissipation of acoustic power.

2.2.4 Properties of Fluids

Properties of fluids play an important role in determining the fluid flow and heat transfer characteristics no matter in experiment of numerical simulation. Some of the important properties of fluids are discussed in this section.

2.2.4.1 Continuum

A fluid is composed of molecules which might be broadly separated apart, especially in the gas phase. However it is advantageously to dismiss the atomic nature of the fluid and view it as homogenous and continuous matter without gaps that is, a continuum. The continuum idealization enable us to regard properties as point functions and to assume that the properties change ceaselessly in space without jump discontinuities.

2.2.4.2 Viscosity

According to Merriam-Webster Dictionary (2018), viscosity of a fluid is defined as the measure of its internal resistance to gradual deformation by shear stress. The gradual deformation of velocity profile due to shear stress is as shown in Figure 2.8. Shear Stress is defined as Eq. (2.4) below:

$$\tau = \mu \frac{du}{dy} \tag{2.4}$$

where τ is shear stress (SI units: N/m^2), μ is dynamic viscosity (SI units: $Pa{\cdot}s = N{\cdot}s/m^2$), du/dy = rate of deformation (SI units: 1/s).

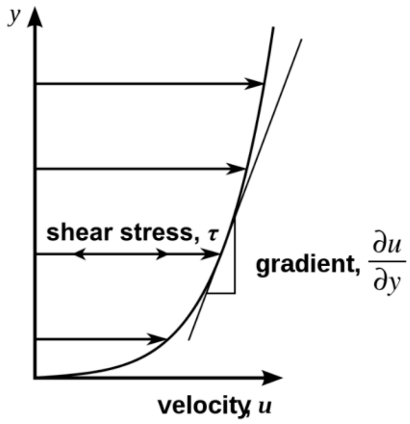

Figure 2.8: Shear stress is proportional to velocity gradient (Cengel and Cimbala, 2014)

According to Patnana et al. (2010), they find that heat transfer characteristics are influenced by the value of flow behavior index, *n* heavily. They also find that as Re and/or Pr increases, Nu also increases regardless of the value of *n*. However, according to their findings, *n* gives significant influence on both local and time-averaged Nu. In their conclusion, pseudoplastic promotes heat transfer whereas dilatant impedes it.

Viscosity is caused by the molecular collisions in gases and by the cohesive forces between molecules in liquids, and temperature plays a huge role in it. The viscosity of liquids decreases with temperature because at higher temperature, the liquid molecules are more active and have more energy, so they can oppose the large cohesive intermolecular between the molecules. As a result the energized liquid molecules can have more freedom in motion. In a gas, although the intermolecular forces are negligible, but at high temperature the gas molecules move randomly faster. This results in more molecular collisions per unit volume per unit time and the viscosity increases. The changes of viscosity values for liquid and gases are as illustrated in the graph shown in Figure 2.9. Values of viscosity for selected fluids are as shown in Table 2.4.

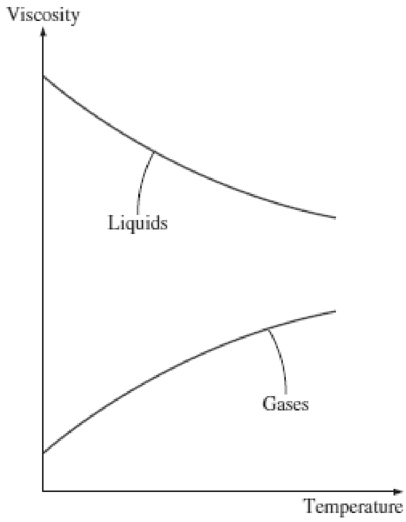

Figure 2.9: Viscosities of liquids and gases against temperature (Cengel and Cimbala, 2014)

Table 2.4: Dynamic viscosity of fluids at 1atm and 20 °C (Cengel and Cimbala, 2014)

Fluid	**Dynamic viscosity, μ (kg/m·s)**
Glycerin:	
-20 °C	134.0
0 °C	10.5
20 °C	1.52
40 °C	0.31
Engine oil:	
SAE 10W	0.10
SAE 10W30	0.17
SAE 30	0.29
SAE 50	0.86
Mercury	0.0015
Water:	
0 °C	0.0018
20 °C	0.0010
100 °C (liquid)	0.00028
100 °C (vapor)	0.000012
Blood, 37 °C	0.00040
Air	0.000018

2.2.5 Governing equations

Fluid flow can be represented by mathematical equations. There are several sets of equations that can be used to constitute fluid flow conditions and these equations are discussed in this section.

2.2.5.1 Navier-Stokes equations

Incompressible Navier-Stokes equation:

$$\rho \frac{DV}{Dt} = -\nabla P + \rho g + \mu \nabla^2 V \tag{2.5}$$

Euler equation:

For irrotational regions of flow,

$$\rho \left[\frac{\partial V}{\partial t} + (V \cdot \nabla) V\right] = -\nabla P + \rho g \tag{2.6}$$

For a simpler form,

$$Eu = \frac{\Delta P}{\rho_a V^2} \tag{2.7}$$

2.2.5.2 Continuity equation

Conservation of mass:

$$\frac{\partial \rho}{\partial t} + \nabla \cdot (\rho V) = 0 \tag{2.8}$$

Conservation of momentum:

$$\rho(V \cdot \nabla)V = -\nabla P + \mu \nabla^2 V \tag{2.9}$$

The momentum equation can also be written in another form of:

$$\frac{\partial V}{\partial t} + (V \cdot \nabla)V = -\nabla P + \frac{1}{Re}\Delta V \tag{2.10}$$

Conservation of energy:

$$\rho C_p(V \cdot \nabla \mathrm{T}) = \lambda \nabla^2 T \tag{2.11}$$

The energy equation can also be written as:

$$\frac{\partial T}{\partial t} + (V \cdot \nabla)T = \frac{1}{RePr}\Delta T \tag{2.12}$$

The equations of mass, momentum, and energy form the basic mathematical representation of fluid flow cases. They are used in many commercial CFD software including Ansys CFX and Ansys Fluent.

2.2.5.3 Bernoulli's equation

The Bernoulli's equation is an expression for an approximate relation between pressure, velocity and elevation, and is only valid in regions of steady, incompressible flow where viscous forces are negligibly small compared to inertial, gravitational, pressure effects. Equation (2.13) states that:

$$\frac{P}{\rho}+\frac{V^2}{2}+gz=constant \tag{2.13}$$

where P/ρ is flow energy, $V^2/2$ is kinetic energy, gz = potential energy

Limitations on the use of Bernoulli's equation:

1. Steady flow
2. Negligible viscous effect
3. No shaft work
4. Incompressible flow
5. Negligible heat transfer
6. Flow along a streamline

2.2.5.4 Womersley number

Womersley number is a dimensioness number used most commonly in biofluid mechanics. It is named after British Mathematician John R. Womersley (1907 – 1958). He is most notable for his contribution in work regarding blood flow in arteries. It is in Eq. (2.14) defined as the ratio of transient inertial force to viscous force.

$$\alpha = L_C\sqrt{\frac{\omega\rho}{\mu}} \tag{2.14}$$

where α is Womersley number, L_C is characteristic length (SI units: m), ω is angular frequency of oscillation (SI units: rad/s), ρ is density of fluid (SI units: kg/m^3), μ is dynamic viscosity (SI units: Pa·s = N·s/m^2)

2.2.6 Friction and pressure drag

Drag force is the net force exerted by a fluid on a body in the direction of flow due to the combined effects of wall shear and pressure forces. There are two types of drag forces and they are:

1. Skin friction drag – drag caused by wall shear stress.
2. Pressure drag – drag caused by pressure.

Reynolds number is inversely proportional to the viscosity of the fluid. At low Reynolds number, friction drag plays a dominant role. This is because friction drag is proportional to frontal area. Thus, larger friction drag will be imposed on the bodies with larger frontal area. However, at high Reynolds number, friction drag may be ignored and total drag in this case is mostly contributed by pressure drag. Pressure drag is proportional to the difference between pressures acting on the front and back of submerged body. The justification is that when the stream velocity of the fluid is extremely high for the fluid to be able to trace the curvature of the submerged body, thus a low pressure region is created at the back of the submerged body as the fluid separated from it. Besides, in similar way as in friction drag situation, pressure drag is also proportional to the frontal area. It is especially significant for blunt bodies.

One of the effective methods to tackle the drag is by streamlining the body. Streamlined body can effectively reduce flow separation and pressure drag. Streamlining can also reduce vibration and noise. However, it has opposite effects on friction drag. The way it works is that streamlining delays the separation of boundary layer, and thus diminishing the pressure difference between the front and back of the submerged body, but it amplifies the effect of friction drag due to large surface area of the body that increases the friction drag as the flow increases.

One of the criteria to be considered before streamlining is identification of body's geometry and flow parameter. Bluff bodies that are subjected to high stream velocity (high Reynolds number) is a suitable candidate where flow separation is plausible. This is because drag in cases where Reynolds number is low (laminar flow) is mostly caused by friction drag. By streamlining it, the surface area will be increased and thus the friction drag since pressure drag is insignificant in such cases.

2.2.7 Flow separation

Flow separation is a phenomenon where the fluid stream disconnects itself from the surface of the submerged body at high stream velocity. A separated region between the body and the fluid stream is formed when the fluid detaches from the body. This low-pressure zone is called separated region where recirculating and backflows occur. The larger the separated region, the larger the pressure drag. Wake region is the region of flow dragging the body and the effect of the body on velocity are felt is known as wake. The phenomena of flow separation and wake region are illustrated for fluid over cylinder is as shown in Figure 2.10.

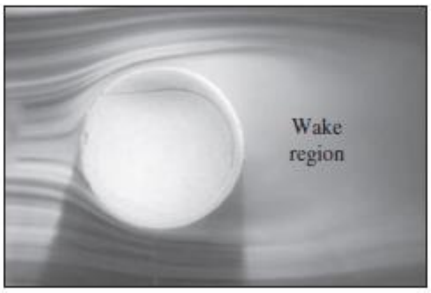

Figure 2.10: Flow separation and wake region (Cengel and Cimbala, 2014)

When the two separated flow streams recombine, it marks the end of separated region. In other words, the wake will keep growing in separated region until the fluid in that region regains its velocity. Formation and shedding of vortices in the wake region is one of the repercussions of flow separation. Vortex shedding is the recurrent creation of vortices downstream and it happens during normal flow over spheres or long cylinders for $Re \geq 90$. Body will resonate to an alarming and life-threatening levels if the frequency of the vortices (due to vibrations caused by the vortices) is in close proximity to natural frequency of the body.

2.3 Principles behind cross flow over tube banks

Convection is one of the major heat transfer modes (the others being conduction and radiation) and it relies on the presence of medium especially fluids. The mechanism of convection heat transfer depends on bulk motion of fluids' molecules. Convection is categorized as natural and forced convection. With the assistance of external means (fan, pump, etc.), forced convection can be realized. Besides, depending on whether the fluid is flowing within a pipe or over a body, it can be further classified as internal and external flows as well. External forced convection is further discussed in this section.

2.3.1 Heat transfer and equations

Heat transfer performance can be expressed or computed by using mathematical equations. Some of the equations are discussed in details in this section.

2.3.1.1 Convection heat transfer coefficient

As mentioned earlier, convection heat transfer coefficient, *h* plays a huge role in convection heat transfer. It is not a fundamental properties of the fluid but it can be discovered via experiment. It is defined in Eq. (2.15) as the rate of heat transfer per unit surface per unit temperature difference.

$$h = \frac{\dot{Q}}{A(T_S - T_\infty)} \tag{2.15}$$

where h is convection heat transfer coefficient (SI units: W/m^2·K), $\dot{Q}$ is rate of heat convection (SI units: W), A is heat transfer area (SI units: m^2), T_s is surface temperature (SI units: K), T_∞ is temperature of fluid sufficiently far from surface (SI units: K).

2.3.1.2 Nusselt number

Nusselt number, Nu is named after German engineer Sir Wilhelm Nusselt (1882 – 1957), who single-handedly pioneered the science of heat transfer and made exceptional contribution towards convective heat transfer. Nusselt number is defined in Eq. (2.16) as the ratio of convective heat transfer to conductive heat transfer.

$$Nu = \frac{hL_c}{k} \tag{2.16}$$

where Nu is Nusselt number, h is convection heat transfer coefficient (SI units: W/m^2·K), L_C is characteristic length (SI units: m), k is thermal conductivity of material (SI units: W/m·K).

The higher the value of Nusselt number, the more effective the convection part of heat transfer. Pure conduction is happening for a fluid surface if the Nusselt number equals to one. Nusselt number usually indicates the heat transfer performance for a system especially in relation to fluid flow situation.

2.3.1.3 Prandtl number

The Prandtl number is named after German physicist Sir Ludwig Prandtl (1875 – 1953), who introduced the concept of boundary layer and made exceptional contribution to the theory of boundary layer. It is defined in Eq. (2.17) as the ratio of momentum diffusivity to thermal diffusivity.

$$Pr = \frac{v}{\alpha} = \frac{\mu C_p}{k} \tag{2.17}$$

where Pr is Prandtl number, v is kinematic viscosity (SI units: m^2/s), α is thermal diffusivity (SI units: m^2/s), μ is dynamic viscosity, (SI units: $Pa \cdot s = N \cdot s/m^2$), C_p is specific heat (SI units: J/kg·K), k is thermal conductivity of material, (SI units: W/m·K).

Prandtl number signifies the relative thickness of momentum and thermal boundary layers. When Pr < 1, thermal diffusivity dominates the behavior of fluids, the heat can diffuse rather quickly. However, when Pr > 1, the momentum diffusivity takes over, and the heat diffuses rather slowly. Last but not least, when Pr = 1, heat and momentum diffuse through the fluid at the equal rate.

Table 2.5: Typical ranges of Prandtl numbers for common fluids (Cengel and Ghajar, 2015)

Fluid	Prandtl number, Pr
Liquid metals	0.004 – 0.030
Gases	0.7 – 1.0
Water	1.7 – 13.7

2.3.1.4 Reynolds number

Reynolds number is named after English engineer and physicist Sir Osbourne Reynolds (1842 – 1912). He had made extraordinary contribution in the field of fluid mechanics. He is well known for this work in hydrodynamics and hydraulics. Reynolds number is the ratio of inertia forces to viscous forces in fluids. It is used to characterize the transition between laminar flow and turbulent flow. In general terms:

$$Re = \frac{\rho V D}{\mu} = \frac{V D}{v} \tag{2.18}$$

where Re is Reynolds number, ρ is density (SI uis nits: kg/m^3), V is free stream velocity (SI units: m/s), D is characteristics length (SI unit: m), μ is dynamic viscosity (SI units: Pa·s = N·s/m^2), v is kinematic viscosity (SI units: m^2/s).

At large Reynolds number, it implies that the velocity of fluid is fast, thus the inertia forces (which is proportional to velocity) is big relative to viscous forces, so the flow becomes turbulent because the viscous forces can't put a stop to the rapid and random fluctuations of fluid. On the other hand, at lower Reynolds number, the flow is laminar because the viscous forces are able to suppress the fluctuations and keep the fluid straight. Critical Reynolds number is the number in which the flow starts to become turbulent.

2.3.1.5 Rayleigh number

Rayleigh number (Ra) is a dimensionless number that describe the flow region of a fluid, and it is usually associated with natural convection. It depicts the relationship between momentum diffusivity and thermal diffusivity by combining buoyancy, viscosity, and Prandtl number. Its relationship with Nusselt number is inseparable. Rayleigh number is defined in Eq. (2.19):

$$Ra = \frac{\rho\beta\Delta T D^3 g}{\mu} \tag{2.19}$$

where Ra is Rayleigh number, ρ is density, β is thermal expansion coefficient, ΔT is temperature difference, D is characteristic length, g is gravitational acceleration, μ is dynamic viscosity. Equation (2.20) shows a simpler form of Rayleigh number,

$$Ra = GrPr \tag{2.20}$$

where Gr is Grashof number.

2.3.1.6 Grashof number

Grashof number (Gr) is a dimensionless number that describe the ratio of buoyancy force to viscous force acting on fluids. It is used frequently in problems involving natural convection. Natural convection is caused by a change in density of fluid due to temperature change. The density of fluid will decrease when the temperature rises, causing the fluid to rise due to buoyancy force. Viscous force is the force that will resist the buoyancy force. Equation (2.21) shows the Grashof number and its variables:

$$Gr_D = \frac{g\beta(T_s - T_\infty)D^3}{v^2} \tag{2.21}$$

where β is the thermal expansion coefficient (approximately 1/T, for ideal gas), T_s is the surface temperature, T_∞ is the bulk temperature, D is diameter, v is kinematic viscosity.

2.3.2 Flow across cylinders

Flow over cylinders is frequently encountered in practice. For example, the tubes in a shell-and-tube heat exchanger involve both internal flow through the tubes and external flow over the tubes, and both flows must be considered in the analysis of heat exchanger.

The characteristic length for a circular cylinder is the external diameter, *D*. The critical Reynolds number for flow across cylinder is about Re $\approx 2 \times 10^5$. The boundary layer will remain laminar if the Reynolds number is less than 2×10^5, otherwise it will become turbulent. At low Re, the flow is laminar with separation occurring resulting in formation of vortices behind each cylinder. For staggered banks, the upstream flow is typically a maximum between the preceding tubes, so the impinging flow bifurcates at the front-leading edge of each cylinder. For in-line banks, cylinders are in a comparatively dead zone downstream of the preceding cylinder's wake. As Re increases, vortices are shed from each cylinder in an alternate fashion. Due to the overall pressure gradient, transient motion tends to occur at higher Re than for single tubes, particularly for compact banks. Wake-switching is observed in staggered tube banks, while in in-line banks there is an instability in the shear-layer between the wake and main flow with some of the detached vortices being entrained by the free-stream flow. As Re further increases, the wake becomes turbulent, and there is substantial free-stream turbulence, due to the influence of the preceding upstream rows. Engineers should be aware that both vortex-shedding and turbulent buffeting can induce vibrations in tube banks.

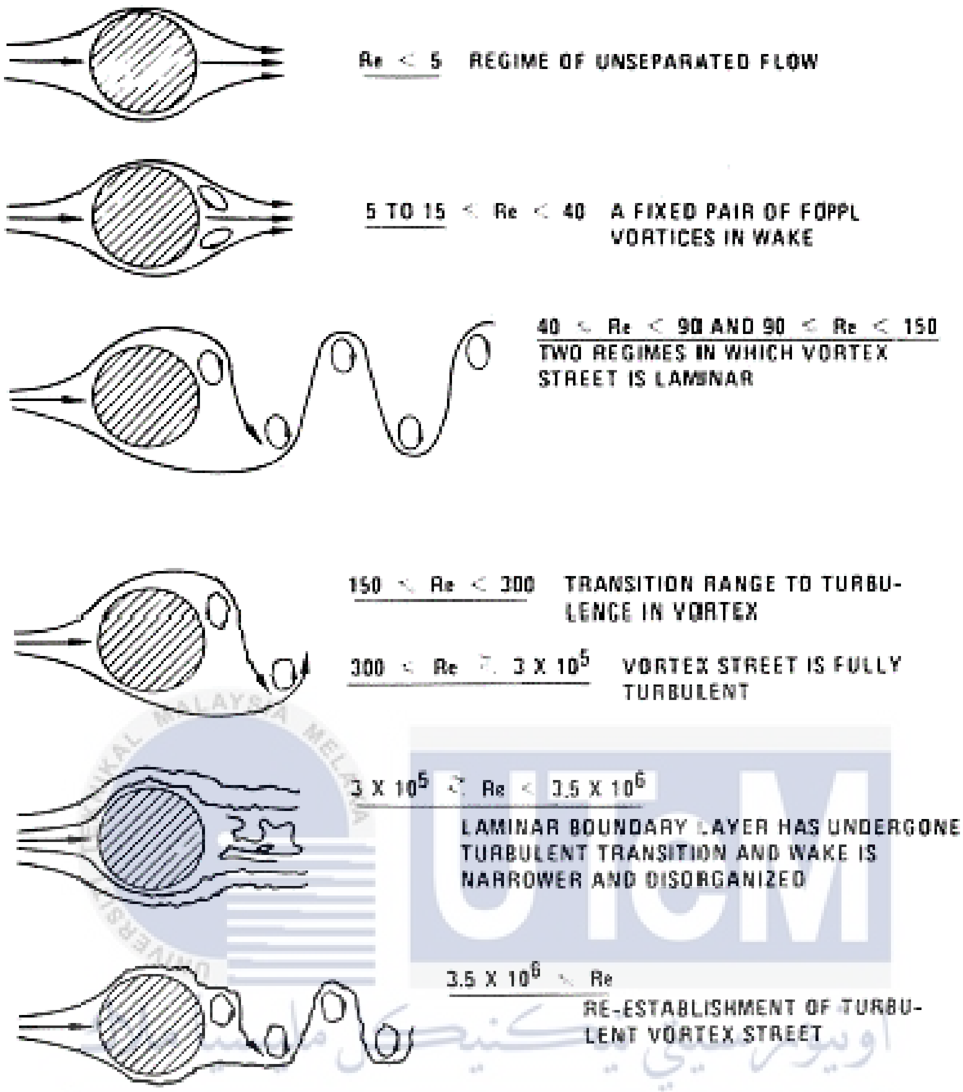

Figure 2.11: Regimes of fluid flow across cylinder (Blevin, 1990)

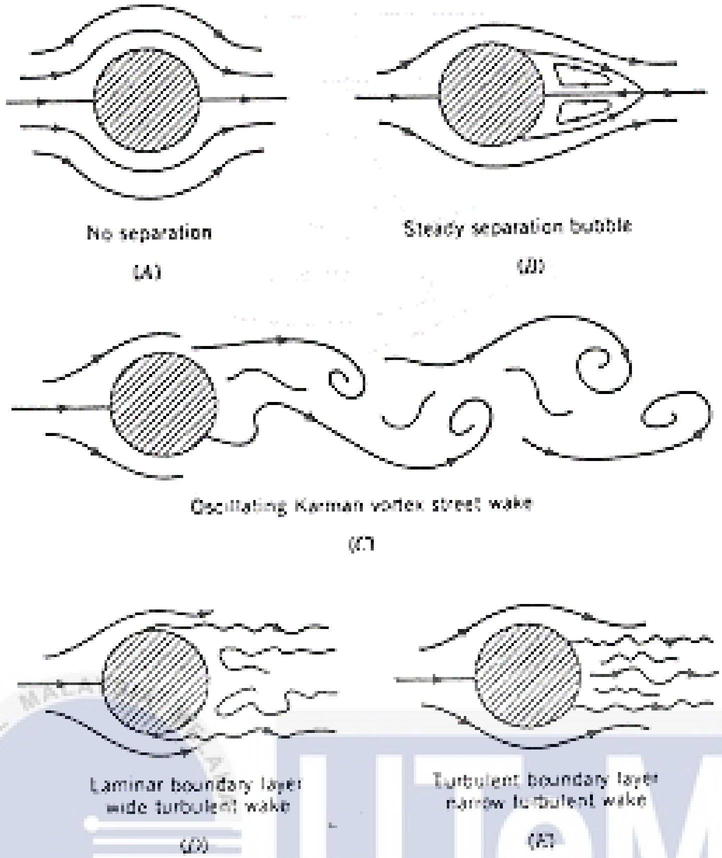

Figure 2.12: Examples of fluid flow over cylinder (Blevin, 1990)

Flow over cylinder manifested complicated flow pattern. Some of the examples are shown in Figure 2.11 and Figure 2.12. Usually what happen is that when the stream velocity is low (Re < 1), the fluid is able to follow the curvature of the cylinder. However, when the stream velocity is high, flow separation is involved in which the boundary layer detaches from the surface, forming a separation region at the back of the cylinder. Vortex is formed in the wake region and the pressure at this region is usually much lower than the stagnation point pressure. Figure 2.13 shows the change of drag coefficient for flow over cylinder and sphere. Drag is related to the behaviour fluid across the object as fluid accelerates to higher Reynolds number.

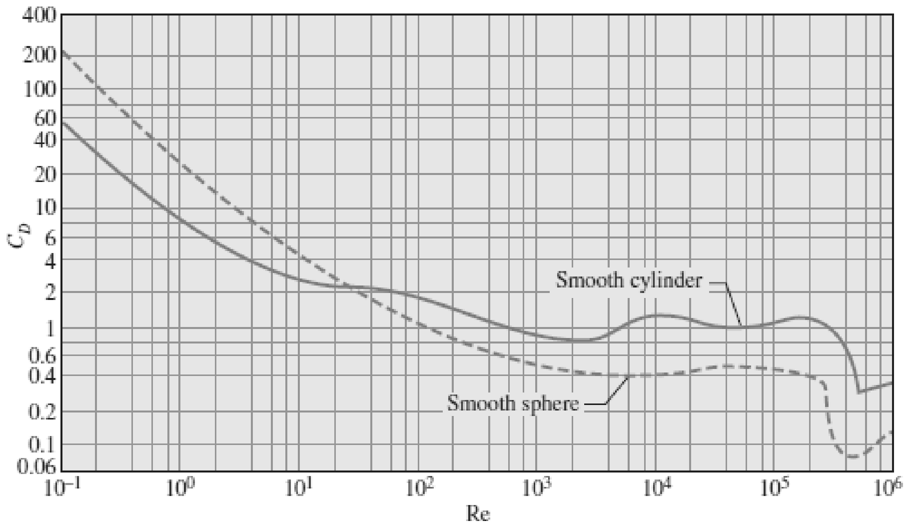

Figure 2.13: Average drag coefficient for flow over smooth cylinder and sphere

(Schlichting, 1974)

2.3.2.1 Effect of surface roughness

As aforementioned, surface roughness has excellent effect on increasing the drag coefficient in turbulent flow for streamlined body. On the other hand, it has detrimental effect for blunt body such as circular cylinder as it could decrease the drag coefficient. Surface roughing can induce the boundary layer into turbulence at low Reynolds number, and therefore stalling the flow separation. The wake region is now narrowed as the fluid is able to reattach at the back of the body and the pressure drag is reduced. Therefore, it is appropriate to rough up the surface of cylinders in order to decrease the drag coefficient as cylinder is a blunt body that experience flow separation at relatively low Reynolds number (Cengel and Cimbala, 2014).

2.3.3 Heat transfer coefficient for horizontal cylinders

In general, flow across cylinders usually involve flow separation which is easy to diagnose numerically or experimentally but extremely difficult to compute analytically. This is because the flow pattern across the cylinders is very complicated and unpredictable, and there is not a single mathematical equation that can predict and solve every possible outcomes at once except for Navier-Stokes equations. Figure 2.14 shows the impact of flow behaviour across a cylinder on the local heat transfer at the surface of the cylinder. Evidently, heat transfer at local points changes depending on the fluid flow characteristics which is represented by Reynolds number. This is related to the changes in separation point and size of wake region as Reynolds number changes.

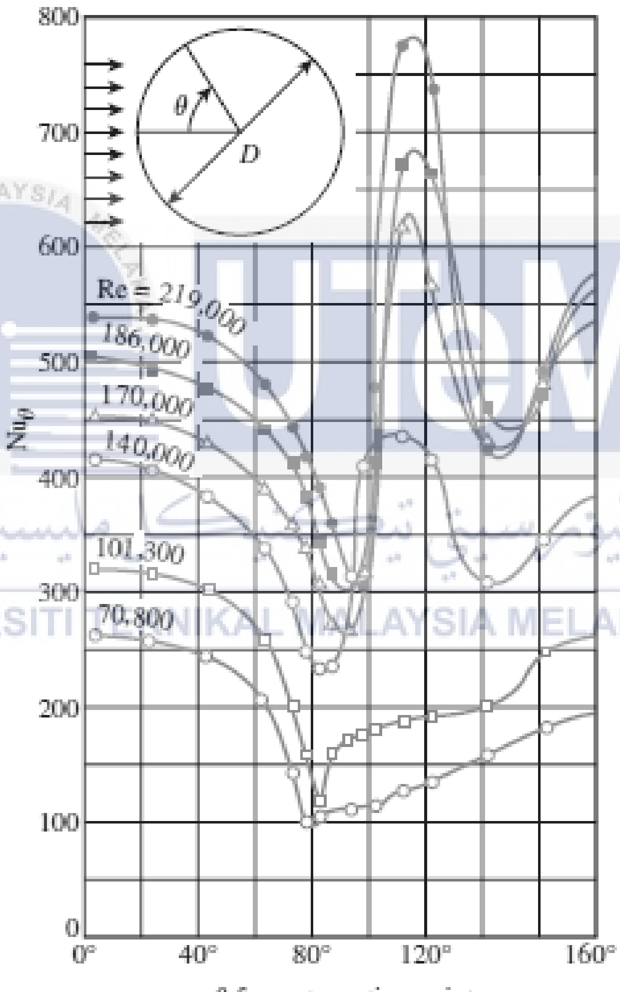

Figure 2.14: Variation of local heat transfer coefficient along the circumference of cylinder in cross flow of air (Giedt, 1949)

According to Churchill and Bernstein (1977), they proposed an equation for heat transfer that requires average heat transfer coefficient over the entire surface for cylinder. It is shown in Eq. (2.22):

$$Nu_{cyl} = \frac{hD}{k} = 0.3 + \frac{0.62Re^{1/2}Pr^{1/3}}{[1 + \left(\frac{0.4}{Pr}\right)^{\frac{2}{3}}]^{1/4}}[1 + \left(\frac{Re}{282000}\right)^{\frac{5}{8}}]^{4/5} \tag{2.22}$$

According to Sparrow et al. (2004), average Nusselt number for flow across cylinders can be expressed like in Eq. (2.23):

$$Nu = C \cdot Re^{m} \cdot Pr^{n} \tag{2.23}$$

where n is 1/3. Constant C and m are given in the Table 2.6 below.

Table 2.6: Empirical correlations for the average Nusselt number for flow across cylinders (Jakob, 1949, Zukaukas, 1972, and Sparrow et al. 2004)

Cross-section of the cylinder	Fluid	Range of Re	Nusselt number
Circle 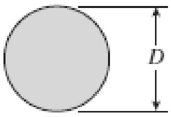	Gas or liquid	0.4–4 4–40 40–4000 4000–40,000 40,000–400,000	$Nu = 0.989Re^{0.330}\,Pr^{1/3}$ $Nu = 0.911Re^{0.385}\,Pr^{1/3}$ $Nu = 0.683Re^{0.466}\,Pr^{1/3}$ $Nu = 0.193Re^{0.618}\,Pr^{1/3}$ $Nu = 0.027Re^{0.805}\,Pr^{1/3}$
Square 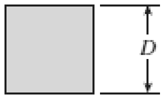	Gas	3900–79,000	$Nu = 0.094Re^{0.675}\,Pr^{1/3}$
Square (tilted 45°) 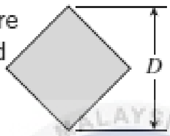	Gas	5600–111,000	$Nu = 0.258Re^{0.588}\,Pr^{1/3}$
Hexagon 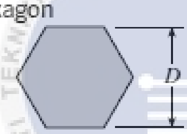	Gas	4500–90,700	$Nu = 0.148Re^{0.638}\,Pr^{1/3}$
Hexagon (tilted 45°) 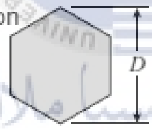	Gas	5200–20,400 20,400–105,000	$Nu = 0.162Re^{0.638}\,Pr^{1/3}$ $Nu = 0.039Re^{0.782}\,Pr^{1/3}$
Vertical plate 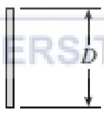	Gas	6300–23,600	$Nu = 0.257Re^{0.731}\,Pr^{1/3}$
Ellipse 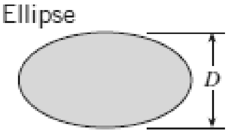	Gas	1400–8200	$Nu = 0.197Re^{0.612}\,Pr^{1/3}$

2.3.4 Flow across tube banks

Cross flow over circular cylinder represents a classical conundrum in fluid mechanics and heat transfer. Therefore it has obtained considerable amount of attention over the past 50 years or so (Patnana et al, 2010). Cross flow over tube banks symbolizes idealization of many industrial applications such as the cross flow in heat exchangers, condensers and evaporators in power plants, air conditioners and refrigerators, etc.

In order to analyze the heat transfer from a tube bank in a cross flow, instead of analyzing the flow through a single tube (analysis multiplied by number of tubes), all the tubes in the bank must be considered at once since they have effect on the flow pattern and turbulence level downstream.

2.3.4.1 Configurations of tube banks

There are two major configurations of tube banks (Cengel and Ghajar, 2015):

1. In-line
2. Staggered

The two configurations of tube banks are as shown in Figure 2.15.

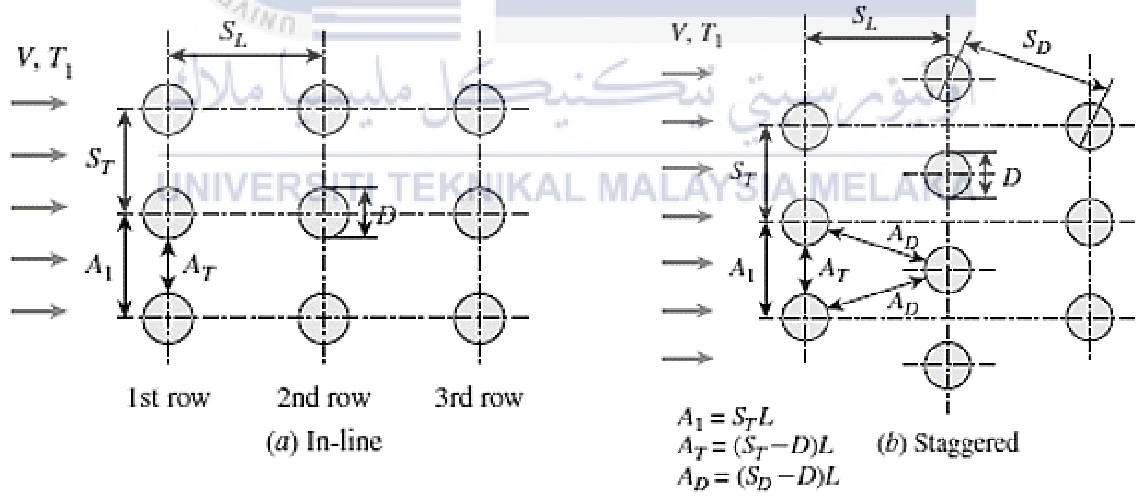

Figure 2.15(a): In-line configuration of tube bank

Figure 2.15(b): Staggered configuration of tube bank

The characteristic length of a cylinder, in this case a tube, is its outer tube diameter, *D*. The parameters involved in the analysis of tube bank are as follow:

1. Transverse pitch, S_T

2. Longitudinal pitch, S_L

3. Diagonal pitch, S_D

Diagonal pitch in tube bank is defined as in Eq. (2.24):

$$S_D = \sqrt{S_L^2 + (\frac{S_T}{2})^2} \tag{2.24}$$

As the fluid enters the in-line tube bank, according to Bernoulli's principle, as the area of flow decreases from $A_I = S_T L$ to $A_T = (S_T - D)L$, the stream velocity should increase. For staggered configuration, the velocity may even increase more if the tube rows are near to each other.

One of the uniqueness about tube bank is that maximum flow velocity, V_{max} within the tube bank is considered in analysis instead of the incoming flow velocity, V. It can be obtained from Eq. (2.25):

$$Re_D = \frac{\rho V_{max} D}{\mu} = \frac{V_{max} D}{v} \tag{2.25}$$

For staggered configuration, maximum velocity is determined as in Eq. (2.26):

$$V_{max} = \frac{S_T}{2(S_D - D)} V \tag{2.26}$$

Condition: $S_D < (S_T + D)/2$. Besides of the conventional in-line and staggered tube bank configuration, many other arrangements of tubes have been look onto, such as tube bank with finned surfaces. Tahseen et al. (2015) concluded that staggered configuration gives better heat transfer performance compared to the in-line configuration for finned and un-finned tube heat exchangers regardless of the tube shape.

Mirzakhanlari et al. (2015) found that thermal performance can be improved by increasing the number of tubes and setting the optimum distance (longitudinal and transverse pitch ratio) between tubes in tube bank. Bender et al. (2018) has put a new trapezoidal tube bank arrangement into test with circular tube bank as reference. Trapezoidal factor $t/d = 3/16$ in high Reynolds number range gives the best fluid flow and thermal transfer performance. They deduced that by increasing the trapezoidal factor, average Nusselt number, pressure drop, and entropy production can be increased.

Mangrulkar et al. (2017) found that thermal performance of cam-shaped tube is more superior to normal circular tube in terms of friction factor, heat transfer, Webb efficiency, and area goodness factor. This is because formation of high-intensity vortex at the downstream and the accretion in length of boundary layer which delay the separating point. By installing splitter plate onto the tube bank, it increases the heat transfer performance and pressure drop compared to bare tube. Overall thermal performance was increased by 60 – 82 % at Reynolds number of 5500. Lotfi et al. (2016) found that heat transfer performance of smooth wavy fin-and-elliptical tube heat exchanger can be enhanced by flow velocity and wavy fin height. In the meantime, tube ellipticity ratio shall be reduced.

According to Ibrahim and Gomaa (2009), elliptic tubes in staggered arrangement contributes significantly to energy conservation compared to circular tube bank. Maximum heat transfer coefficient is obtained when the flow is parallel to major axis of tube and vice versa. Increasing the angle of attack until 90^{o} amplifies the heat transfer performance drastically. He et al. (2012) had the same conclusion in which increasing the angle of attack of punched winglet-type vortex generator arrays in fin-and-tube heat exchangers can increase the heat transfer coefficient and pressure drop. According to Lu et al. (2011), geometric parameters play a big role on the performance of a fin-and-tube heat exchanger. Heat transfer performance, in terms of $Q/\Delta P$ and COP increases, as the longitudinal and transverse tube pitch increase, and as the larger tube diameter and fin thickness decrease. Kim (2013) obtained the similar results provided that the longitudinal pitch ratio is less than 2.7.

Han et al. (2013) examined the effect of oval tubes in finned (enhanced fin, wavy fin, and louvered fin) tube heat exchanger compared to circular tube. They found that flow resistance and pressure drop can be reduced effectively by using oval tube with fin, thus improved the heat transfer performance and fin efficiency.

Gharbi et al. (2015) claimed that it is best to avoid using circular tube while designing a heat exchanger as circular tube can cause severe flow separation and large wakes that lead to high pressure drop compared to streamlined tube. However it still depends on the flow parameter whether it is laminar or turbulent. According to Hsieh and Jang (2012), they found that fin collar outside diameter, transverse tube pitch and fin pitch are the main influencers on determining the fluid flow and heat transfer characteristics of louver fin-and-tube heat exchanger.

2.3.4.2 Nature of flow across tube banks

When the tubes are not too close to each other, first row of tubes can be treated as single tube in cross-flow because there is minor change in turbulence level and the heat transfer coefficient remains controlled. For second and subsequent rows, due to the formation of wakes and turbulence caused by the flow in upstream location while passing across the tubes, heat transfer coefficient and level of turbulence increase with the number of rows.

According to Zukauskas (1987), a correlation is proposed for the average Nusselt number of cross flow over tube banks based on the experimental data obtained which is defined as shown in Eq. (2.27):

$$Nu_D = \frac{hD}{k} = CRe_D^m Pr^n (\frac{Pr}{Pr_s})^{0.25} \tag{2.27}$$

The conditions and limitations of the use of Eq. (2.27) are:

1. Tube bank must be more than 16 rows ($N_L > 16$)
2. $0.7 < \mathrm{Pr} < 500$
3. $0 < \mathrm{Re_D} < 2 \times 10^6$
4. $\mathrm{Pr_s}$ is determined from arithmetic mean temperature, $T_m = (T_i + T_e)/2$

Values of constant C, m, and n can be found in Table 2.7 with corresponding Reynolds number range.

Table 2.7: Nusselt number correlations for cross flow over tube banks (Zukauskas, 1987)

Arrangement	Range of Re_D	Correlation
In-line	0–100	$Nu_D = 0.9\,Re_D^{0.4}Pr^{0.36}(Pr/Pr_s)^{0.25}$
	100–1000	$Nu_D = 0.52\,Re_D^{0.5}Pr^{0.36}(Pr/Pr_s)^{0.25}$
	1000–2×10^5	$Nu_D = 0.27\,Re_D^{0.63}Pr^{0.36}(Pr/Pr_s)^{0.25}$
	2×10^5–2×10^6	$Nu_D = 0.033\,Re_D^{0.8}Pr^{0.4}(Pr/Pr_s)^{0.25}$
Staggered	0–500	$Nu_D = 1.04\,Re_D^{0.4}Pr^{0.36}(Pr/Pr_s)^{0.25}$
	500–1000	$Nu_D = 0.71\,Re_D^{0.5}Pr^{0.36}(Pr/Pr_s)^{0.25}$
	1000–2×10^5	$Nu_D = 0.35(S_T/S_L)^{0.2}\,Re_D^{0.6}Pr^{0.36}(Pr/Pr_s)^{0.25}$
	2×10^5–2×10^6	$Nu_D = 0.031(S_T/S_L)^{0.2}\,Re_D^{0.8}Pr^{0.36}(Pr/Pr_s)^{0.25}$

For number of rows that is less than 16 (N_L < 16), Eq. (2.27) can still be used but with consideration of correction factor, *F*. It is shown in Eq. (2.28) below:

$$Nu_{D,N_L<16} = FNu_D \tag{2.28}$$

where *F* = correction factor. Values of correction factors are as listed in Table 2.8.

Table 2.8: Correction factor for N_L < 16, and Re_D > 1000 (Zukauskas, 1987)

N_L	1	2	3	4	5	7	10	13
In-line	0.70	0.80	0.86	0.90	0.93	0.96	0.98	0.99
Staggered	0.64	0.76	0.84	0.89	0.93	0.96	0.98	0.99

According to Guo et al (2018), maldistribution of inlet flow and non-uniformity of inlet temperature could jeopardize the performance of cross flow over tube bank. Abramov et al. (2015) claimed that the numerical simulation and experiment are in good agreement for finding the average heat transfer of liquid metal in turbulent cross flow over tube bank. Minakov et al. (2016) claimed that heat transfer performance is enhanced in cylindrical tube by using nanofluids. As the nanoparticles' size and concentration increase, the heat transfer coefficients in turbulent region increases as well. Ahmed et al. (2017) obtained the similar findings by using Al_2O_3-water nanofluid as medium in investigation of laminar convective heat transfer of flow over circular tube banks with staggered configuration. Lavasani and Bayat (2016) found that using Al_2O_3-water nanofluid for cross flow over tube bank increases the heat transfer rate for both circular and cam-shaped configuration. They also found that the staggered arrangement is better than the in-line arrangement. Cam-shaped tube bank has lower pressure drop than the circular tube bank for all range of Reynolds number.

Based on the findings by Ilori et al. (2018), effect of oscillatory flow on thermal and pressure drop performance of compact tube heat exchanger is examined. Performances are indicated on the drive ratio (measured maximum oscillating pressure to mean pressure of system), edge shape and temperature. They reported that edge shape reduces the minor loss notably with ignorable effect on thermal performance at high amplitude.

2.3.4.3 Pressure drop in tube banks

Pressure drop, *ΔP*, is the irreversible pressure loss between the inlet and outlet of the tube bank. According to Swep (2019), pressure drop can occur whenever a flow is disrupted. In usual situation, the pressure at the inlet is higher than the outlet. Pressure drop can be both beneficial and detrimental depending on the magnitude of it. It is beneficial because large pressure drop suggests that more turbulences are created. Turbulence is prudent in a heat exchanger. This is because in every flow, no matter laminar or turbulent, there's always formation of boundary layer, this layer can act as insulation film to constrict the convective heat transfer. By making the flow turbulent, it can force the boundary layer to be separated and introduce vortex in the flow region. This will enhance the overall heat transfer.

It is detrimental because it implies that the flow is obstructed and requires more pump power to push it through. Besides, it can also damage the interior of a heat exchanger. Pressure drop can be calculated using Eq. (2.29).

$$\Delta P = N_L f \chi \frac{\rho V_{max}^2}{2} \tag{2.29}$$

where *f* is friction factor (refer to Figure 2.16), *X* is correction factor (*X* = 1 for square and equilateral triangle configurations).

Pressure drop is in a proportionate relation with the power needed to transfer the fluid. Equation (2.30) shows the pumping power needed to triumph the drag of cross flow when there is pressure drop:

$$\dot{W}_{pump} = \dot{V}\Delta P = \frac{\dot{m}\,\Delta P}{\rho} \tag{2.30}$$

where $\dot{W}$ is pumping power (SI units: W), $\dot{V}$ is volume flow rate (SI units: m^3/s), $\dot{m}$ is mass flow rate (SI units: kg/s).

Dynamic pressure is the pressure exerted by moving fluids. It is defined as Eq. (2.31) shown below:

$$\Delta P = \frac{\rho V^2}{2} \tag{2.31}$$

where ΔP is pressure drop (SI units: Pa), ρ is density of fluid (SI units: kg/m^3), and V is flow speed (SI units: m/s). It can be used to determine the density of moving fluid when the dynamic pressure and its velocity is determined via Ansys Fluent.

If the flow is fully turbulent, the heat transfer coefficient satisfies the following relation as shown in Eq. (2.32):

$$k \sim \sqrt[3]{\Delta P} \tag{2.32}$$

Figure 2.16 shows the values of friction factor and correction factor for the staggered arrangement of tube bank.

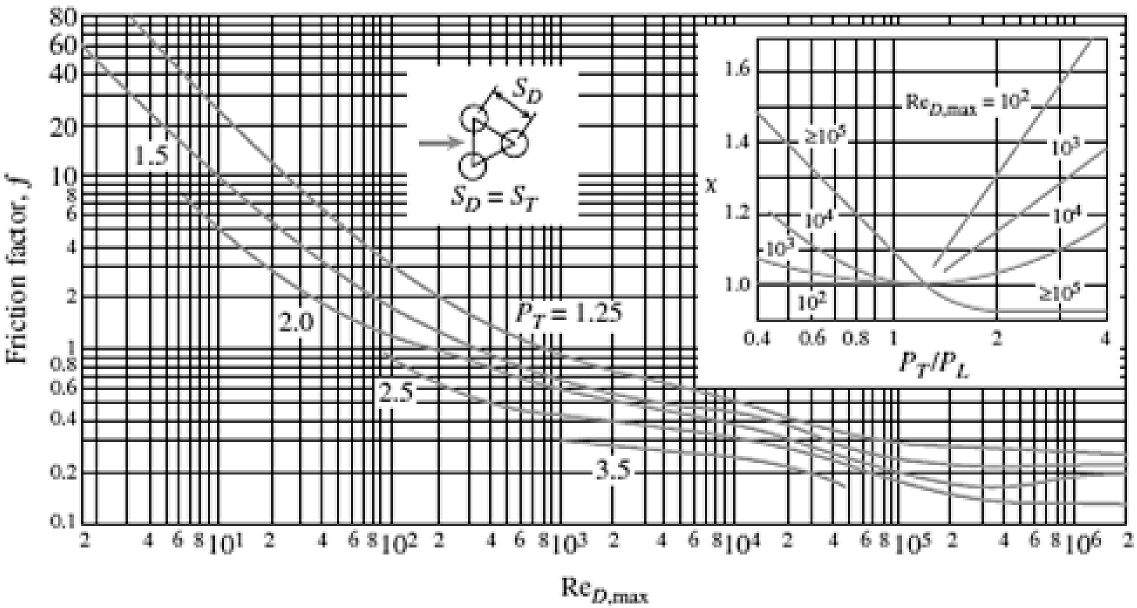

Figure 2.16: Friction factor *f* and correction factor *X* for staggered tube banks

(Cengel and Ghajar, 2015)

2.3.4.4 Brief introduction to heat exchangers

Energy is one of the most important quantity we human can't live without. Sustainable development on energy sector is showing signs that we do care about our next generation. Effective utilization of available energy is the hottest topic among the people (Mohanty et al., 2018).

Heat exchanger is used to transfer or 'exchange' heat from one to another fluids. It is used widely in industries such as power plant, chemical processing plant, vehicle manufacturers, and etc. It is used in both heating and cooling processes (Al-Sammarraie and Vafai, 2017). There are many types of heat exchangers available on the market. Examples of types of heat exchanger are:

1. Double-pipe heat exchanger
2. Shell-and-tube heat exchanger
3. Plate fin heat exchanger

4. Direct contact heat exchanger

5. Waste heat recovery unit

6. Printed circuit heat exchanger

According to labbadlia et al. (2017), efficiency of a shell-and-tube heat exchanger can be affected by the non-uniformity of flow distribution. The flow distribution is greatly affected by arrangement of tubes. Based on the study, by arranging the tubes in 60^{o} configuration, it gives better uniformity in flow distribution compared to conventional configuration (90^{o}) by 21%. Also, 45^{o} configuration exhibits highest mean velocity and uniform pressure distribution compared to other configurations, and it is the most economical because it uses lowest number of tubes. However, Wang et al. (2016) claimed that inclination degree of tube does not give significant impact on characteristics of fluid flow and heat transfer for cross over tube banks, but decreasing the impact angle will reduce the fluid velocity thus weakens heat transfer performance in heat exchanger.

According to Li et al. (2011), slit fin-and-tube heat exchanger with longitudinal vortex generators is studied numerically, and the results showed that vortices generated by slit fin improved the heat transfer performance with modest pressure drop penalty.

Analysis on heat exchangers

Basically there are two methods that can be used for the analysis and selection of heat exchangers, and they are:

1. Log mean temperature method,

$$Q = UA(\Delta T_{lm});\ \Delta T_{lm} = \frac{\Delta T_1 - \Delta T_2}{\ln\left(\frac{\Delta T_1}{\Delta T_2}\right)} \tag{2.33}$$

2. Effective-NTU method

$$\varepsilon = \frac{Q}{Q_{max}};\ NTU = \frac{UA}{C_{min}} \tag{2.34}$$

where Q is heat, U is overall heat transfer coefficient, A is surface area, ΔT_{lm} is log mean temperature difference, ΔT_1 is temperature difference between two streams at end 1, ΔT_2 is temperature difference between two streams at end 2, ε is effectiveness of heat exchanger, Q_{max} is the maximum heat, C_{min} is the lowest heat capacity rate of the fluid in the heat exchanger.

Selection of heat exchangers

Selecting the right heat exchangers can be a challenge as there are so many factors needed to be taken into consideration. Understanding the thermal performance and application of heat exchangers are a must when selecting the heat exchangers. Here are some of the criteria:

1. Heat transfer rate
2. Flow rate
3. Pressure drop
4. Cost
5. Pumping power
6. Size and weight
7. Type
8. Materials
9. Maintenance

2.4 Numerical simulation

A numerical simulation is a very useful tool for the study of collective effects especially for fluid flow and heat transfer applications. It is a calculation that is run on a computer to solve mathematical model implemented by a program for a physical system. It is required when the mathematical models are too complex to be solved analytically, as in most nonlinear systems.

2.4.1 Computational Fluid Dynamics (CFD)

Computer Fluid Dynamics (CFD) is the science of predicting and analysing fluid flow, heat and mass transfer, chemical reactions, etc. using numerical analysis. CFD is a very effective tool and is used in many applications, such as aerodynamics, research and development, weather simulation, etc. CFD solves equations for conservation of mass, momentum, energy, etc. to predict these phenomena.

Although the equations governing the fluid flow such as Bernoulli's equation have been known for over a century, not until the appearance and availability of digital computers till we see massive advances in CFD. Since then, ever-increasing level of investments and resources has been garnered and sectors such as industry, education, etc. has benefited from CFD. CFD has matured to a point where most CFD calculations are undertaken on commercial packages. Here are the examples of the commercial CFD software available in the market:

1. Ansys Fluent
2. Star-CCM+
3. OpenFoam
4. COMSOL
5. Ansys CFX

6. Autodesk CFD

7. SOLIDWORKS Flow Simulation

CFD analysis is without a doubt strenuous. User-friendly interactive graphical presentation becomes necessary during the analysis. Even with these, it is still hard to display all the information in order to get full understanding of the problem.

2.4.2 CFD methodology

Usually, every CFD process starts with preprocessing. Geometry and physical bounds of problem is designed using computer aided design (CAD). Computational domain is chosen and divided into mini elements called cells (Areas for 2-D domain, volume for 3-D domain). Mesh is generated. It can be structured or unstructured, uniform or non-uniform, consisting combination of triangle, quadrilateral, hexahedral, tetrahedral, prismatic, pyramidal or polyhedral elements. Boundary conditions are defined. Fluid behavior, type of fluid and properties at all edges or faces are specified. Initial conditions are defined if it's a transient problem. Numerical parameters and solution algorithms are selected. Grid independent test and mesh convergence study is run if necessary. Simulation commenced and the equations are solved iteratively as steady-state or transient. Analysis and visualization of resulting solution using postprocessor.

2.4.3 Mesh generation

Mesh generation is a preprocessing step for CFD to create mesh. According to Bern and Plassmann (1997), a mesh is a discretization of continuous geometric space into small simple shapes, such as triangles or quadrilaterals in 2D or tetrahedral or hexahedral in 3D. Meshes are generated automatically by computer algorithms, usually accompanied with human guidance. The meshes are used as discrete local approximations of the computational domain. Rivara (1984) has proposed multiple techniques to enhance the quality of mesh generated: Mesh refinement, mesh smoothing, and optimal triangulation.

Meshing is especially important when it comes to more accurate solution. Mesh with higher quality or better shaped will have better numerical properties. There are three major distinctions in mesh grids:

1. Structured – regular lattice with implied connectivity between elements. It's simpler and easier.
2. Unstructured – irregular patterns with varying local neighborhoods. The adaptivity of mesh to complicated domains is higher.
3. Hybrid – contain a mixture of structured and unstructured grids.

According to Ansys Inc. (2009), it is acceptable for 2D meshes to use quadrilateral and triangular cells while polyhedral such as hexahedral, tetrahedral, pyramid, and wedge are suitable for 3D meshes. Figure 2.17 below shows the illustrations of cell types aforementioned.

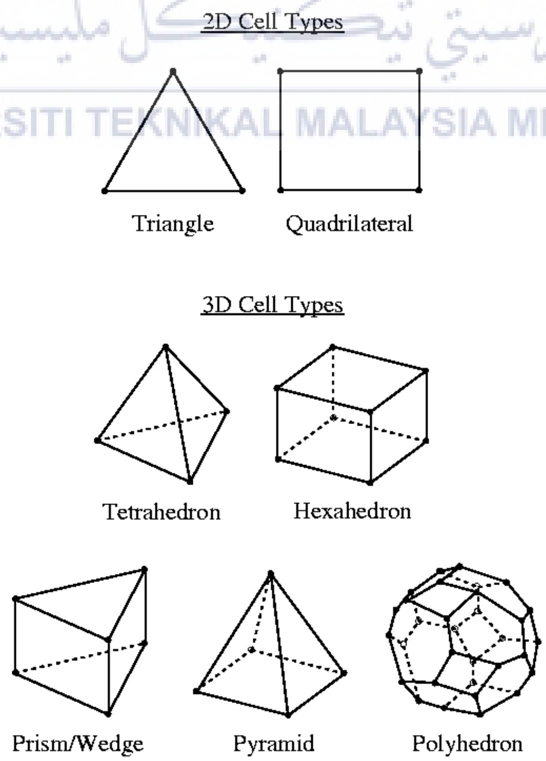

Figure 2.17: Mesh topology (Ansys Inc., 2009)

There are at least three criteria that need to be considered when it comes to choosing the appropriate mesh type. These criteria are:

1. Setup time – unstructured meshes is always preferable compared to structured meshes when it comes to complex geometries as it is very time consuming to create structured meshes for it. However, it doesn't make any difference for simple geometries (Sadrehaghighi, 2019).
2. Computational expense – use quadrilateral or hexahedra meshes for simple geometries and triangular/tetrahedral meshes for complex geometries to reduce computational expense.
3. Numerical diffusion – Numerical diffusion is a major source of error in CFD. It is presented in almost all numerical simulations for fluid flow. This is because of the truncation errors when discretizing the equations. It can be minimized when the flow is in the same direction as the meshes.

2.4.4 Discretization methods

Discretization is a way to convert continuous problems into discrete problem by approximation. Then the problem can be solved discretely by numerical methods. Some of the discretization methods being used are:

1. Finite volume method
2. Finite element method
3. Finite difference method
4. Boundary element method
5. High resolution discretization schemes

Discretization method is selected based on the demanded accuracy of solution. In Ansys Fluent 16.0, there are five options for spatial discretization and there are first order upwind, second order upwind, power law, QUICK, and third-order MUSCL for field variables such as momentum, turbulent kinetic energy, specific dissipation rate and energy.

According to Fluent Inc. (2006), second-order upwind scheme is more accurate than first-order upwind scheme because it will compute the cell faces through a Taylor series expansion of the cell-based solution about the cell's centre but first order upwind scheme will represent values of any field variable to be average and remain the same throughout the entire cell which is rather inaccurate.

Gradients are one of the most essential component used to construct scalar's values at cell faces. They are also used to compute secondary diffusion and velocity derivatives. There are three options for gradients available in Ansys Fluent 16.0, and these are the Green-Gauss Cell-Based, the Green-Gauss Node-Based, and the Least Squares Cell-Based. One of the criteria to be considered when it comes to selecting of the best gradients is the mesh topology. Least squares cell-based gradients are recommended when it comes to solving on polyhedral meshes and it will definitely produce a more accurate solution. Node-based gradients is more stable when solving on triangular and tetrahedral meshes compared to cell-based gradients.

2.4.5 Pressure-velocity coupling

Pressure-velocity coupling is a pressure-based solver that enable the user to solve the flow problem in either segregated or coupled manners (Fluent Inc., 2006). It is attained by revising the continuity equation to derive auxiliary state for pressure. There are 5 options to be chose from Ansys Fluent and there are SIMPLE, SIMPLEC, PISO, Fractional Step, and Coupled. SIMPLE and SIMPLEC algorithms are suitable for relatively simple problems such as laminar flows without extra models activated. PISO algorithms is highly recommend for all transient flow solution with large time step. However, it does not shows any significant difference over SIMPLE or SIMPLEC algorithms for steady state problems. Last but not least, the coupled scheme is different than the aforementioned algorithms because it is a coupled solution scheme and enables full pressure-velocity coupling. It offers a powerful and effective solution for steady-state flows, with superior performance compared to the segregated solution schemes. Besides, using the coupled algorithm is recommended when the quality of the mesh is poor or large time steps are used for transient problem.

2.4.6 Turbulence models

Turbulent models are in different realm compared to laminar models. There are a lot of uncertainties involved and it is far more complex to be solved. Vendors have been developing suitable models from differential forms of Navier-Stokes equation and continuity equations in order to predict the fluid flow in turbulent region. Some of the computational models for turbulent flow being used are:

1. Reynolds-Averaged Navier Stokes (RANS)
2. Large Eddy Simulation (LES)
3. Detached Eddy Simulation (DES)
4. Direct Numerical Simulation (DNS)
5. k-ε two equation model
6. k-ω two equation model

According to Mohd Saat and Jaworski (2017), SST-k-ω turbulence model can produce the most accurate depiction of velocity profile and calculated heat flux for oscillatory flow.

2.4.7 Flow patterns and flow visualization

Flow visualization is the visual examination of flow field. It is highly useful not only in physical experiments, but also in numerical solutions (CFD).

2.4.7.1 Plots of fluid flow data

It is really important to plot flow data in details to inform the user on the useful flow data regardless of how the results are obtained (computationally or experimentally). Examples of useful plots are:

1. Profile plots – indicates the variation of scalar properties such velocity at a specific direction in flow field.
2. Vector plots – Array of arrows indicating the magnitude and direction of vector properties at an instant of time.
3. Contour plots – Curves of constant values of a scalar property or magnitude of a vector property at an instant of time.

Figure 2.18 to 2.20 show the illustration of the plots; the profile plot, the vector plot, and the contour plot.

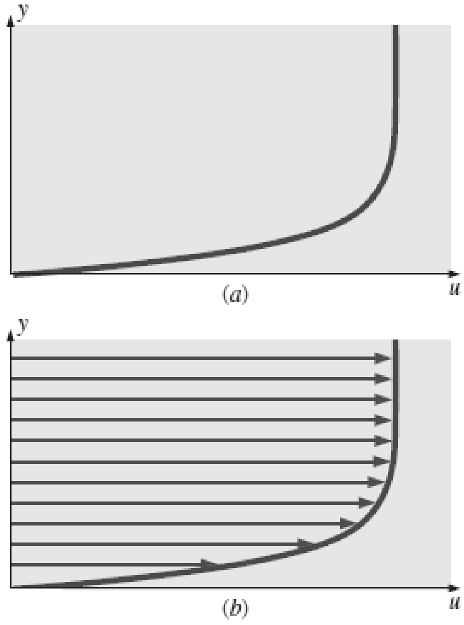

Figure 2.18(a): Standard profile plot

Figure 2.18(b): Profile plot with arrows

(Cengel and Cimbala, 2014)

Figure 2.19: Vector plot (Cengel and Cimbala, 2014)

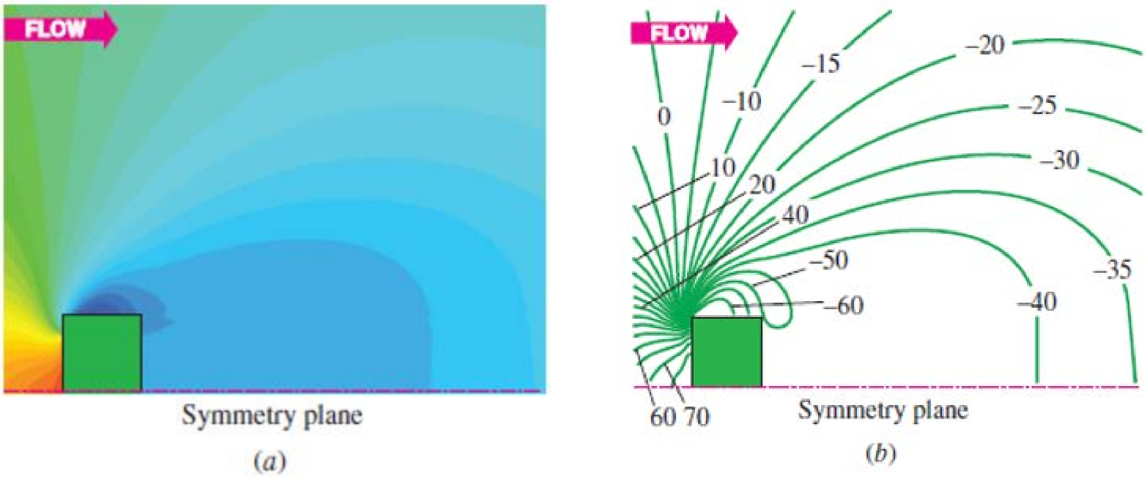

Figure 2.20(a): Filled color contour plot

Figure 2.20(b): Contour plot with pressure values

(Cengel and Cimbala, 2014)

CHAPTER 3

METHODOLOGY

3.0 Introduction

This chapter describes the framework of the project which cover the outline of implementation of project. It also covers methodology used in this project to obtain the data and results for project entitled “CFD Investigation of Cross Flow over Tube Banks”.

3.1 Overall project planning

This project is divided into Final Year Project I and Final Year Project II. They are to be completed in Semester I and Semester II, respectively. At the beginning of Semester I, project title has been selected and it is called “CFD Investigation of Cross Flow over Tube Banks”. Throughout Semester I, literatures such as books, articles, etc. regarding the project have been reviewed and related information are relayed into this report.

At the end of Semester I, some of the criteria regarding to the CFD simulation of cross flow over tube banks were completed. For example, tube banks model with suitable arrangement, geometry, and dimensions was designed based on literatures reviewed. Boundary conditions, flow materials, wall condition, meshing criteria were identified. Fluid flow criteria such as steady, incompressible, one-dimensional flow, transient oscillatory flow were also determined via literature review. Ansys Fluent was used in the CFD investigation of cross flow over tube banks.

3.1.1 Overall project planning flow chart

Figure 3.1 shows the flow chart that describes the overall process of this final year project.

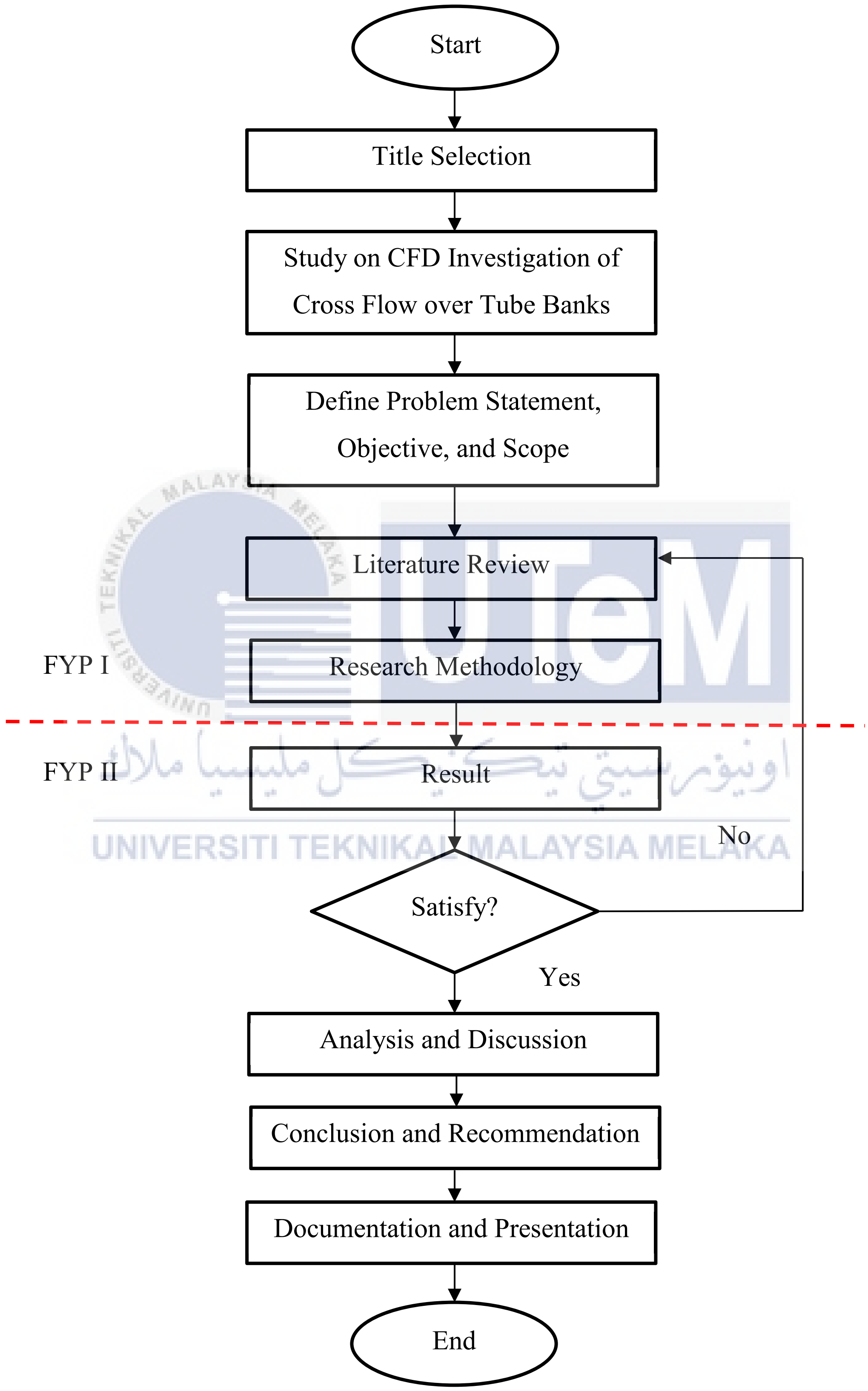

Figure 3.1: Overall project planning flow chart

3.2 Research methodology

The section provide an insight into the research methodology employed in order to obtain the needed criteria to fulfil the objectives for the project to be completed smoothly and successfully. Figure 3.2 shows the flow of the research methodology in CFD investigation of cross flow over tube banks.

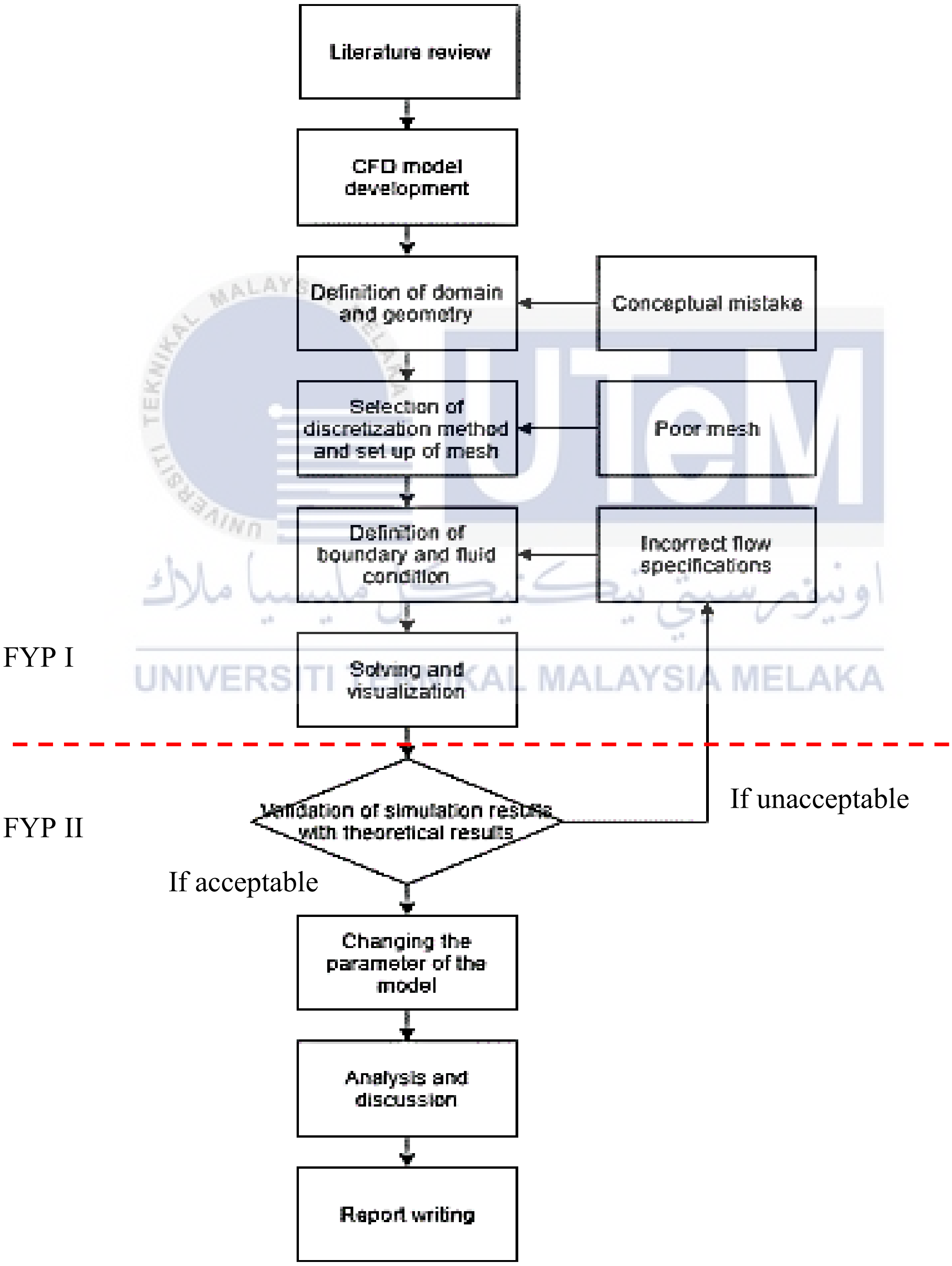

Figure 3.2: Research methodology flow chart

3.2.1 Literature review

Literature review was done on the project with a topic of "CFD Investigation of Cross Flow over Tube Banks". Literature review is a powerful and valuable part of the project as it allows extraction and evaluation of the available literatures done by the other researchers in conjunction to the current research topic. Literatures regarding the project title were obtained from different sources such as papers, journals, books, reports, relevant works, publications, etc. Synthesis of data and information collected regarding to the project topic were inserted into Chapter 2.

3.2.2 CFD model development

Based on the reviewed literature, a 2D model of a staggered tube bank was produced using SOLIDWORKS, a software by Dassault Systemes. The model was sketched according to the dimensions as stated in Table 3.1 below. The sketches were then converted into surface layer using the surface feature and imported into Ansys Fluent 16.0. Later, the model was generated within Ansys Design Modeler. Analysis type was toggled to 2D. The sketch of the 2D staggered tube banks is as shown in Figure 3.3.

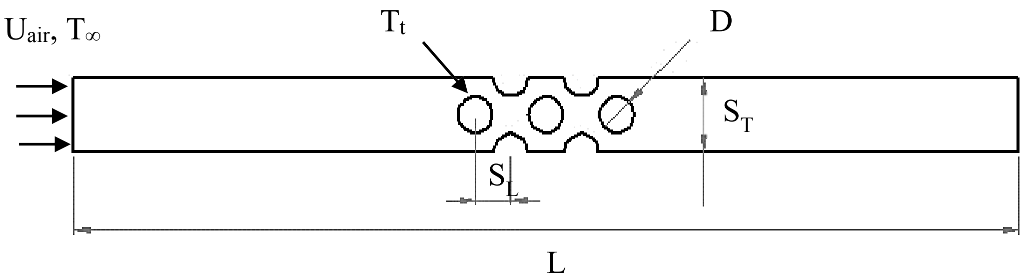

Figure 3.3: Design of staggered tube banks

Table 3.1: Description of tube banks

Description	**Details**
Shape of tubes	Circular
Diameter of tube, *D* (mm)	21.7
Length of bank array, *L* (mm)	600
Longitudinal pitch, S_L (mm)	22.5
Transverse pitch, S_T (mm)	45
Angle of attack, θ (°)	0

3.2.3 Definition of domain and geometry

Commercial CFD package Ansys Fluent 16.0 was used in this numerical simulation. Fluent module was selected from the workbench to begin the setting up process for simulation. After the process of importing the geometry as was discussed in previous section, the computational domain of the model was set to be a fluid domain and named selections were done as shown in Figures 3.4.

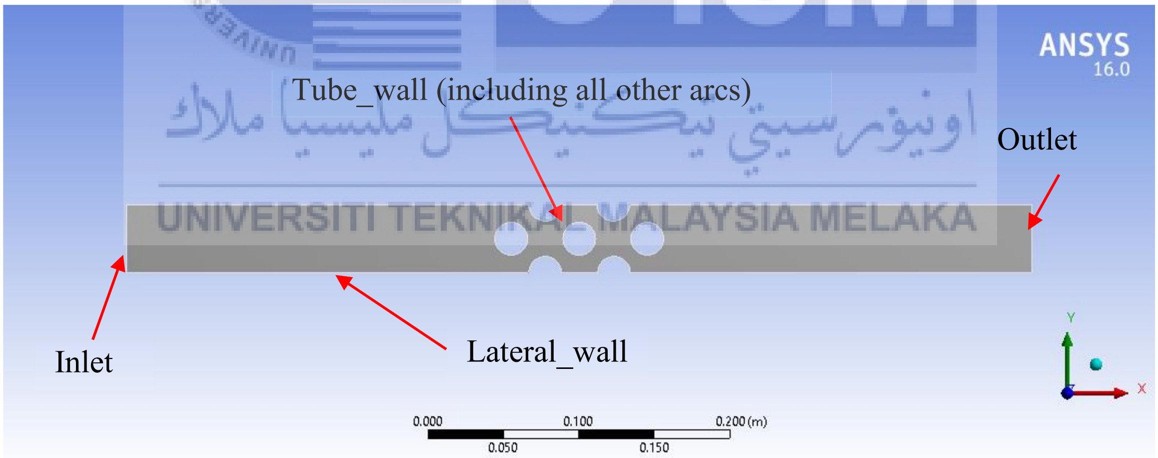

Figure 3.4: Named selections for the surfaces of the model

3.2.4 Selection of discretization method and set up of mesh

Before conducting the mesh convergence test, default sizing method was used for the model. Table 3.2 provides the details for mesh sizing option. Figures 3.5 and 3.6 show the default mesh setting and the enlarged view of the quality of mesh around the wall respectively.

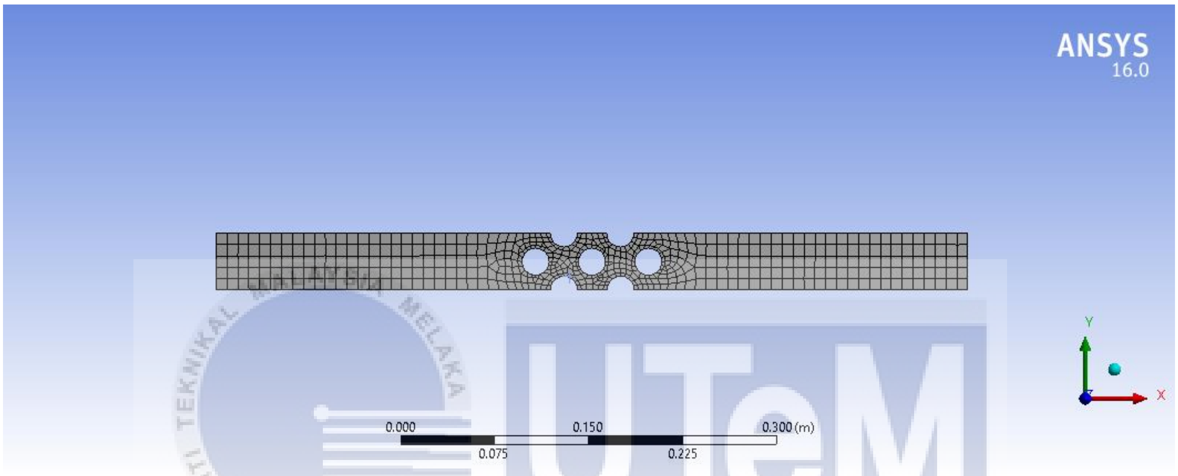

Figure 3.5: Default meshing

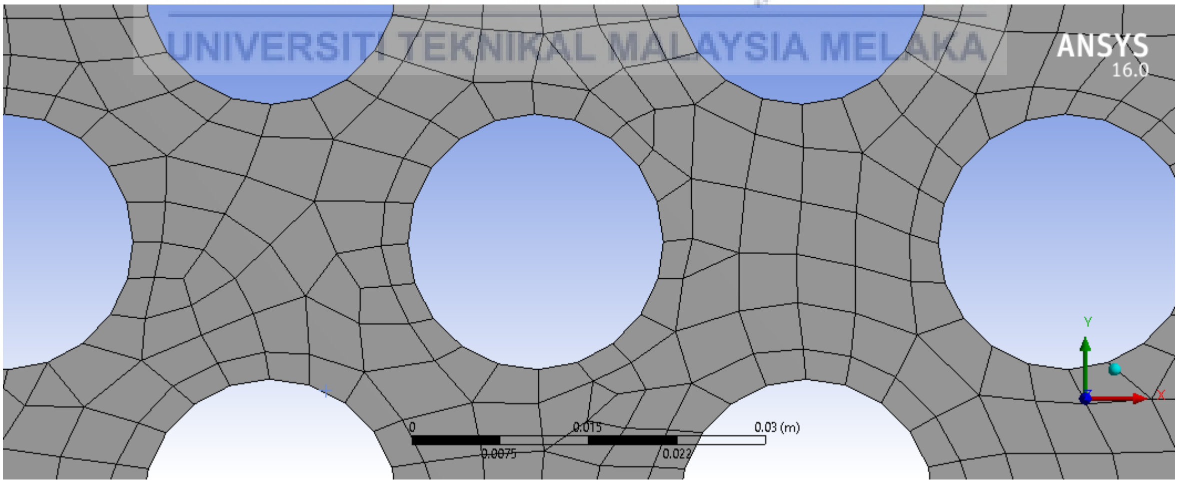

Figure 3.6: Mesh around tube walls

Table 3.2: Mesh sizing option

Description	Details
Use advanced size function	On: proximity and curvature
Relevance center	Fine
Initial size seed	Active assembly
Smoothing	High
Proximity size function sources	Faces and edges
Min size	8.7837e-05
Proximity min size	8.7837e-05
Max face size	8.7837e-05
Max size	1.7567e-02
Growth rate	1.2

The number of nodes was 654, and the total number of elements was 531 for this mesh. The discretization method of second order upwind scheme was chosen for all the governing equations involved in the model.

3.2.5 Definition of boundary and fluid condition

The model was solved for two different flow conditions: the steady flow and the oscillatory flow conditions.

3.2.5.1 Setup for steady flow model

The boundary conditions for steady flow model are as shown in Table 3.3.

Table 3.3: Boundary conditions for steady flow model

Location	Boundary condition
Inlet	Velocity inlet, free stream turbulence intensity = 1%, $2000 \leq Re \leq 24000$
Outlet	Neumann-type pressure outlet
Lateral wall	Symmetry
Tube wall	Non-slip

The Reynolds number for the flow is calculated as in Eq. (3.1):

$$Re_{D,eq} = \frac{\rho_{air} U_{max} D_{eq}}{\mu_{air}} \tag{3.1}$$

where $Re_{D,eq}$ is the Reynolds number, ρ_{air} is density of air, U_{max} is maximum velocity that occurs within the tube banks, D_{eq} is the diameter of the tube, μ_{air} is the dynamic viscosity. Flow range of interest is $2000 \leq Re_{D,eq} \leq 24000$.

The maximum air velocity, U_{max} for staggered tube bank arrangement can be calculated by using Eq. (3.2):

$$U_{max} = U_{air} \frac{S_T}{2(S_D - D)} \tag{3.2}$$

Where

$$S_D = \sqrt{S_L^2 + (\frac{S_T}{2})^2} \tag{3.3}$$

The fluid flow is modelled as an air and aluminium is applied at the tube walls. Table 3.4 shows the physical properties of air and aluminium as defined in the CFD model.

Table 3.4: Physical properties of material used in steady flow model

Material	**Properties**	**Values**
Air	Density (ρ_{air})	1.1459 kg/m^3
	Specific heat (Cp_{air})	1006.43 J/kg·K
	Thermal conductivity (λ_{air})	0.02671 W/m·K
	Viscosity (μ_{air})	1.8915 x 10^{-5} m/s^2
	Prandtl number (Pr)	0.71289

	Inlet temperature (T_{air})	35 ºC
Aluminium	Density (ρ_t)	2700 kg/m^3
	Heat capacity (Cp_t)	879 J/kg·K
	Thermal conductivity (λ_t)	229 W/m·K
	Tube temperature (T_t)	10 ºC

The Reynolds number of the flow changes with the change of velocity following the Eq. (3.1) Table 3.5 shows the velocity of air that was assigned as inlet condition for the model corresponding to the Reynolds number of the flow.

Table 3.5: Air velocity corresponding to Reynolds number

Reynolds number, $Re_{D, eq}$	**Air velocity, U_{air} (m/s)**
2000	0.684
5000	1.710
8000	2.737
15000	5.132
24000	8.211

3.2.5.2 Setup for oscillatory flow model

For case of comparison between the cases of steady flow and oscillatory flow conditions, the drive ratios (DR) of the oscillatory flow were set to be at 0.3% and 1.2%. Drive ratio represents the strength of the flow amplitude and it was defined as the ratio between the maximum amplitude of pressure to the mean value of pressure. The drive ratio of 0.3% and 1.2% were found to provide inlet conditions with Reynolds number almost similar to the steady flow cases of Re = 2000 and Re = 8000. Drive ratios (DR) of 0.3% and 1.2% were therefore chosen to set up the oscillatory flow model. The frequency of the flow is set to 13.1Hz (Mohd Saat and Jaworski, 2017). Equations (3.4) and (3.5) governed the inlet and outlet conditions for the model:

$$P = P_a \cos(kx_1) \cos(2\pi f t) \tag{3.4}$$

$$m' = \frac{P_a}{c}\sin(kx_2)\cos(2\pi ft + \theta) \tag{3.5}$$

where P is pressure, P_a is maximum pressure at a location of antinode which can be determine using Eq. (3.6), k is a wave number which can be determined by using Eq. (3.7), f is frequency, t is time, m' is mass flux, θ is phase difference between pressure and velocity, 1.75 radian, c is the speed of sound, 346m/s.

$$Drive\ ratio, DR = \frac{P_a}{P_m} \tag{3.6}$$

where P_m is the mean pressure, 100000Pa.

$$k = \frac{2\pi f}{c} \tag{3.7}$$

Wavelength, λ can be determined using Eq. (3.8):

$$\lambda = \frac{c}{f} \tag{3.8}$$

The tube banks were placed at the centre location of the model which is equal to a location of 0.17λ. This particular location is then offset to both end of the bank array. It leads to values of x_1 = 4190 mm and x_2 = 4790 mm from the pressure antinode location of a quarter wavelength resonator. Table 3.6 summarizes the boundary conditions for the oscillatory flow model.

Table 3.6: Boundary conditions for oscillatory flow model

Location	**Boundary condition**
Inlet	Pressure inlet, DR = 0..3% & 1.2%
Outlet	Mass flux inlet, DR = 0..3% & 1.2%
Lateral wall	Symmetry
Tube wall	Non-slip

The properties of fluid and tube walls for the oscillatory flow model are as shown in Table 3.7.

Table 3.7: Physical properties of materials used in oscillatory flow model

Material	**Properties**	**Values**
Air	Density (ρ_{air})	Ideal gas
	Specific heat (Cp_{air})	1006.43 J/kg·K
	Thermal conductivity (λ_{air})	Refer Eq. (3.9)
	Viscosity (μ_{air})	Refer Eq. (3.10)
	Prandtl number (Pr)	0.71289
	Inlet temperature (T_{air})	35 ºC
Tubes wall	Density (ρ_t)	2700 kg/m^3
	Heat capacity (Cp_t)	879 J/kg·K
	Thermal conductivity (λ_t)	229 W/m·K
	Tube temperature (T_t)	10 ºC

Mohd Saat and Jaworski (2017) stated that the use of symmetry conditions is inappropriate when heat transfer is involved due to the existence of temperature-driven buoyancy effect (free convection). Thermal conductivity of air for oscillatory flow was computed using piecewise-polynomial method with temperature and it is defined as in Eq. (3.9).

$$k = 0.023635 + 7.56264 \times 10^{-5}T - 2.51537 \times 10^{-8}T^2 + 4.18521 \times 10^{-12}T^3 + 1.05973 \times 10^{-15}T^4 - 1.12111 \times 10^{-18}T^5 - 5.47329 \times 10^{-22}T^6 - 9.94835 \times 10^{-26}T^7 \quad (3.9)$$

Viscosity of air for oscillatory flow is computed using power-law model where temperature is used as variable. The equation is as shown in Eq. (3.10).

$$\mu = 1.85 \times 10^{-5} (\frac{T}{T_0})^{0.76} \tag{3.10}$$

where T_0 is the reference temperature of 300K.

3.2.5.3 Heat transfer rate and pressure drop

Heat transfer rate for steady flow model can be determined using list of equations as follow:

$$h = \frac{\dot{Q}}{A_t \cdot LMTD} \tag{3.11}$$

$$LMTD = \frac{T_{air} - T_{out}}{\ln \frac{T_{air} - T_t}{T_{out} - T_t}} \tag{3.12}$$

$$Nu = \frac{hD}{\lambda_{air}} \tag{3.13}$$

$$\dot{Q} = \dot{H}_{out} - \dot{H}_{in} \tag{3.14}$$

The pressure drop of flow across the tube banks can be calculated as:

$$\Delta P = P_{in} - P_{out} \tag{3.15}$$

The Euler number is defined as:

$$Eu = \frac{\Delta P}{\rho_{air} U_{max}} \tag{3.16}$$

Heat transfer rate for oscillatory flow can be determined using equations below:

$$q' = \frac{q}{A} \tag{3.17}$$

$$q' = \int_0^T q'dt = \frac{\sum q'_{\Phi 1-\Phi 20}}{20} \tag{3.18}$$

3.2.6 Solving and visualization

Once everything was set up (including selection of suitable mesh grid after mesh test), the simulation was commenced. Fluid flow and heat transfer characteristics over the tube walls were determined by solving continuity, momentum and energy equations. Double precision floating point was activated for faster convergence. In general, pressure-based solver was selected for both steady and oscillatory flow models. Gravitational acceleration of -9.81m/s^2 was imposed at Y-axis to consider for the natural convection effect. In order to study the heat transfer characteristics, energy equations were solved. Viscous model was used in both simulation and the SST k-ω model with low-Re corrections and viscous heating settings was chosen. This is to obtain a more accurate turbulent depictions and more accurate thermal properties near the tube walls with large surface area. Coupled algorithm was selected for pressure-velocity coupling as it is stated to be more accurate than the other segregated algorithm (Fluent Inc, 2006). The gradient scheme chosen for thee spatial discretization method was the least squares cell based scheme. Pressure, density, momentum, turbulent kinetic energy, specific dissipation rate, and energy were solved with second order upwind scheme. First order implicit scheme was used for transient formulation of the transient flow.

For steady flow, the solutions converged within 200 iterations. While for oscillatory flow, the time step size was determined by taking the time period needed to complete one acoustic cycle (1/f) and then divided it by 1000 time steps following the method described by Mohd Saat and Jaworski (2017),. The solution converged within 12 iteration for every time step. According to Mohd Saat and Jaworski (2017), in order for the model to be as accurate as possible, at least seven cycles must be completed (7000 time steps) to achieve steady oscillatory flow condition before further analysis is done. The current model was therefore solved for at least 70000 iterations so that 7000 time steps condition is achieved.

After completing the simulation, validation of both flows were done. For steady flow, the result was validated with theoretical and experimental results done by Gharbi et al. (2015). The findings were also validated using equations as discussed before. For oscillatory flow, velocity profile for one acoustic cycle was collected through the transient model and then was investigated further. The findings were validated by using equations as discussed earlier.

For visualization of fluid flow characteristics, vector plot was produced to investigate the velocity magnitude and direction of flow over tube banks. Besides, vorticity contour was also produced to examine the turbulent intensity for each cases. After that, temperature, velocity, and pressure contours were also be included into the analysis to study the heat transfer characteristics of cross flows over tube banks. Heat transfer coefficient and heat flux was calculated and determined as mentioned earlier. Last but not least, discussion was made based on the obtained data and conclusion is drawn.

3.3 Grid test

Grid independence is one of the crucial part in numerical research. It plays an important role for reliability of the results. A bad grid can lead to significant impacts on the solutions and therefore mesh sensitivity study must be conducted. Mesh sensitivity study consists of refining elements and comparing the refined solutions to the coarse solutions. If further refinement (or other changes) does not significantly change the solution, then the mesh is considered as suitable as it will not give impact on the solution. The mesh is refined by using various techniques, such as increasing number of division at critical region, refining the surface, inflate the required edge, etc. A total of 8 studies on mesh independence were conducted for steady flow. The number of studies needed for oscillatory flow was justified based on the findings.

3.3.1 Mesh quality

The mesh quality of a grid is determined by aspect ratio, orthogonal quality, and orthogonal skewness. Mesh quality of each studies were tabulated in Table 3.8.

Table 3.8: Mesh quality of grid

Study no.	**Number of element**	**Aspect ratio**	**Minimum orthogonal quality (0 to 1, where values close to 0 correspond to low quality)**	**Orthogonal Skewness ((0 to 1, where values close to 1 correspond to low quality)**
1	531	1.934	0.707	0.639
2	1181	1.930	0.748	0.520
3	4713	2.018	0.692	0.543
4	10600	2.097	0.716	0.536
5	14841	2.009	0.686	0.572
6	19170	2.044	0.719	0.553
7	49675	73.0	0.031	0.995
8	86892	60.4	0.037	0.989

3.3.2 Grid independency test

3.3.2.1 Grid test for steady flow model

Mesh test for steady flow model was carried out by using first simulation case of steady flow in which the velocity of air at the inlet location was set to 1.711m/s (corresponds to Re = 5000). Data was obtained by using area-weighted average surface integrals. Study no. 1 to no. 6 represent the evolution of mesh while study no. 7 and no. 8 are extreme cases used to test the grid. The values of temperature, pressure, and velocity as tabulated in Table 3.9 were also plotted in graphs as can be seen in Figures 3.7 and 3.8.

Table 3.9: Grid test for steady flow

Study no.	**Number of element**	**Temperature at outlet (K)**	**Dynamic pressure at outlet (Pa)**	**Velocity at outlet (m/s)**
1	531	305.31	1.722	1.726
2	1181	304.51	1.700	1.719
3	4713	303.81	1.683	1.713
4	10600	303.40	1.682	1.713
5	14841	303.30	1.682	1.713
6	19170	303.30	1.680	1.712
7	49675	303.8	1.679	1.711
8	86892	303.93	1.679	1.711

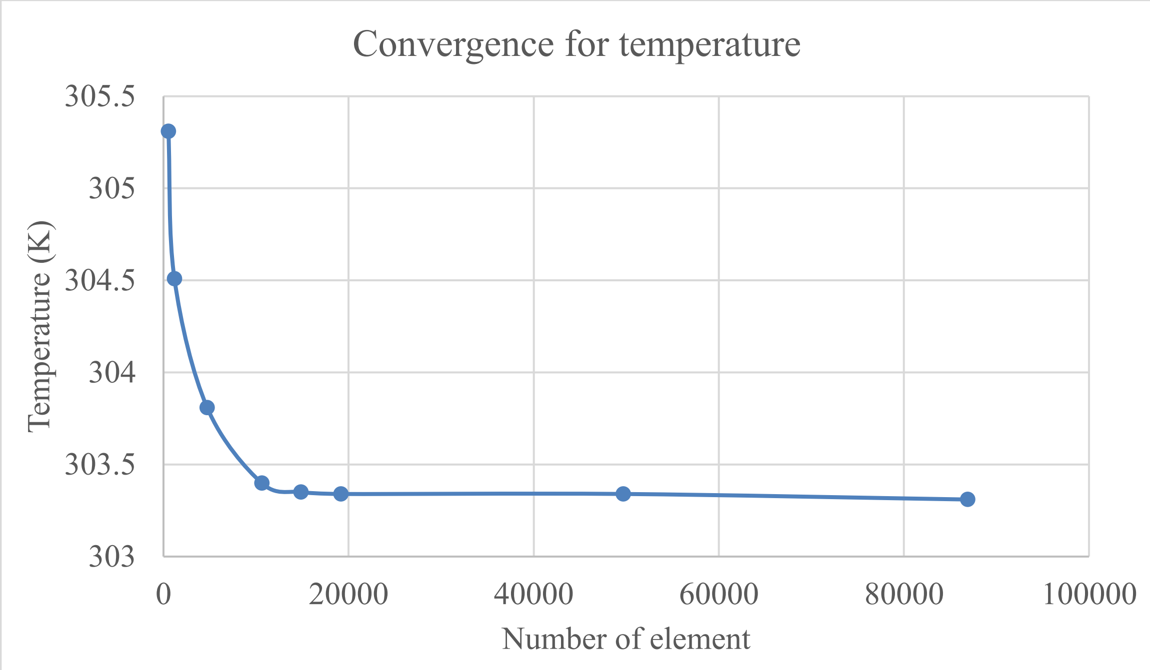

Figure 3.7: Graph of convergence for temperature

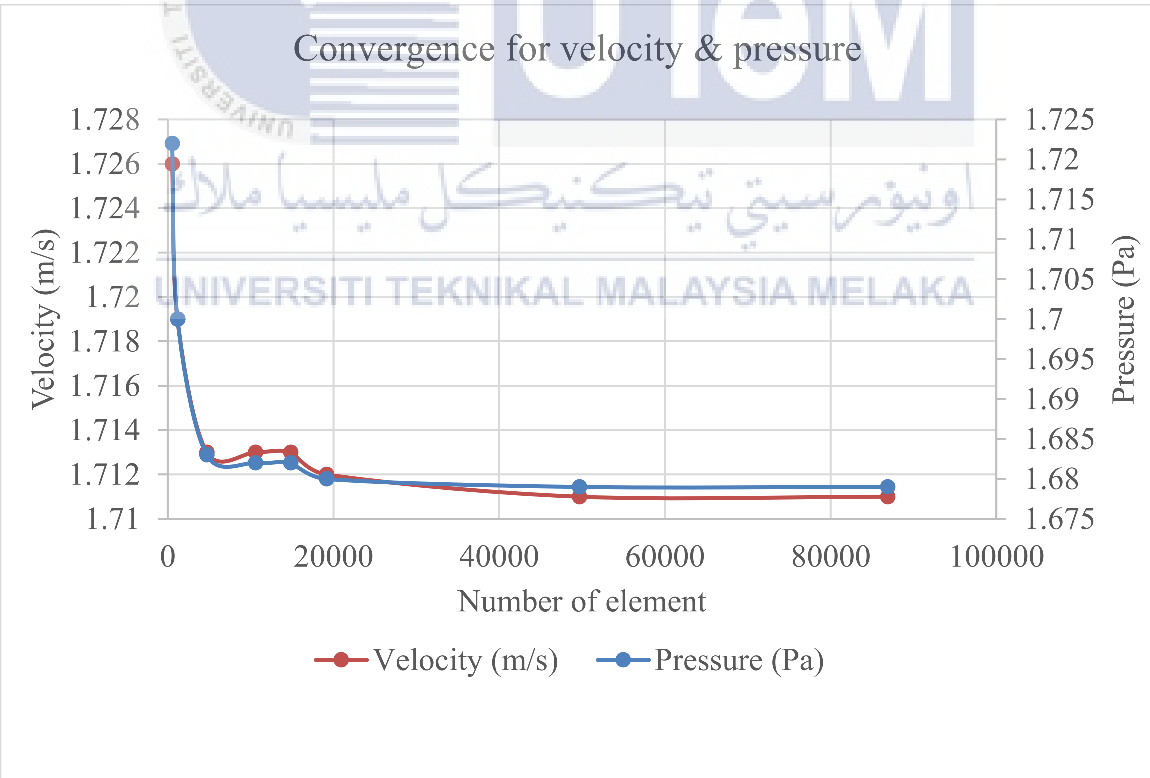

Figure 3.8: Graph of convergence for velocity and pressure

At low number of element (<10000), all temperatures, velocities, pressures were over-predicted, however, all these variables converged with little fluctuation when number of element was above 12000. Therefore it was concluded that this grid was independent of solution when number of element was more than 12000. Case no. 6 with number of element of 19170 was chosen for the simulation model and was set as the benchmark for oscillatory flow's grid test.

3.3.2.2 Grid test for oscillatory flow model

Mesh test was carried out by using the same meshes as defined in Section 3.3.2.1. The drive ratio of 1.2% was used to run the test for the grid independency of the oscillatory flow model. Figures 3.9 and 3.10 show the change of velocity and pressure amplitudes with time for all tested grid sizes for one acoustic cycle.

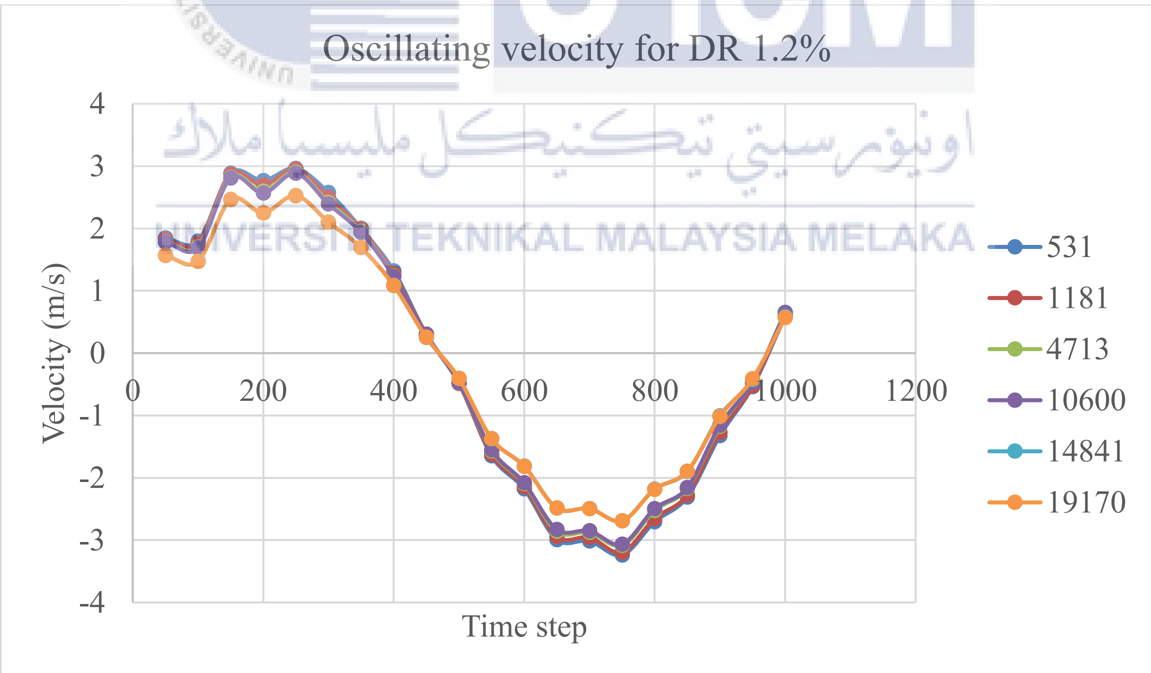

Figure 3.9: Graph of oscillating velocity for DR 1.2%

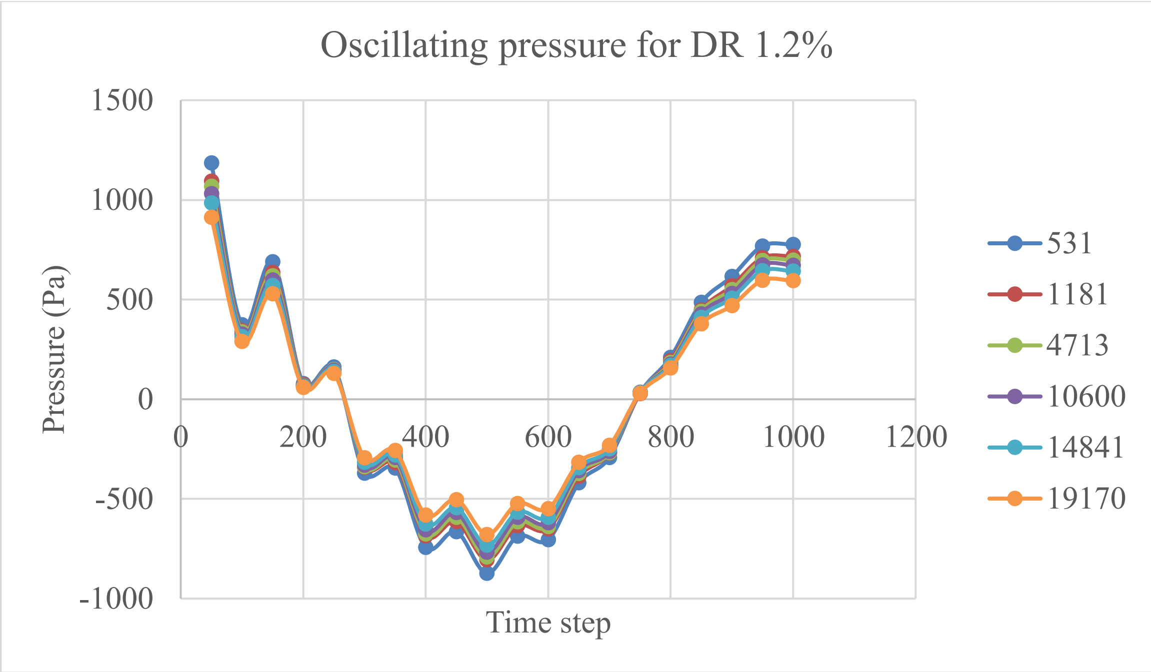

Figure 3.10: Graph of oscillating pressure for DR 1.2%

Based on the data obtained, it was obvious that the previous conjecture's correct. At low number of element, the variables fluctuated at a larger amplitude. However for higher number of element, the fluctuation was rather small and consistent. Verdict's made that the grid was independent if its number of element was higher than 12000.

3.3.3 Grid selection

In order to select the right grid for the simulation, aspect ratio, minimum orthogonal quality, and maximum orthogonal skewness were examined. First of all, in the most ideal situation, the aspect ratio should be equal to 1 or close to 1. This is because a large aspect ratio can jeopardize the calculation and produce unacceptably huge error. The acceptable range of aspect ratio for 2D mesh grid should be less than 5. Next, minimum orthogonal quality is also another measure of mesh quality, the closer it is to 1, the better the solution will become. The acceptable range of orthogonal quality is 0.7. Last but not least, orthogonal skewness is defined as the difference between the shape of the cell and its equivalent cell with the same volume. The closer it is to 0, the lower the skewness of the cell as the higher the accuracy and the solution is more stable. The acceptable range of orthogonal skewness is 0.5.

In conclusion, after reviewing all the criteria, mesh grid with number of element of 19170 is selected for this simulation.

CHAPTER 4

RESULT AND DISCUSSION

4.1 Validation of result

Validation of results is exceptionally crucial in a research. It is a necessity for every researcher in order to ensure that the result is legit, correct, and useful. Validation can be done by reviewing previous work, journals, publication, etc.

4.1.1 Validation of steady flow's result

Figure 4.1 shows comparison of results between published works and the current work. The comparison was made based on the change of Nusselt number as a function of Reynolds number.

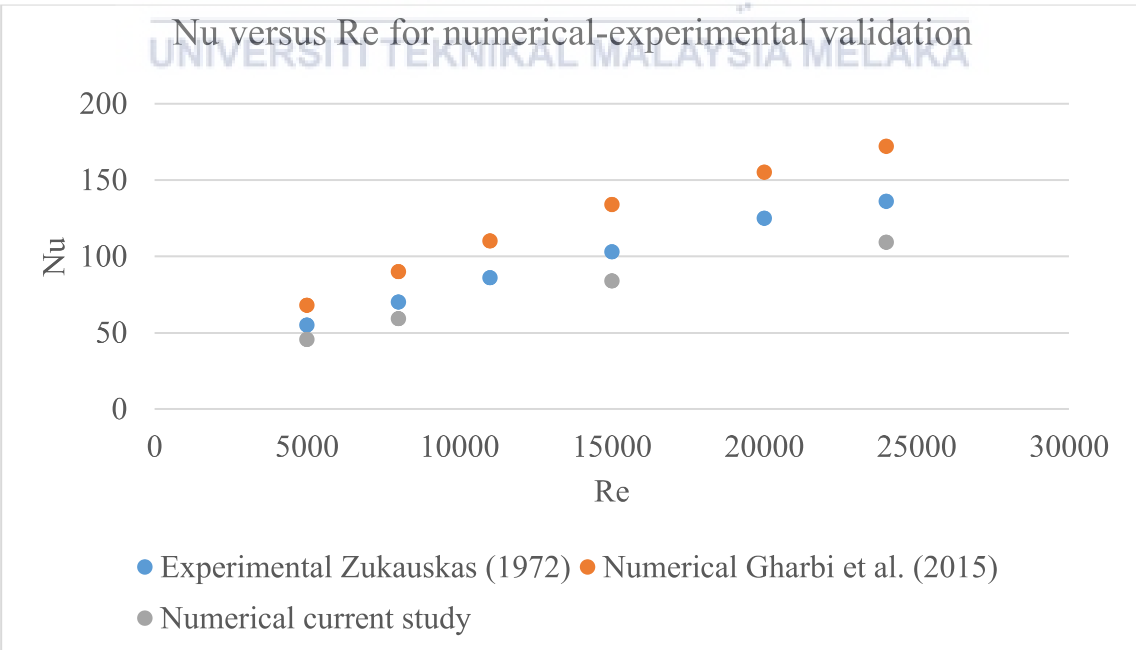

Figure 4.1: Nu versus Re for numerical-experimental validation

The findings of the simulation for steady flow were compared with experimental results of Zukauskas (1972), and numerical results of Gharbi et al. (2015). The results have shown sufficient consistency with the compared results and manifested the same trend as predicted. However, it deviated slightly when Re increased from 10000 and above. This is because the density of medium (1.987kg/m^3) that Gharbi et al. (2015) used for their simulation was a lot higher than that of standard air (1.1.459 kg/m^3) at 35^{o}C compared to that's been used in current simulation. Convection is a heat transfer mode caused by bulk motion of fluid. Therefore the denser the fluid is, the more heat can be transferred via convection. And since Nusselt number is the ratio of convective to conductive heat transfer therefore it is logical for the published Nu to be higher than the current study.

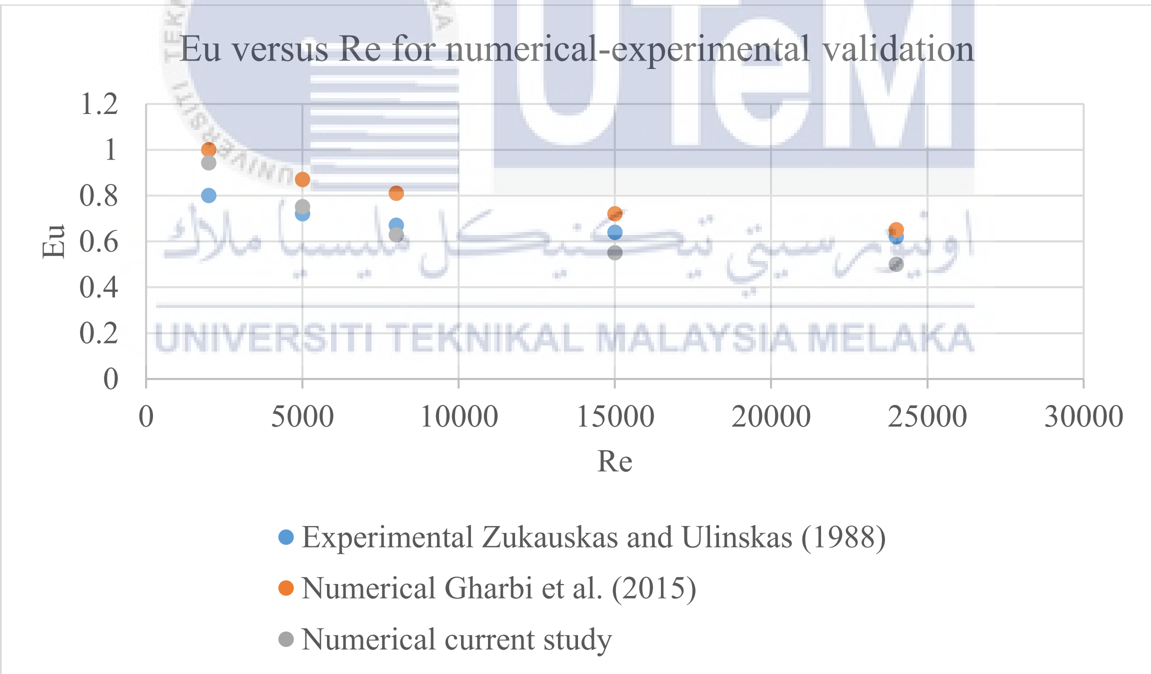

Figure 4.2: Eu versus Re for numerical-experimental validation

Based on Figure 4.2, it can be seen that the results from current study was in good agreement with the previous works done by others. As Re increases, Eu decreases. It was also noticeable that Eu is in a reciprocal relationship with Nu. This is based on the observation made when examining both Figure 4.1 and 4.2, as Re increases, Nu increases while Eu decreases. Thus we can relate both of them in an expression shown in Eq. (4.1) below:

$$Eu \propto \frac{1}{Nu} \tag{4.1}$$

4.1.2 Validation of oscillatory flow's result

The validation of oscillatory flows' results was done by comparing the theoretical predictions of linear thermoacoustic theory with the results obtained from the current CFD models. If the results are valid, the pressure and velocity should follow what was predicted by linear model. In order to do that, a point was set up at x = 150 mm from the inlet of the tube bank. The inlet (pressure) and outlet (velocity) conditions were calculated using Eq. (3.4) and (3.5) with location of x with respect to the location of pressure antinode. If the simulation results matched the pressure and velocity for all phases, then the results are conclusive for oscillatory flow. Figures 4.3 and 4.4 show the comparison between theory and CFD for oscillating pressure and oscillating velocity when the fluid flows with drive ratio of 0.3%. The results of higher drive ratio of 1.2% are as shown in Figures 4.5 and 4.6.

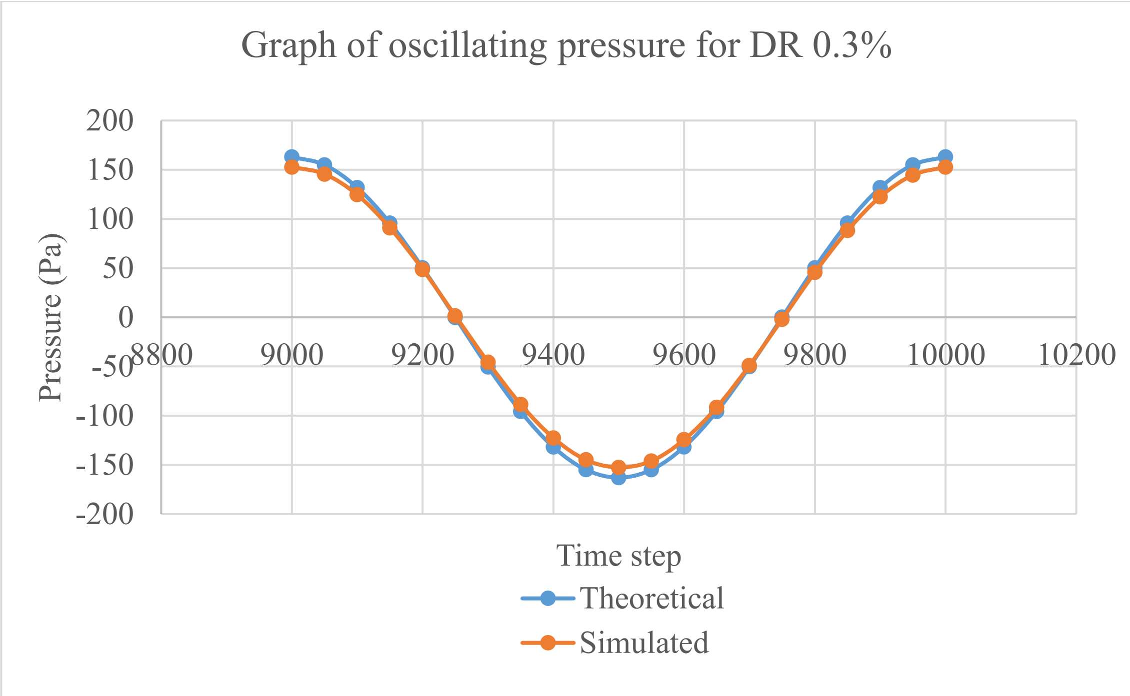

Figure 4.3: Comparison between theoretical and simulation oscillating pressure for DR 0.3%

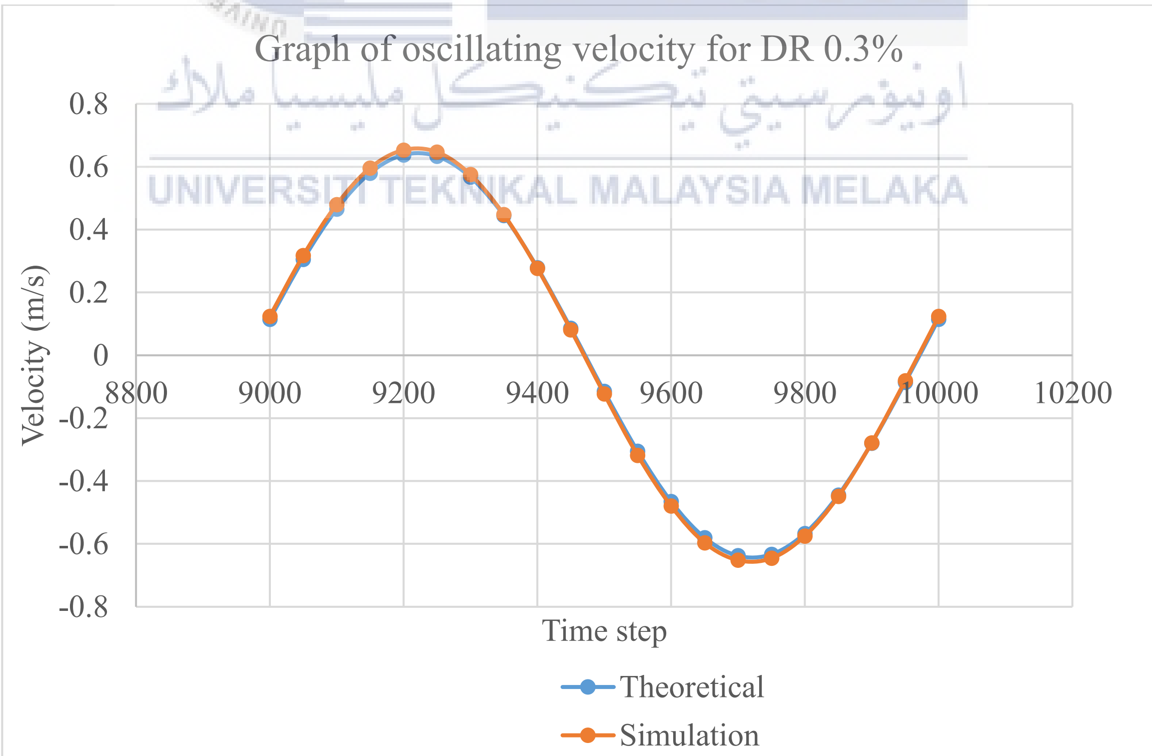

Figure 4.4: Comparison between theoretical and simulation oscillating velocity for DR 0.3%

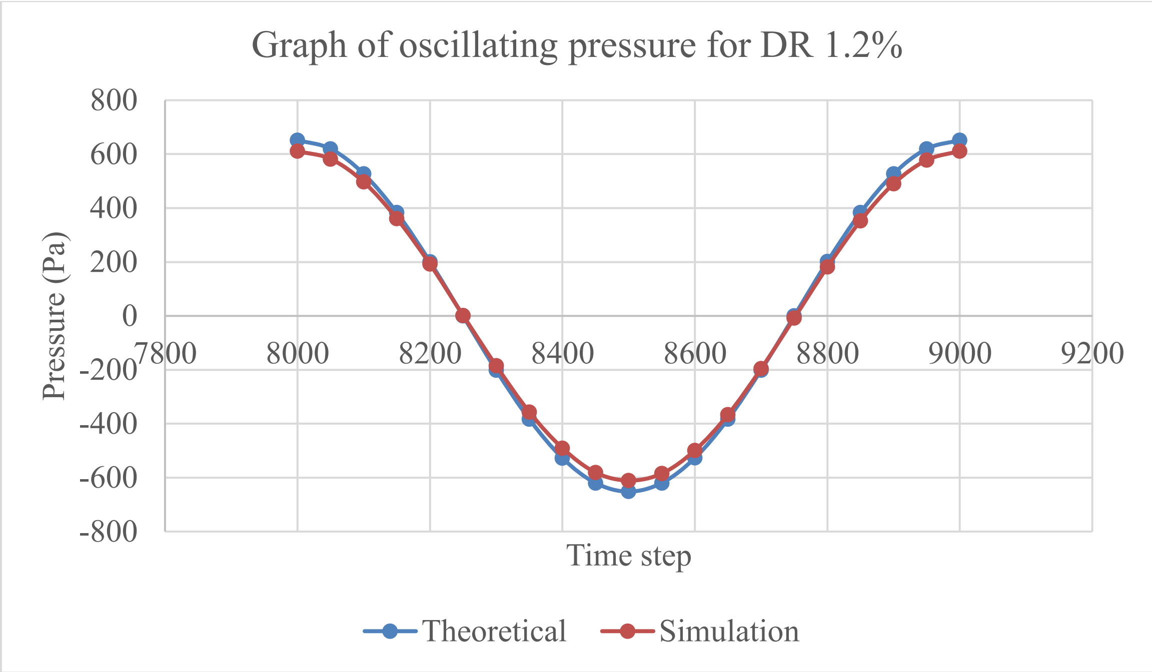

Figure 4.5: Comparison between theoretical and simulation oscillating pressure for DR 1.2%

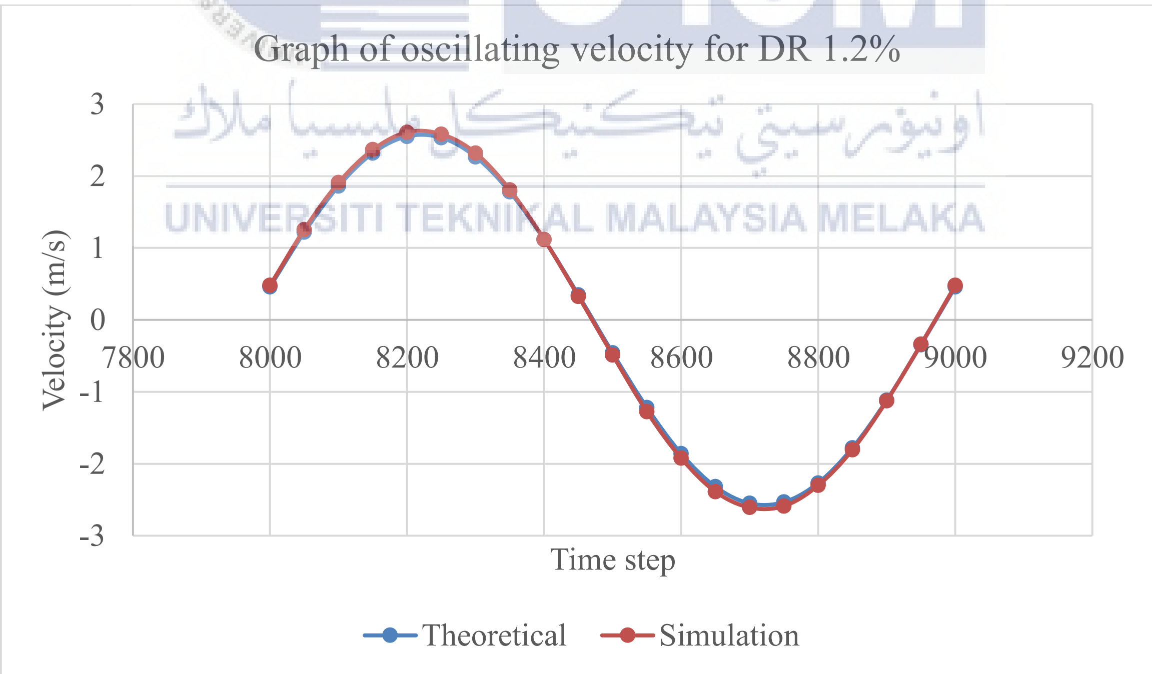

Figure 4.6: Comparison between theoretical and simulation oscillating velocity for DR 1.2%

Based on the observation on all Figure 4.3 to Figure 4.6, it was obvious that the simulation model was fairly accurate and stable since it didn't deviate from the linear thermoacoustic theoretical data. Results for both steady and oscillatory flows were therefore validated and the models were used for further analysis.

4.2 Fluid flow characteristics – vector & vorticity

4.2.1 Steady flow – vector & vorticity

Table 4.1 and 4.2 show the vector plot and vorticity contour respectively for steady flow model with Reynolds number that varies from 2000 to 24000.

Table 4.1: Vector plot for steady flow model

Re	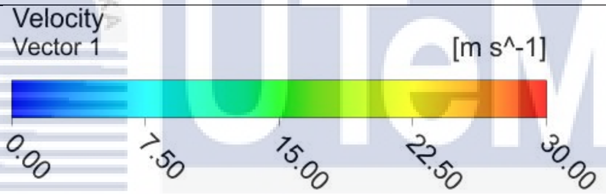
2000	
5000	
8000	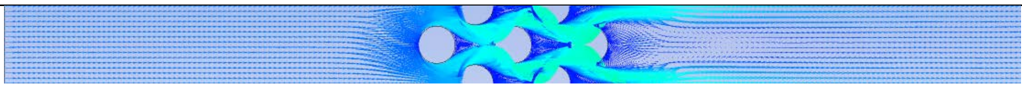
15000	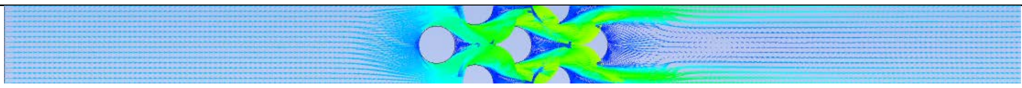
24000	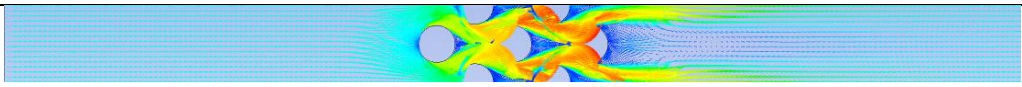

Table 4.2: Vorticity contour for steady flow model

Re	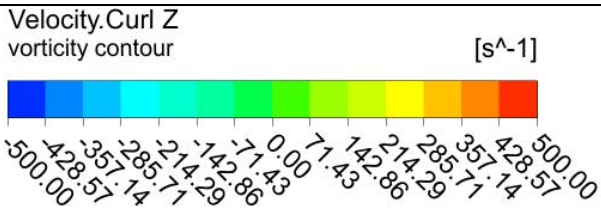
2000	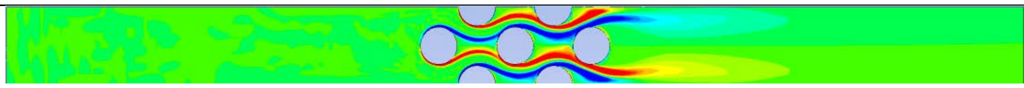
5000	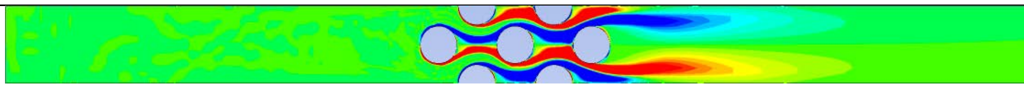
8000	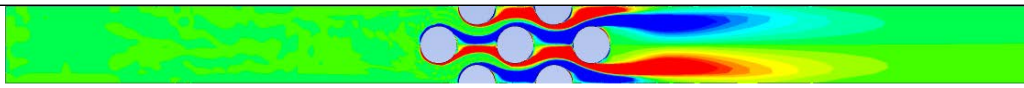
15000	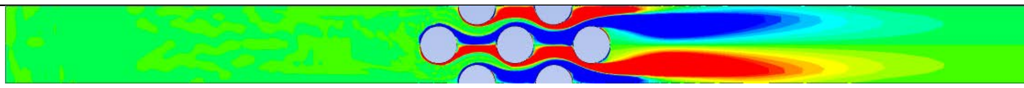
24000	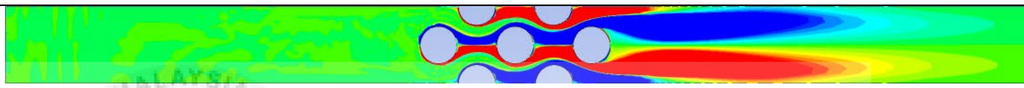

Based on Table 4.1 and Table 4.2, as expected, the flows came to a stop when they hit the tubes and started developing boundary layer due to no-slip condition. For Re = 2000, the flow is categorized as laminar flow in which the flow is flowing in smooth and highly ordered motion. The thickness of boundary layer is relatively thinner and the vorticity which is a measure of rotationality of fluid is significantly less than the other cases. The separated flows due to the tube geometry reattached rather quickly. At high Re (Re = 24000), the flow is turbulent and highly disordered. The fluctuation of velocity is significantly higher than in low Re cases. The wake region is also larger than the others based on the vorticity contour because wake region is a region consists of recirculating flows that have high vorticity. The vortex elongates to further distances as Reynolds number increases but never detached from the tube.

4.2.2 Oscillatory flow – vector & vorticity

Oscillatory flow is a condition of flow where fluid flows back and forth across the tube banks in a cyclic manner. For this research, the analysis of oscillatory flow conditions were made based on the cyclic behavior of flow. This was done by extracting the data for several instantaneous points across one cycle of flow. Figures 4.7 and 4.8 show the instantaneous points labelled as Φ1 to Φ20 for one flow cycle with drive ratio of 0.3% and 1.2% respectively.

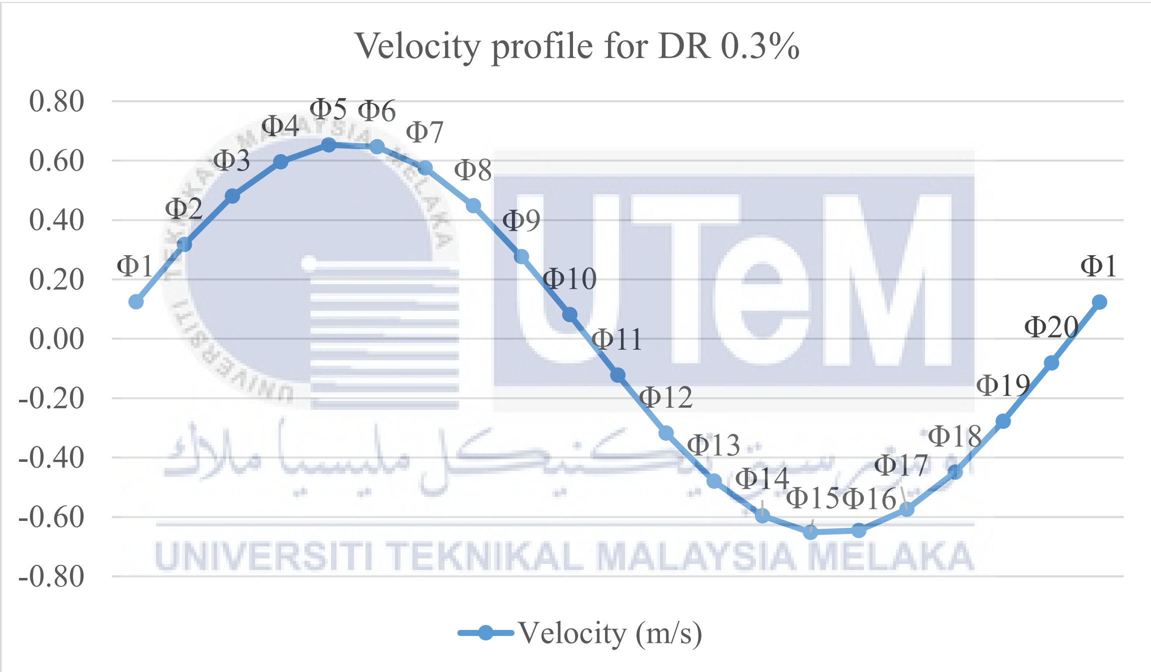

Figure 4.7: Velocity profile for DR 0.3%

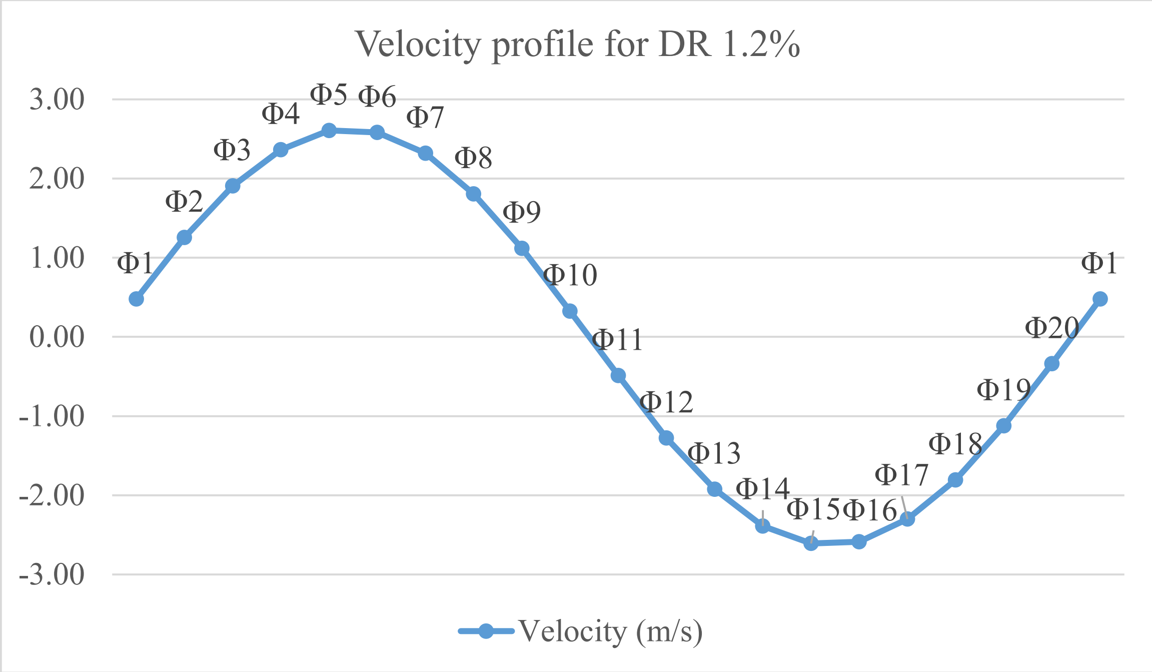

Figure 4.8: Velocity profile for DR 1.2%

In general, the instantaneous points in Figure 4.7 and 4.8 represent the condition of flow forcing forward (Φ1 – Φ10) and then flow reverses (Φ11 – Φ20). The vector plots for all the instantaneous points are as shown in Table 4.3. The results were shown for the flow amplitude with drive ratio of 0.3% (left) and the drive ratio of 1.2% (right). At drive ratio of 0.3%, the maximum velocity is 9 m/s while for drive ratio of 1.2%, the maximum velocity is 25 m/s.

Table 4.3: Vector plot for oscillatory flow model

DR 0.3%		**DR 1.2%**
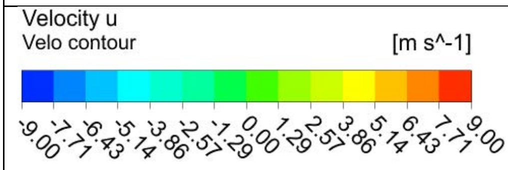		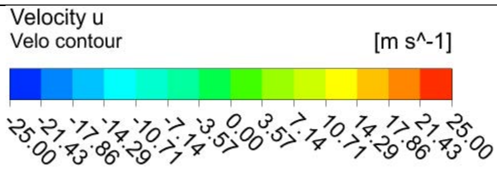
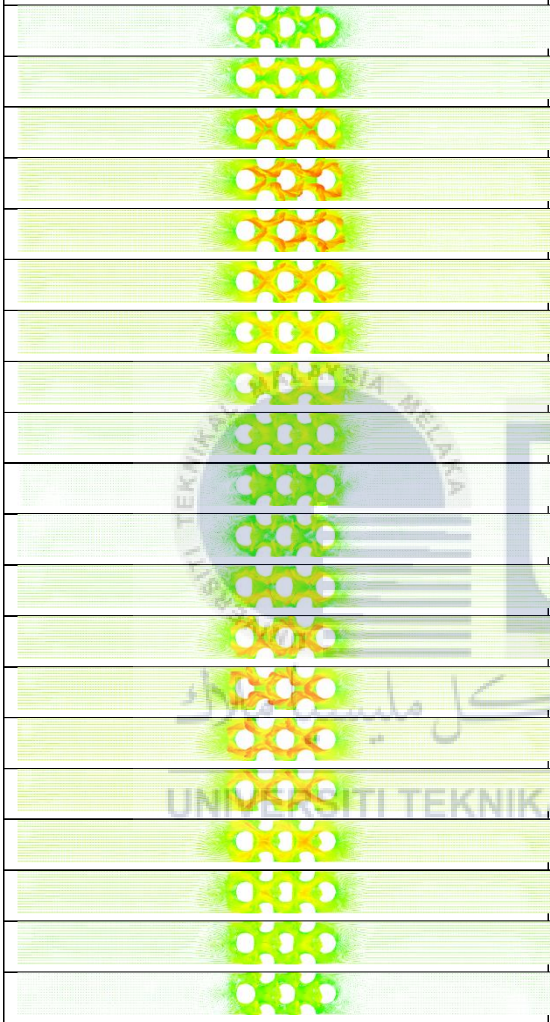	Φ1	
	Φ2	
	Φ3	
	Φ4	
	Φ5	
	Φ6	
	Φ7	
	Φ8	
	Φ9	
	Φ10	
	Φ11	
	Φ12	
	Φ13	
	Φ14	
	Φ15	
	Φ16	
	Φ17	
	Φ18	
	Φ19	
	Φ20	

Table 4.4 shows the evolution of vortex structures as fluid flows back and forth for twenty instantaneous points over one flow cycle. The contours on the left are the results for the drive ratio of 0.3% while the contours on the right are for the drive ratio of 1.2%.

Table 4.4: Vorticity contour for oscillatory flow model

<table>
<tr><th>DR 0.3%</th><th></th><th>DR 1.2%</th></tr>
<tr><td colspan="3">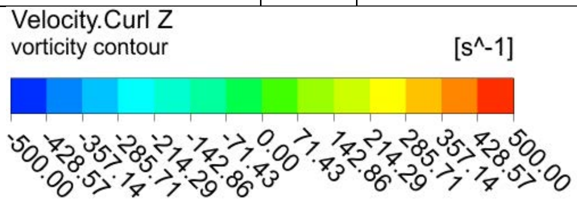
</td></tr>
<tr><td rowspan="20">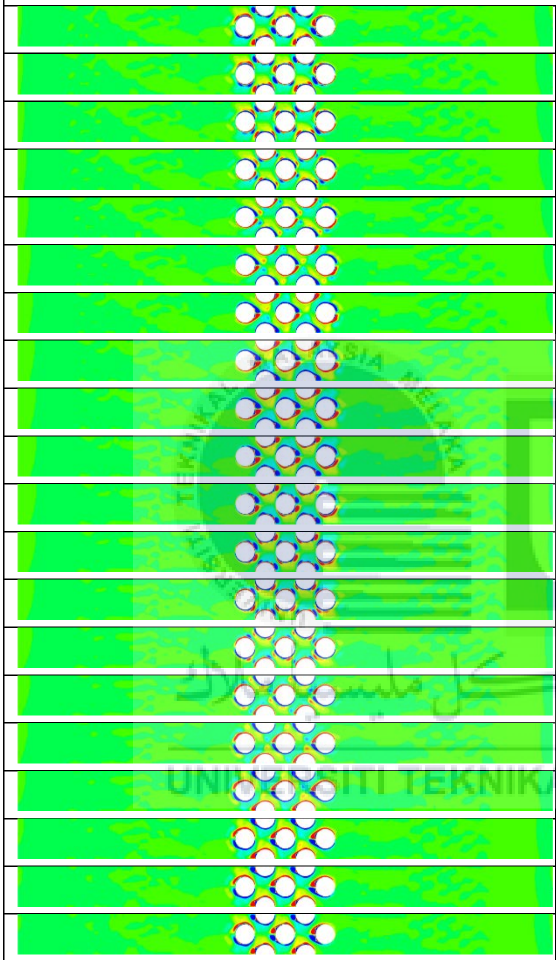</td><td>Φ1</td><td rowspan="20">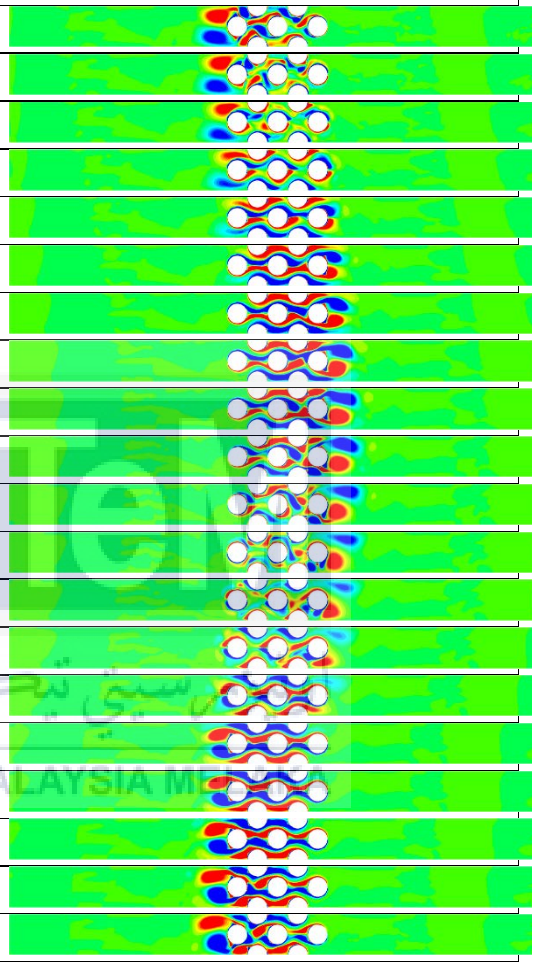</td></tr>
<tr><td>Φ2</td></tr>
<tr><td>Φ3</td></tr>
<tr><td>Φ4</td></tr>
<tr><td>Φ5</td></tr>
<tr><td>Φ6</td></tr>
<tr><td>Φ7</td></tr>
<tr><td>Φ8</td></tr>
<tr><td>Φ9</td></tr>
<tr><td>Φ10</td></tr>
<tr><td>Φ11</td></tr>
<tr><td>Φ12</td></tr>
<tr><td>Φ13</td></tr>
<tr><td>Φ14</td></tr>
<tr><td>Φ15</td></tr>
<tr><td>Φ16</td></tr>
<tr><td>Φ17</td></tr>
<tr><td>Φ18</td></tr>
<tr><td>Φ19</td></tr>
<tr><td>Φ20</td></tr>
</table>

Vorticity is the measure of rotationality (quality of rotation) of the fluid. It is twice the value of angular velocity. It is apparent that the flow in DR 0.3% is in laminar region as there are little more than zero formation of vortex. As for DR 1.2%, there are huge formation of turbulences behind the tube as the flow passed by, especially at Φ1 and Φ11 where the flow direction is about to change. Otherwise, the flows behaved like what were discussed back at steady flow section. The elongation of the vortex at the end of tube banks is shorter compared to that of the steady flow presumably due to the effect of frequency where fluid is forced into different direction as instantaneous point Φ1 and Φ11 are reached.

4.3 Temperature, velocity, and pressure contours

4.3.1 Contour plots for steady flow model

Table 4.5 shows the temperature contour of the fluid for steady flow model.

Table 4.5: Temperature contour for steady flow model

Re	
	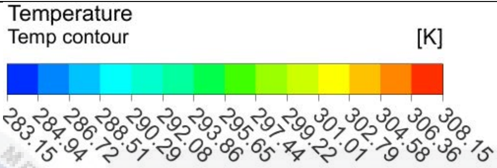
2000	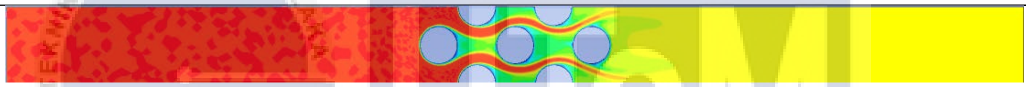
5000	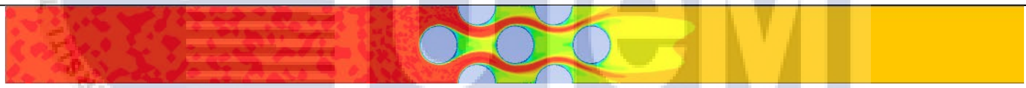
8000	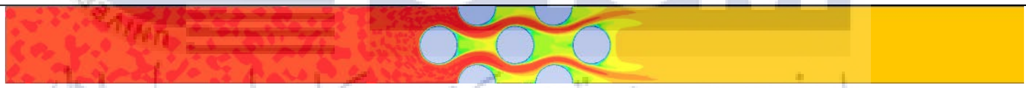
15000	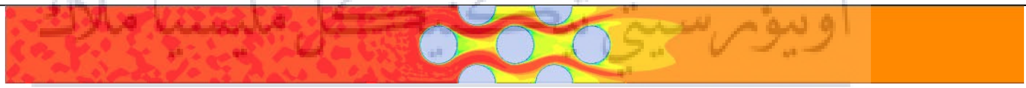
24000	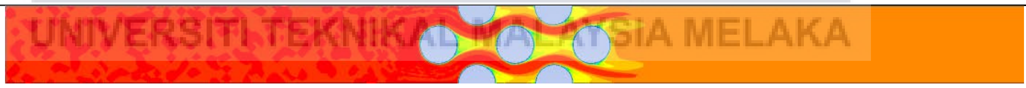

As expected, heat transfer performance was better for flow with high Reynolds number compared to the one with low Reynolds number. This is because the outlet temperature for flow with Re = 24000 is much higher than the flow with less Re. Convective heat transfer mainly relies on the fluid's bulk movement. Therefore, the more turbulences there are in a flow, the more heat can be transferred. However, the risk of vortex shedding and possible structural damage to the tube banks will also increase at high Re. Therefore, an appropriate range of Re for fluids must be determined when designing a heat exchanger.

Table 4.6 shows the velocity contour of the fluid for steady flow model.

Table 4.6: Velocity contour for steady flow model

Re	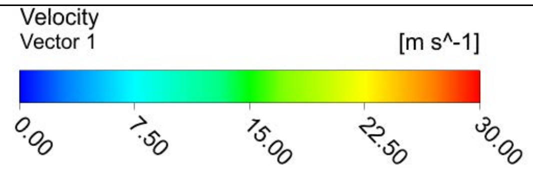
2000	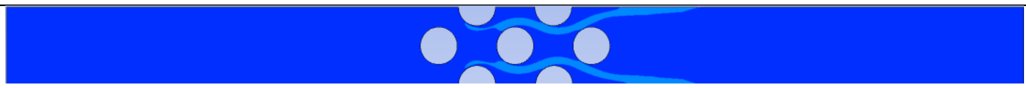
5000	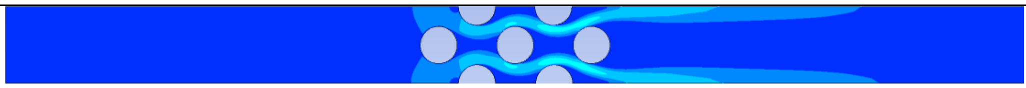
8000	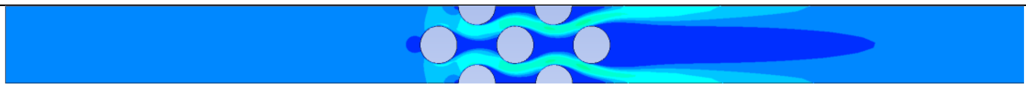
15000	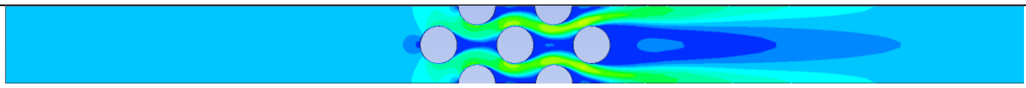
24000	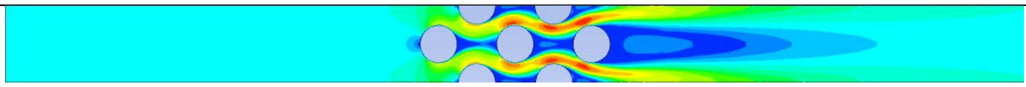

Velocity contour of steady flow matched the discussion made in Section 4.2.1. The flow with high Re came to a sudden stop at the wall, then flowed cross the wall, and separated heavily, leaving a big wake region at downstream. There's no wake region for low Re. From here, we can say that heat transfer performance is directly proportional to Re. The higher the Re, the better the heat transfer performance as discussed in Table 4.5.

Table 4.7 shows the pressure contour of the fluid for steady flow model.

Table 4.7: Pressure contour for steady flow model

Re	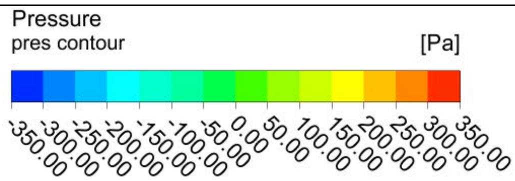
2000	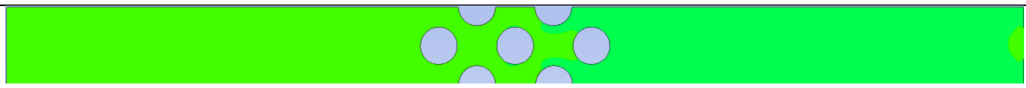
5000	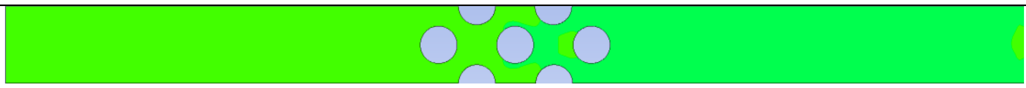
8000	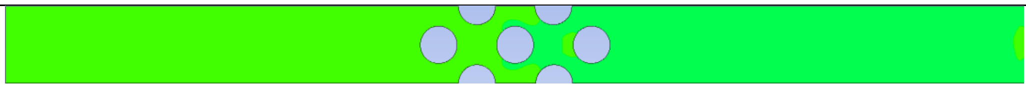
15000	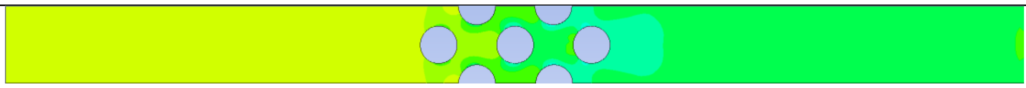
24000	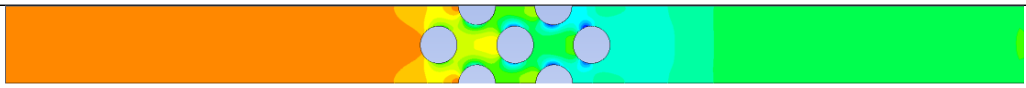

The point of contact between the fluid and the wall yielded the highest pressure. As fluid passed by, depending on the Re, the wake region yields the lowest pressure. This scenario satisfied the Bernoulli's principle where a drop in speed of fluid occurs simultaneously with an increase in pressure. It is clear that at higher Re, the pressure drop is much larger than those in lower Re. High pressure drop means that there is a huge difference between inlet pressure and outlet pressure. This can be achieved for high turbulent flow. As discussed before, turbulent flow comes with the formation of low-pressure wake at downstream of tubes. The more turbulent a flow is, the higher the chance of formation of wake and the size of it. Although turbulent flow is desired in heat transfer application, the operational cost (fan, pump, etc.) must be taken into account as high pressure drop implies that more power is needed to push the fluid forward (and to achieve turbulent flow with high velocity in the first place as well).

4.3.2 Contour plots for oscillatory flow model

Table 4.8 shows the evolution of temperature contour as the fluid flows in oscillatory manner across the tube banks. The left column represents the drive ratio of 0.3% while the right column represents the drive ratio of 1.2%.

Table 4.8: Temperature contour for oscillatory flow model

DR 0.3%		DR 1.2%
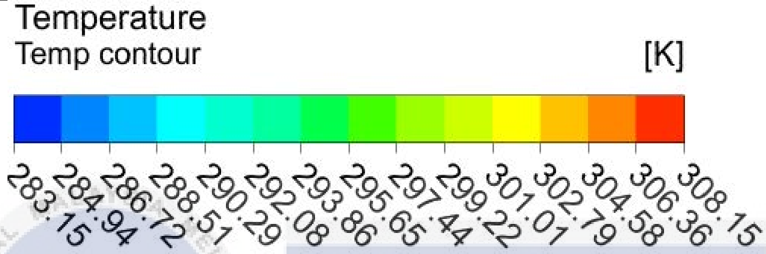		
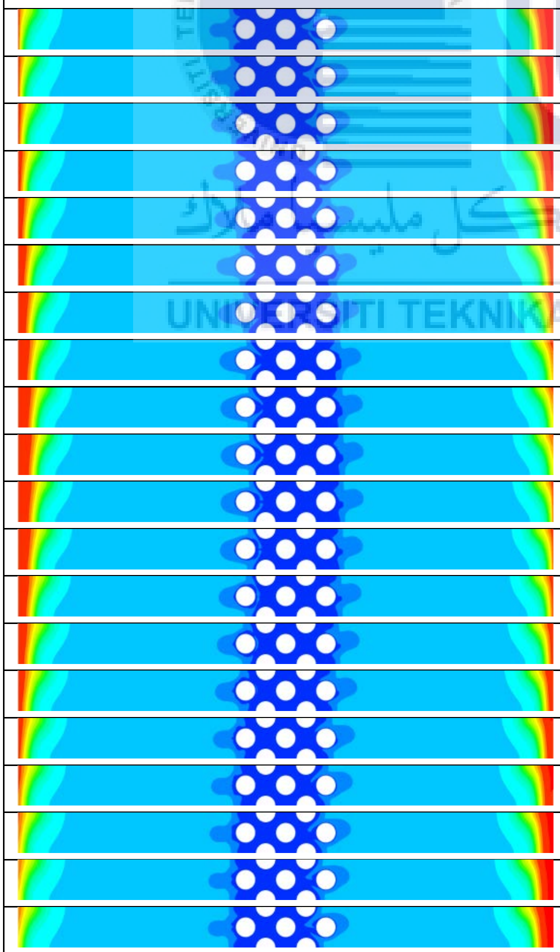	Φ1	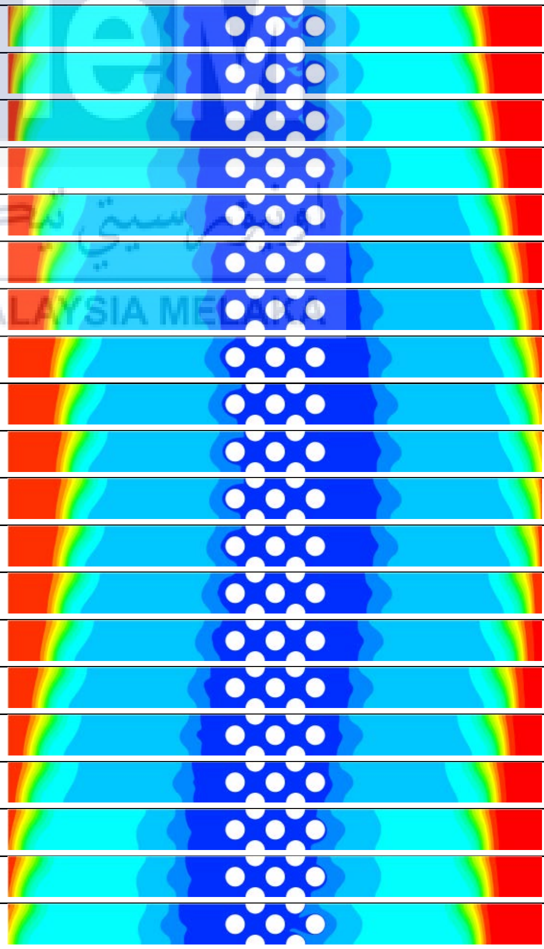
	Φ2	
	Φ3	
	Φ4	
	Φ5	
	Φ6	
	Φ7	
	Φ8	
	Φ9	
	Φ10	
	Φ11	
	Φ12	
	Φ13	
	Φ14	
	Φ15	
	Φ16	
	Φ17	
	Φ18	
	Φ19	
	Φ20	

As expected, the area of dark blue region (low temperature) around the tube banks were higher as drive ratio increased. This meant that more heat was able to be transferred at higher drive ratio (thus higher Re). Table 4.9 shows the velocity contour for the twenty instantaneous points across one flow cycle for both the drive ratios of 0.3% (left column) and 1.2% (right column). The maximum velocity was observed to happen at Φ5 and Φ6 within the region of the tube banks.

Table 4.9: Velocity contour for oscillatory flow model

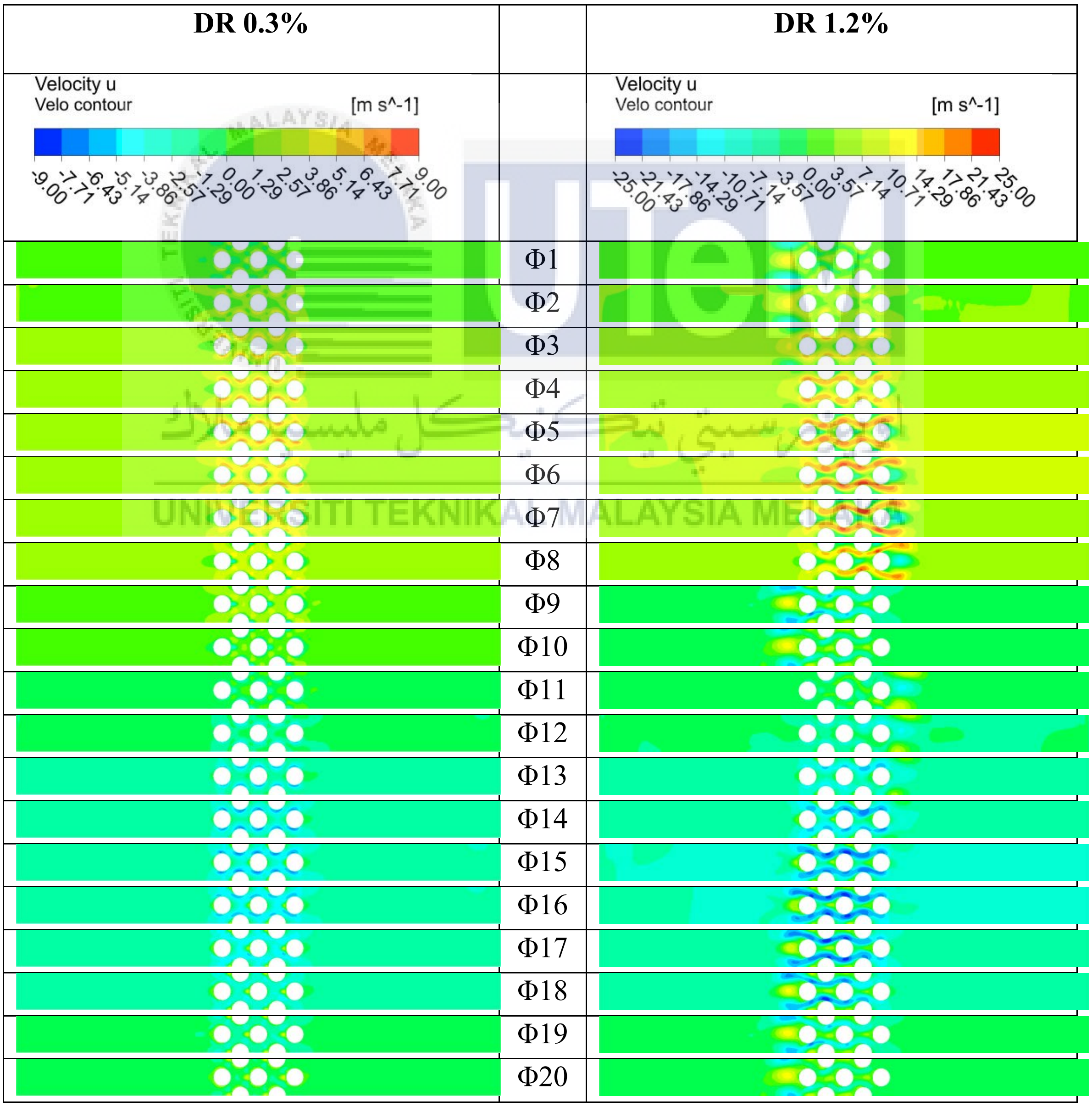

In general, DR 1.2% had higher velocity and velocity fluctuation compared to DR 0.3%. It suggested that DR 1.2% is more turbulent and has higher heat transfer rate than DR 0.3%. Table 4.10 shows the pressure contour of the fluid within the computational domain of the oscillatory flow models. The pressure amplitude is higher for drive ratio of 1.2%. For both drive ratios, the pressure amplitude is highest at Φ1 and Φ20 when the velocity is the smallest. This is consistent with Bernoulli's principle.

Table 4.10: Pressure contour for oscillatory flow

DR 0.3%		**DR 1.2%**
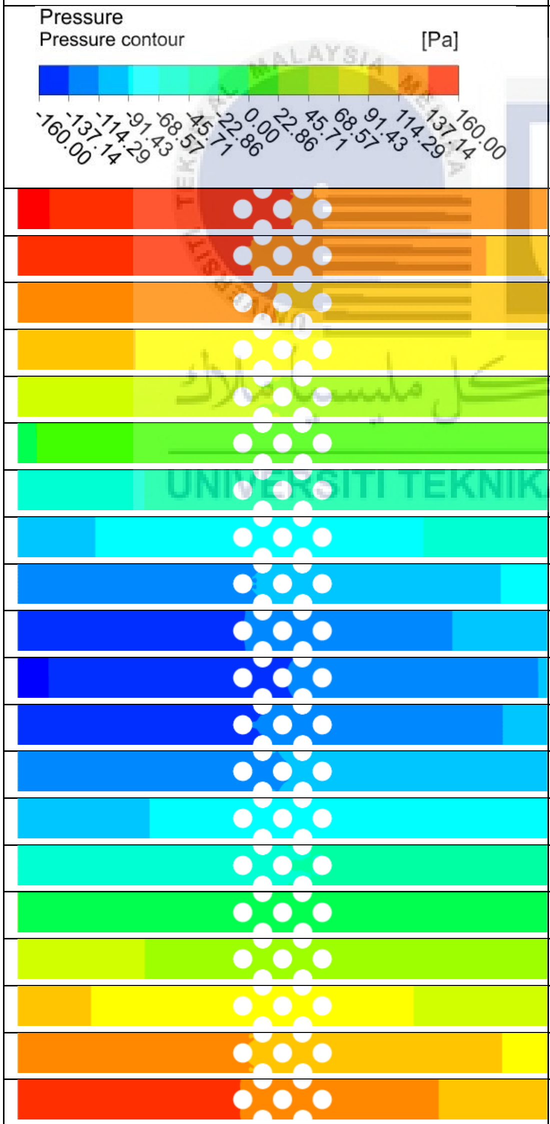		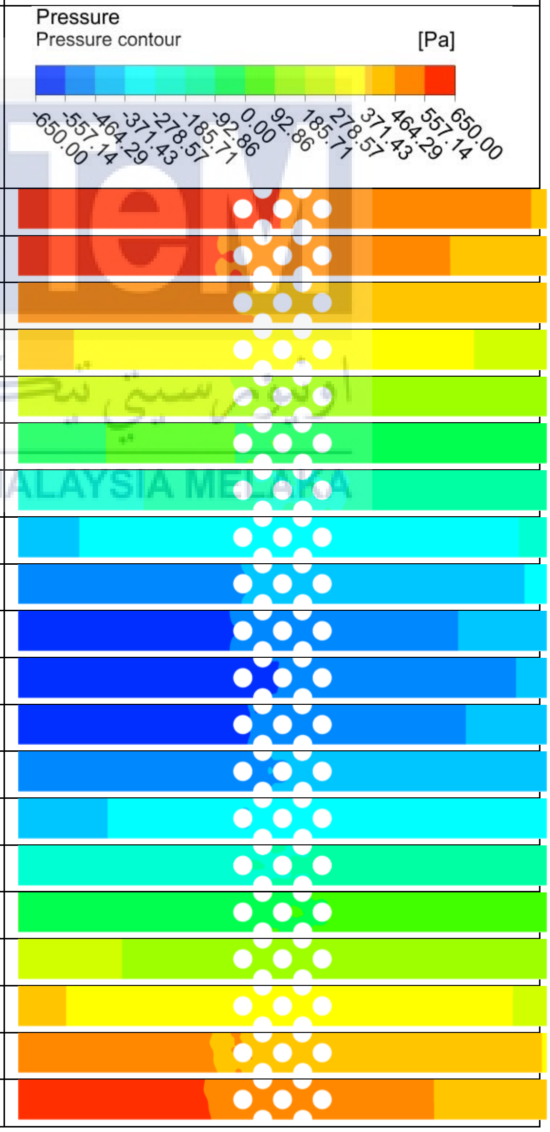
	Φ1	
	Φ2	
	Φ3	
	Φ4	
	Φ5	
	Φ6	
	Φ7	
	Φ8	
	Φ9	
	Φ10	
	Φ11	
	Φ12	
	Φ13	
	Φ14	
	Φ15	
	Φ16	
	Φ17	
	Φ18	
	Φ19	
	Φ20	

Both contours displayed similar pattern of pressure distribution yet non-identical pressure values as denoted by their respective drive ratios. The pressure distribution was based on the oscillating nature of the flow model. The interaction between the flows and the tube banks were exactly the same as explained in Section 4.3.1, under Table 4.7. From Table 4.10, we can say that the higher the pressure drop, the better the heat transfer performance.

4.4 Heat transfer coefficient

Table 4.11 shows the measure of heat transfer coefficient which is Nusselt number for steady flow model while Table 4.12 shows the Nusselt number for oscillatory flow model. Nusselt number for both models were obtained by using Eq. (3.11) to Eq. (3.14). The total heat transfer rates for inlet and outlet were obtained via the built-in function of Ansys Fluent 16.0 (Reports – Fluxes – Total Heat Transfer Rate). Since there is no documented record on how to represent the heat transfer rate for oscillatory flow especially for flow over tube banks, peak value was selected to represent the overall heat transfer performance for oscillatory flow over tube banks. The area-weighted average outlet temperatures were obtained for steady flow model. And again, since there is no predecessor on the study, the minimum temperature was chosen from all twenty phases of both oscillatory flow models. Thermal conductivity of air is fixed for both models in this computation which is 0.02671 W/m·K.

Table 4.11: Nusselt number for steady flow model

Reynolds number, Re	**Nusselt number, Nu**
2000	24.7
8000	59.1

Table 4.12: Nusselt number for oscillatory flow model

Drive ratio (%)	**Nusselt number, Nu**
0.3 (Re ≈ 2000)	7.8
1.2 (Re ≈ 8000)	20.7

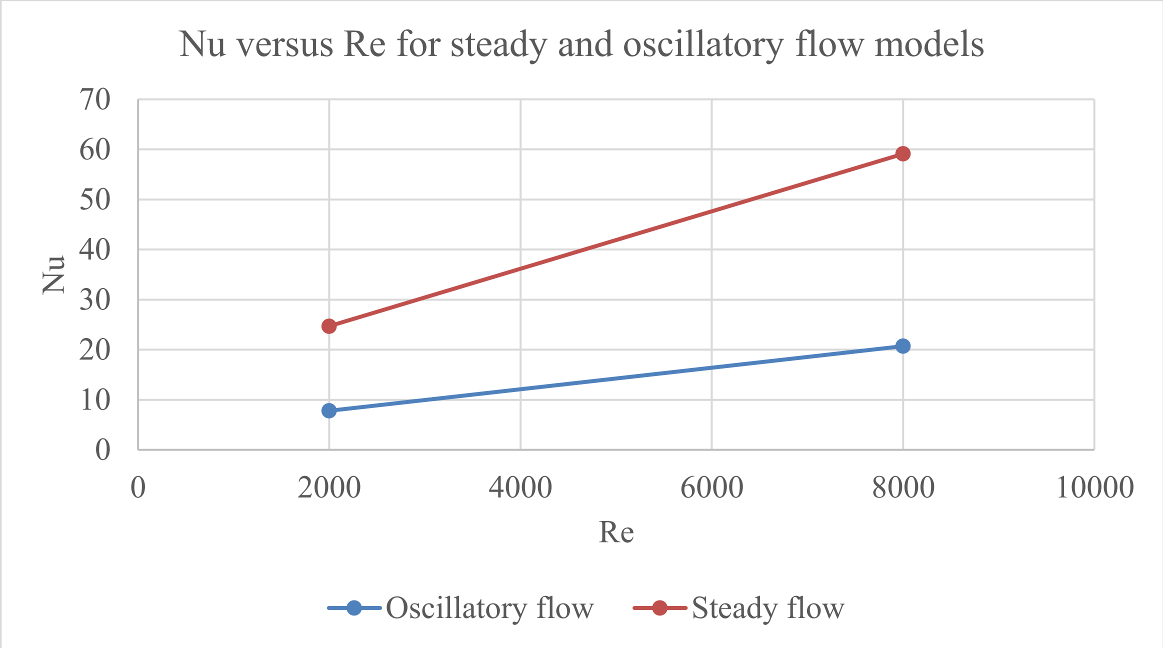

Figure 4.9: Nu versus Re for steady and oscillatory flow models

Based on Figure 4.9, both of the models showed similar upward trend, therefore the numerical simulation was sound. In general, the higher the Reynolds number of a flow, the better the heat transfer performance. Out of expectation, steady flow has a better heat transfer performance compared to oscillatory flow. The original hypothesis was that oscillatory flow should outperform the steady flow in term of heat transfer. This is because oscillatory is an ever-changing flow, it is much more chaotic and disordered compared to steady flow even for laminar region of flow. Turbulence can be induced when the flows are moving back and forth. As explained before, turbulence is an excellent medium in transferring heat. Oscillatory flow can induce an early transition to turbulent flow regime, forcing the boundary layer to become turbulent and eliminates laminar insulating blanket over the tube banks, so the heat can be transferred rapidly by large bulk motion of fluids. It can also cause the low-pressure wake region to break by making the separated flows to reattach and thus reducing the pressure drop and pump power needed. However, for steady flow, since the flow is ‘steady’, once it is stable, there will be persisting low-pressure wake regions at downstream of flow. This can increase the pump power needed and decrease the efficiency of heat exchanger. Besides, the formation of wake can also limit the transfer of heat because the effective heat transfer surface are reduced since the flow is separated over the tube at relatively higher Reynolds number. However, the results proved otherwise, therefore appropriate explanation will be discussed in next section.

4.5 Discussion

After thorough analysis on both models, verdicts were made. For steady flow, it was apparent that the higher the Re, the more vorticity on it, the better the heat transfer performance. By looking at the vorticity contour, the flow separation was getting severe as Re increased. It implied that there were wakes forming at downstream of tubes, along with flow separation and formation of vortex. The statement was valid after referring the velocity contour and vector plot. The deduction was that the flow came to an abrupt stop in front of the tubes, then accelerate along the tube surface (due to formation of boundary layer) and separated downstream, leaving a wake region behind tube. The wake region is highly unsteady and consists of recirculating flows that could lead to pressure drop. The wake is then destroyed when the separated flows reattached which is highly unlikely in turbulent flow. Therefore, large eddies or vortices are shed downstream. Vortex shedding is the oscillating flow that are formed at regular frequency at the wake. The formation of wake can be both beneficial and detrimental, it is beneficial in way that it implies the flow is turbulent. Usually, turbulence is good for heat transfer as explained in previous section. However, it is detrimental if the magnitude is too large because it requires more power to compensate the losses, and this is not economical at all.

Generally, turbulent flow is better in heat transfer compared to laminar flow because it is faster and more chaotic. For laminar flow, the only mean of heat transfer is by molecular diffusion. The heat energy is carried by the movement of molecules from one place to another based on concentration gradient. For turbulent flow it has one more mean of heat transfer other than molecular diffusion, and that is by the formation of eddies. These eddies are formed at wake region. It can transport mass, momentum, and energy quicker than molecular diffusion. Therefore turbulent flows will always have higher heat transfer coefficient compared to laminar flows. Another explanation is that boundary layer can act as an insulating film to constrict heat transfer. Heat is transferred from the fluid through the tube wall, and boundary layer will be formed definitely due to no-slip condition. There are three general types of boundary layers: laminar, transitional, and turbulent. Laminar boundary layer formed on the tube wall is smooth and calm like a blanket and constrict the heat transfer while turbulent boundary layer is agitated and contains a lot of vortices. Therefore turbulent flow is better than laminar flow in terms of heat transfer application. This is why there are vortex generators used to induce earlier onset of turbulent flows.

Next, moving on to oscillatory flow, DR 0.3% operated in laminar region, as the vorticity and velocity contours suggested, while DR 1.2% was fully developed turbulent flow. By looking at the comparison of vorticity contours between both oscillatory flow model and steady flow model, and results obtained from simulation especially velocities for both models, the corresponding Reynolds number for drive ratio 0.3% is 2000, and 8000 for drive ratio 1.2%. To continue on the previous discussion in Section 4.4, steady flow has better heat transfer performance than oscillatory flow. This can be explained by referring the Figure 4.10 and 4.11. Figure 4.10 and 4.11 show the Nusselt number development for both numerical models.

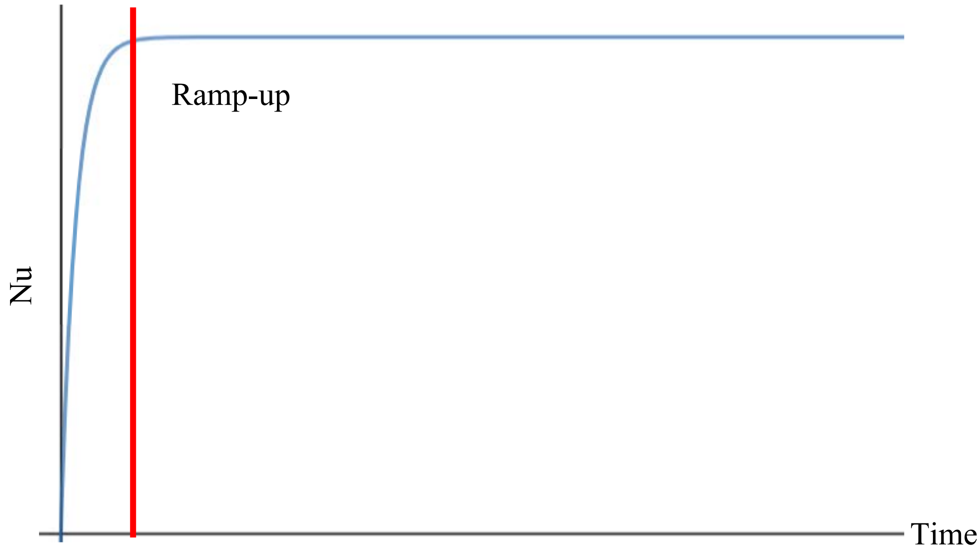

Figure 4.10: Nusselt number development for steady flow model

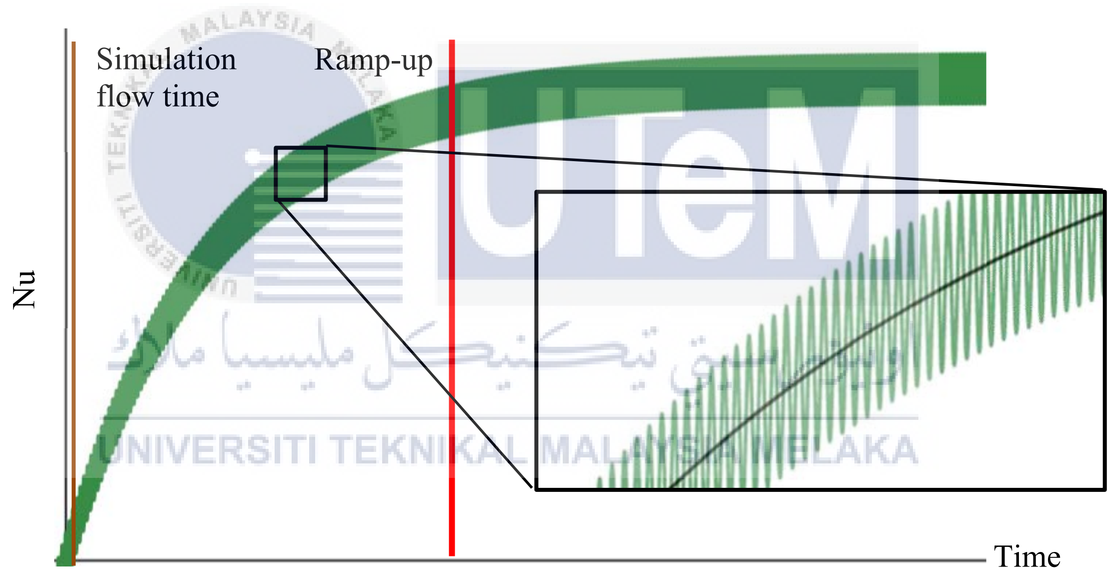

Figure 4.11: Nusselt number development for oscillatory flow model

In reality, it takes time for a heat exchanger to warm up to a ‘steady’ state, and it is usually different for a number of variables such as types of flows, types of heat exchangers, etc. The time taken is known as ramp up period and it is represented by the red lines found in Figure 4.10 and 4.11. Based on the Figure 4.10 and 4.11, it is clear that the ramp up period for both models are different. The steady flow has significantly shorter ramp up period than oscillatory flow because of its ‘steady’ nature. Oscillatory flow takes more time to reach steady oscillatory state than steady flow. In simulation, Ansys Fluent 16.0 is able to compute the steady flow model with ease since time is not a variable in play, therefore it can solve the model until it reached the aforementioned 'steady' state. However, oscillatory flow model is a transient model, therefore time is an important variable that must be taken into account. Although the simulation has been ran for more than 7 cycles (7000 time steps), the total flow time is merely 0.53 second. It takes a lot more time (simulation flow time to ramp up) for the model to reach steady oscillatory flow. The software can only solve the transient model according to the time step size and number of time steps defined by the user. It can't work on its own and produce result which is at steady oscillatory state. Therefore, by taking results at 7 cycles, the heat transfer has yet to reach its peak performance although the amplitude of function is the same (refer to the amplified view of waveform in Figure 4.11). Based on Figure 4.11, the overall performance will increase as time progresses (more time steps) and reach steady oscillatory state. By then, the results will be meaningful and the original hypothesis saying that oscillatory flow has better heat transfer performance than steady flow will be established. However, the steady flow has better heat transfer performance than oscillatory flow for now.

CHAPTER 5

CONCLUSION & RECOMMENDATIONS FOR FUTURE WORK

In conclusion, the objectives were achieved. The CFD model was successfully developed using Ansys Fluent. Mesh independent test had been carried out with multiple grids with different number of element. Results obtained were validated by reviewing literatures. The fluid flow and heat transfer characteristics of both steady and oscillatory flows were identified and examined via the CFD models developed. Plots and contours were set up for visualization of results. Heat transfer coefficient was determined using equations mentioned in methodology and also literature review, and built-in function of Ansys Fluent. It is found that steady flow with higher Re has better heat transfer performance compared to those with low Re. Oscillatory flow with higher drive ratio has better heat transfer performance. Steady flow has better heat transfer performance compared to oscillatory flow. However this statement is inconclusive and more works are required to substantiate it. Recommendation for future work is to develop appropriate correlation or equation to compute or validate heat transfer coefficient for oscillatory cross flow over tube banks.

REFERENCES

Abramov, A.G., Levchenya, A.M., Smirnov, E.M. and Smirnov, P.E., 2015. Numerical simulation of liquid metal turbulent heat transfer from an inline tube bundle in cross-flow. St. Petersburg Polytechnical University Journal: Physics and Mathematics, 1(4), pp.356-363.

Ahmed, M.A., Yaseen, M.M. and Yusoff, M.Z., 2017. Numerical study of convective heat transfer from tube bank in cross flow using nanofluid. Case studies in thermal engineering, 10, pp.560-569.

Al-Sammarraie, A.T. and Vafai, K., 2017. Heat transfer augmentation through convergence angles in a pipe. Numerical Heat Transfer, Part A: Applications, 72(3), pp.197-214.

Ansys, Inc., 2009. 6.1.3 Choosing the Appropriate Mesh Type. [online] Available at: http://www.afs.enea.it/project/neptunius/docs/fluent/html/ug/node164.htm [accessed on 12 November 2019]

Bender, A., Meier, A.M., Vaz, M. and Zdanski, P.S.B., 2018. A numerical study of forced convection in a new trapezoidal tube bank arrangement. International Communications in Heat and Mass Transfer, 91, pp.117-124.

Bern, M.W. and Plassmann, P.E., 1997. Mesh generation. Pennsylvania State University, Department of Computer Science and Engineering, College of Engineering.

Bhutta, M.M.A., Hayat, N., Bashir, M.H., Khan, A.R., Ahmad, K.N. and Khan, S., 2012. CFD applications in various heat exchangers design: A review. Applied Thermal Engineering, 32, pp.1-12.

Blevins, R.D., 1990. Flow-induced vibration.

Bochev, P.B. and Gunzburger, M.D., 1994. Analysis of least squares finite element methods for the Stokes equations. Mathematics of Computation, 63(208), pp.479-506.

Cengel, Y.A. and Cimbala, J.M., 2014. Fluid Mechanics: Fundamentals and Applications 3rd. New York, McGraw-Hill.

Cengel, Y.A. and Ghajar, A.J., 2015. Heat and Mass Transfer: Fundamentals and Applications 5th. New York, McGraw-Hill.

Churchill, S.W. and Bernstein, M., 1977. A correlating equation for forced convection from gases and liquids to a circular cylinder in crossflow. Journal of Heat Transfer, 99(2), pp.300-306.

Churchill, S.W. and Chu, H.H., 1975. Correlating equations for laminar and turbulent free convection from a horizontal cylinder. International journal of heat and mass transfer, 18(9), pp.1049-1053.

Day, M.A., 1990. The no-slip condition of fluid dynamics. Erkenntnis, 33(3), pp.285-296.

El Gharbi, N., Kheiri, A., El Ganaoui, M. and Blanchard, R., 2015. Numerical optimization of heat exchangers with circular and non-circular shapes. Case Studies in Thermal Engineering, 6, pp.194-203.

Evans, P., 2015. Properties of Air at atmospheric pressure. [online] Available at: https://theengineeringmindset.com/properties-of-air-at-atmospheric-pressure/ [accessed on 10 July 2019]

Feldmann, D. and Wagner, C., 2012. Direct numerical simulation of fully developed turbulent and oscillatory pipe flows at. Journal of Turbulence, (13), p.N32.

Fluent Inc., 2006. 25.3.2 Temporal Discretization. [online] Available at: https://www.sharcnet.ca/Software/Fluent6/html/ug/node993.htm [accessed on 12 November 2019]

Fluent Inc., 2006. 25.3.3 Evaluation of Gradients and Derivatives. [online] Available at: https://www.sharcnet.ca/Software/Fluent6/html/ug/node994.htm [accessed on 12 November 2019]

Fluent Inc., 2006. 25.9.1 Choosing the Pressure-Velocity Coupling Method. [online] Available at: https://www.sharcnet.ca/Software/Fluent6/html/ug/node1021.htm [accessed on 12 November 2019]

Gerritsma, M. and Bochev, P., 2016. A spectral mimetic least-squares method for the Stokes equations with no-slip boundary condition. Computers & Mathematics with Applications, 71(11), pp.2285-2300.

Giedt, W.H., 1949. Investigation of variation of point unit heat transfer coefficient around a cylinder normal to an air stream. Trans. ASME, 71, pp.375-381.

Guo, J., Huai, X., Cheng, K., Cui, X. and Zhang, H., 2018. The effects of nonuniform inlet fluid conditions on crossflow heat exchanger. International Journal of Heat and Mass Transfer, 120, pp.807-817.

Han, H., He, Y.L., Li, Y.S., Wang, Y. and Wu, M., 2013. A numerical study on compact enhanced fin-and-tube heat exchangers with oval and circular tube configurations. International Journal of Heat and Mass Transfer, 65, pp.686-695.

He, Y.L., Han, H., Tao, W.Q. and Zhang, Y.W., 2012. Numerical study of heat-transfer enhancement by punched winglet-type vortex generator arrays in fin-and-tube heat exchangers. International Journal of Heat and Mass Transfer, 55(21-22), pp.5449-5458.

Hsieh, C.T. and Jang, J.Y., 2012. Parametric study and optimization of louver finned-tube heat exchangers by Taguchi method. Applied Thermal Engineering, 42, pp.101-110.

Ibrahim, T.A. and Gomaa, A., 2009. Thermal performance criteria of elliptic tube bundle in crossflow. International Journal of Thermal Sciences, 48(11), pp.2148-2158.

Ilori, O.M., Jaworski, A.J. and Mao, X., 2018. Experimental and numerical investigations of thermal characteristics of heat exchangers in oscillatory flow. Applied Thermal Engineering, 144, pp.910-925.

Jakob, M., 1949. Heat transfer in evaporation and condensation', Mech. Engng 1936 58 (October), 643; also. Heat transfer, 1.

Kim, T., 2013. Effect of longitudinal pitch on convective heat transfer in crossflow over in-line tube banks. Annals of Nuclear Energy, 57, pp.209-215.

Labbadlia, O., Laribi, B., Chetti, B. and Hendrick, P., 2017. Numerical study of the influence of tube arrangement on the flow distribution in the header of shell and tube heat exchangers. Applied Thermal Engineering, 126, pp.315-321.

Lavasani, A.M. and Bayat, H., 2016. Numerical study of pressure drop and heat transfer from circular and cam-shaped tube bank in cross-flow of nanofluid. Energy Conversion and Management, 129, pp.319-328.

Li, J., Wang, S., Chen, J. and Lei, Y.G., 2011. Numerical study on a slit fin-and-tube heat exchanger with longitudinal vortex generators. International Journal of Heat and Mass Transfer, 54(9-10), pp.1743-1751.

Lotfi, B., Sundén, B. and Wang, Q., 2016. An investigation of the thermo-hydraulic performance of the smooth wavy fin-and-elliptical tube heat exchangers utilizing new type vortex generators. Applied energy, 162, pp.1282-1302.

Lu, C.W., Huang, J.M., Nien, W.C. and Wang, C.C., 2011. A numerical investigation of the geometric effects on the performance of plate finned-tube heat exchanger. Energy Conversion and Management, 52(3), pp.1638-1643.

Mandhani, V.K., Chhabra, R.P. and Eswaran, V., 2002. Forced convection heat transfer in tube banks in cross flow. Chemical Engineering Science, 57(3), pp.379-391.

Mangrulkar, C.K., Dhoble, A.S., Chakrabarty, S.G. and Wankhede, U.S., 2017. Experimental and CFD prediction of heat transfer and friction factor characteristics in cross flow tube bank with integral splitter plate. International Journal of Heat and Mass Transfer, 104, pp.964-978.

Mangrulkar, C.K., Dhoble, A.S., Deshmukh, A.R. and Mandavgane, S.A., 2017. Numerical investigation of heat transfer and friction factor characteristics from in-line cam shaped tube bank in crossflow. Applied Thermal Engineering, 110, pp.521-538.

Minakov, A.V., Guzei, D.V., Pryazhnikov, M.I., Zhigarev, V.A. and Rudyak, V.Y., 2016. Study of turbulent heat transfer of the nanofluids in a cylindrical channel. International Journal of Heat and Mass Transfer, 102, pp.745-755.

Mirzakhanlari, S., Pourjalali, B., Sheikhrobat, A.A. and Behzadi, T., 2015. Numerical Investigation of Natural Convection Heat Transfer on Aligned Arrangement Tube Banks. Procedia Engineering, 127, pp.148-154.

Mohanty, R.L., Swain, A. and Das, M.K., 2018. Thermal performance of mixed tube bundle composed of circular and elliptical tubes. Thermal Science and Engineering Progress, 5, pp.492-505.

Mohd Saat, F. and Jaworski, A., 2017. Numerical predictions of early stage turbulence in oscillatory flow across parallel-plate heat exchangers of a thermoacoustic system. Applied Sciences, 7(7), p.673.

Mohd Saat, F. and Jaworski, A., 2017. The effect of temperature field on low amplitude oscillatory flow within a parallel-plate heat exchanger in a standing wave thermoacoustic system. Applied Sciences, 7(4), p.417.

Patnana, V.K., Bharti, R.P. and Chhabra, R.P., 2010. Two-dimensional unsteady forced convection heat transfer in power-law fluids from a cylinder. International Journal of Heat and Mass Transfer, 53(19-20), pp.4152-4167.

Prabhakara, S. and Deshpande, M.D., 2004. The No-Slip Boundary Condition in Fluid Mechanics – 2. Solution of the Sticky Problem. Resonance.

Rivara, M.C., 1984. Mesh refinement processes based on the generalized bisection of simplices. SIAM Journal on Numerical Analysis, 21(3), pp.604-613.

Sadrehaghighi, I., 2019. Mesh Generation in CFD. 10.13140/RG.2.2.26522.54721/2.

Schlichting, H., 1974. Boundary-layer theory. McGraw-Hill 1968.

Schoenmaker, L., 2017. Simulations of steady and oscillating flow in diffusers.

Shu, J.J., Teo, J.B.M., Chan, W.K., 2017. Fluid velocity slip and temperature jump at a solid surface. Applied Mechanics Reviews, 69(2).

Smith, B.L. and Swift, G.W., 2003. Power dissipation and time-averaged pressure in oscillating flow through a sudden area change. The Journal of the Acoustical Society of America, 113(5), pp.2455-2463.

Sparrow, E.M., Abraham, J.P. and Tong, J.C., 2004. Archival correlations for average heat transfer coefficients for non-circular and circular cylinders and for spheres in cross-flow. International Journal of Heat and Mass Transfer, 47(24), pp.5285-5296.

Swep, 2019. 1.8 Pressure drop. [online] Available at: https://www.swep.net/refrigerant-handbook/1.-basic-heat-transfer/as/ [accessed on 22 November 2019]

Swift, G.W., 1988. Thermoacoustic engines. The Journal of the Acoustical Society of America, 84(4), pp.1145-1180.

Swift, G.W., 1988. Thermoacoustic engines. The Journal of the Acoustical Society of America, 84(4), pp.1145-1180.

Tahseen, T.A., Ishak, M. and Rahman, M.M., 2015. An overview on thermal and fluid flow characteristics in a plain plate finned and un-finned tube banks heat exchanger. Renewable and Sustainable Energy Reviews, 43, pp.363-380.

Viscosity. 2018. In Merriam-Webster.com. Retrieved October 22, 2018, from https://www.merriam-webster.com/dictionary/viscosity

Wang, Y., Gu, X., Jin, Z. and Wang, K., 2016. Characteristics of heat transfer for tube banks in crossflow and its relation with that in shell-and-tube heat exchangers. International Journal of Heat and Mass Transfer, 93, pp.584-594.

Whitaker, S., 1972. Forced convection heat transfer correlations for flow in pipes, past flat plates, single cylinders, single spheres, and for flow in packed beds and tube bundles. AIChE Journal, 18(2), pp.361-371.

Žukauskas, A., 1987. Heat transfer from tubes in crossflow. In Advances in heat transfer (Vol. 18, pp. 87-159). Elsevier.

Žukauskas, A., 1972. Heat transfer from tubes in crossflow. In Advances in heat transfer (Vol. 8, pp. 93-160). Elsevier.

APPENDICES

APPENDIX A

Grid no.2, No of elements: 1181, Relevance centre: fine, smoothing: high, number of division: 30, behaviour: hard

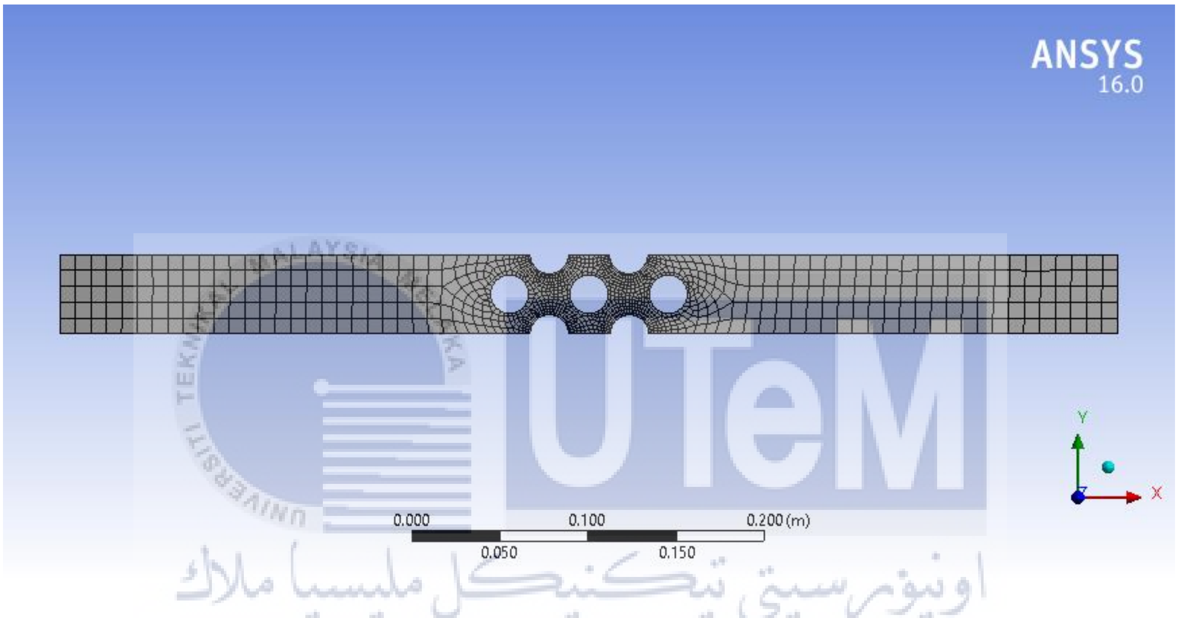

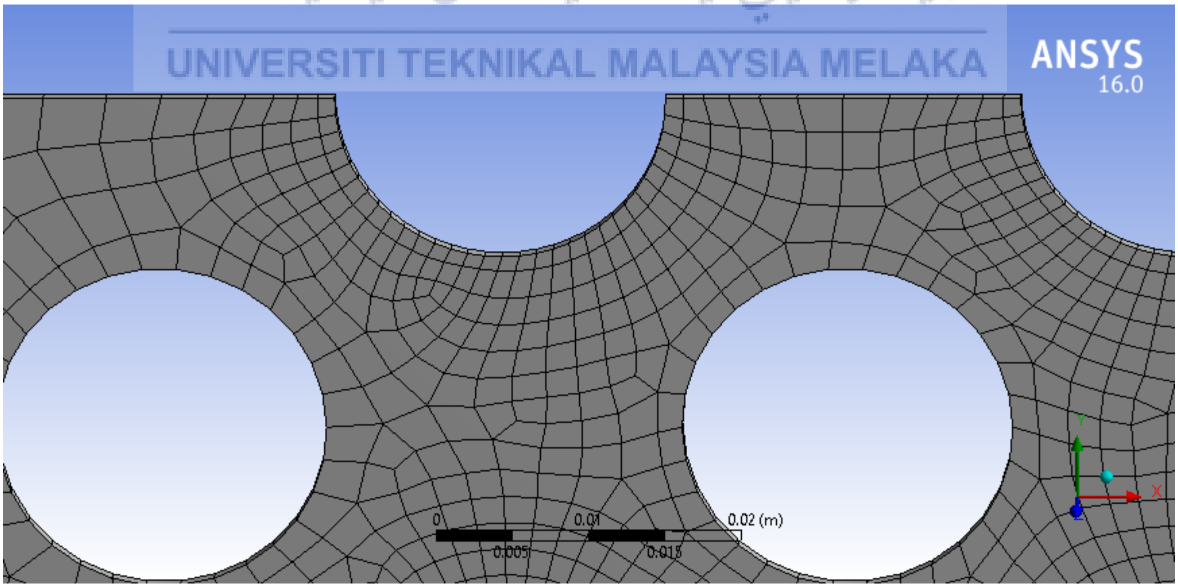

APPENDIX B

Grid no. 3, No of elements: 4713, Relevance centre: fine, smoothing: high, number of division: 30, behavior: hard, face refinement: 1

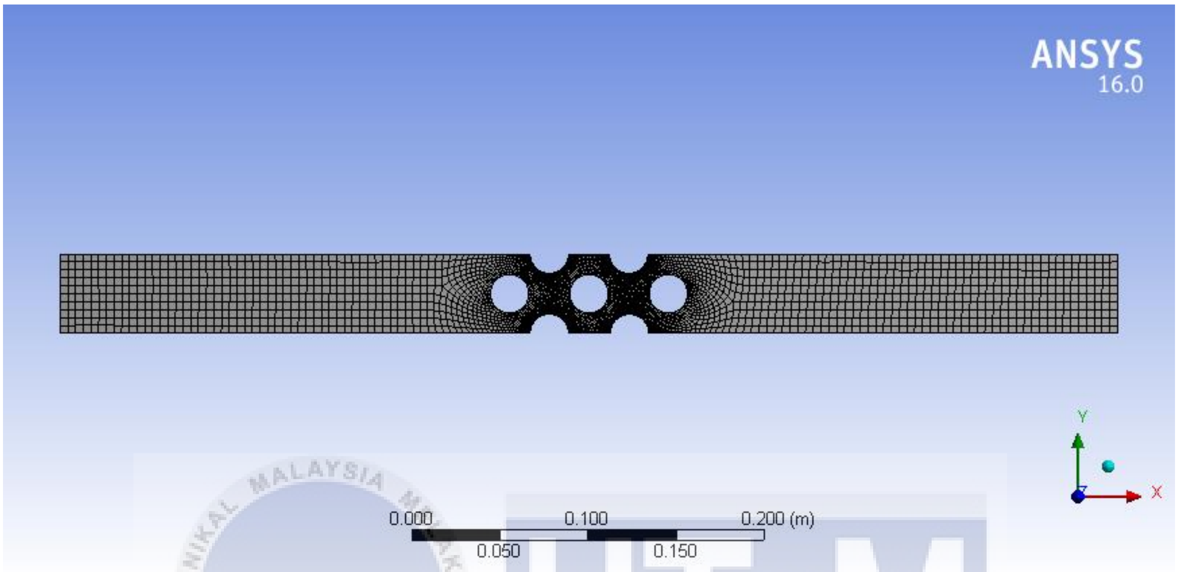

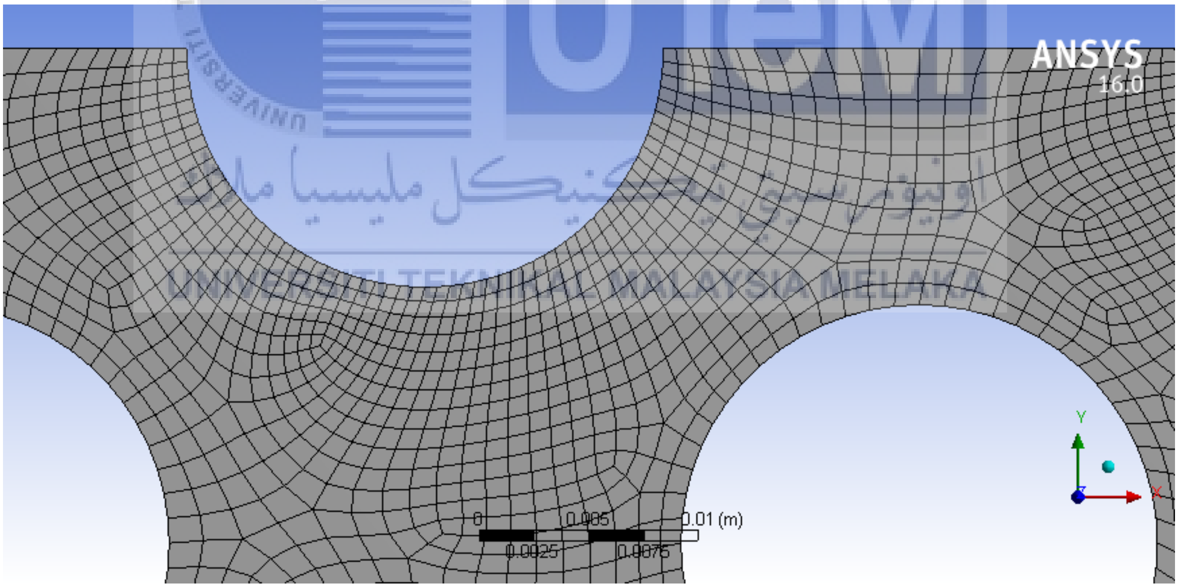

APPENDIX C

Grid no. 4, No of elements: 10600, Relevance centre: fine, smoothing: high, number of division: 30, behavior: hard, face refinement: 2

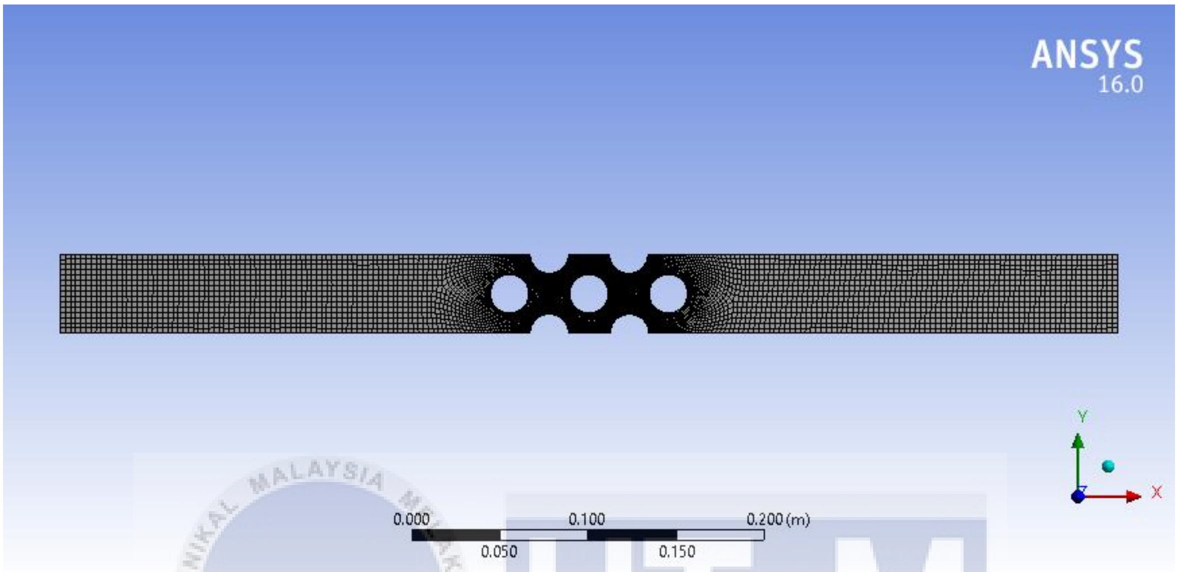

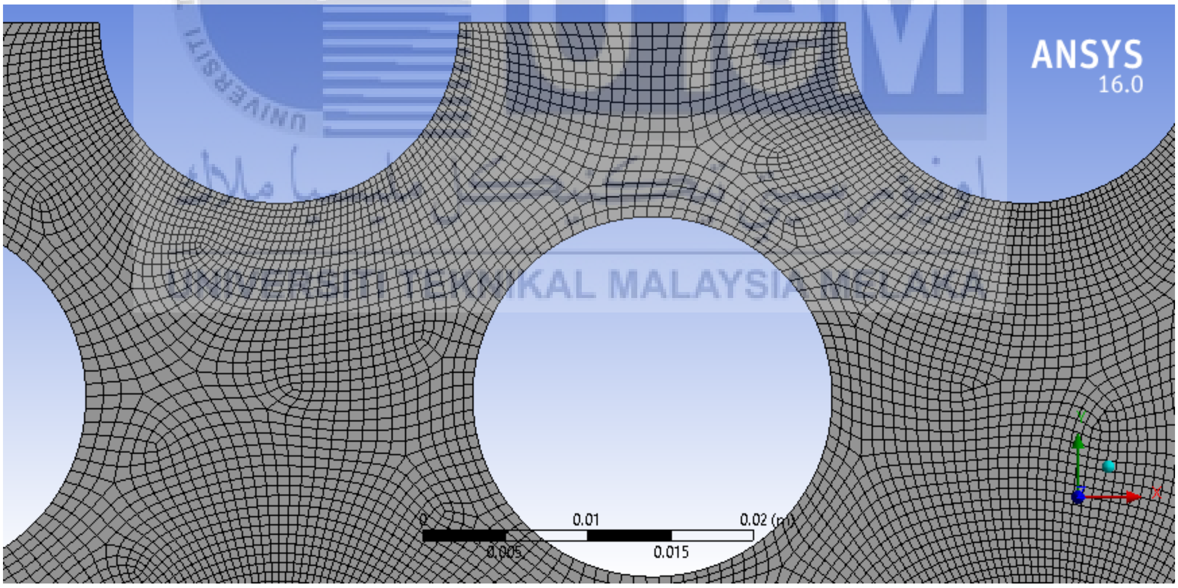

APPENDIX D

Grid no. 5, No of elements: 14841, Relevance centre: fine, smoothing: high, number of division: 30, behavior: hard, face refinement: 2

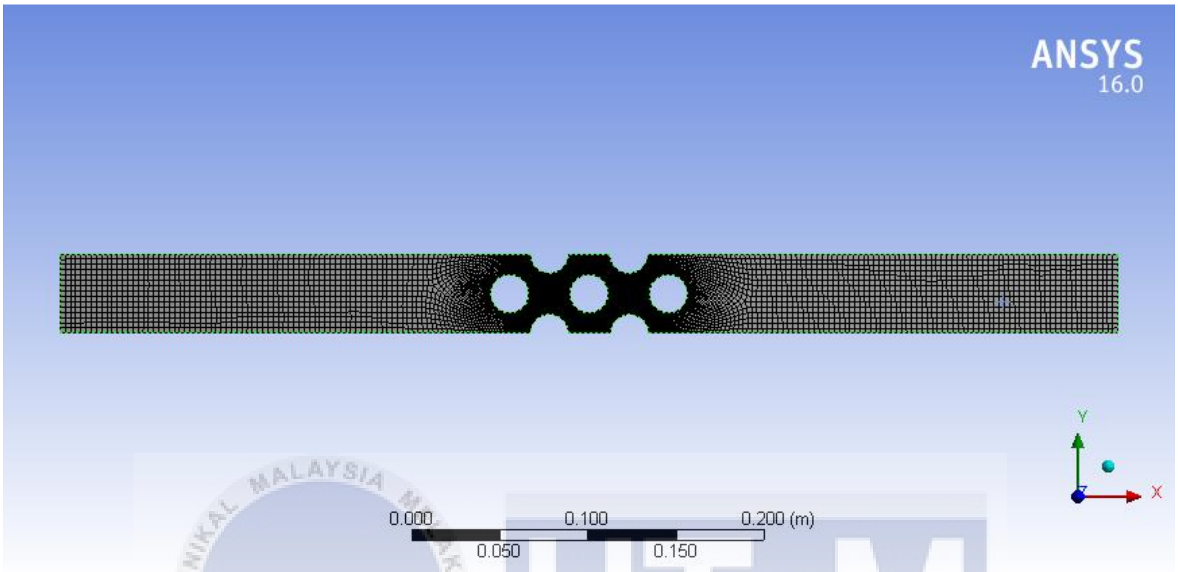

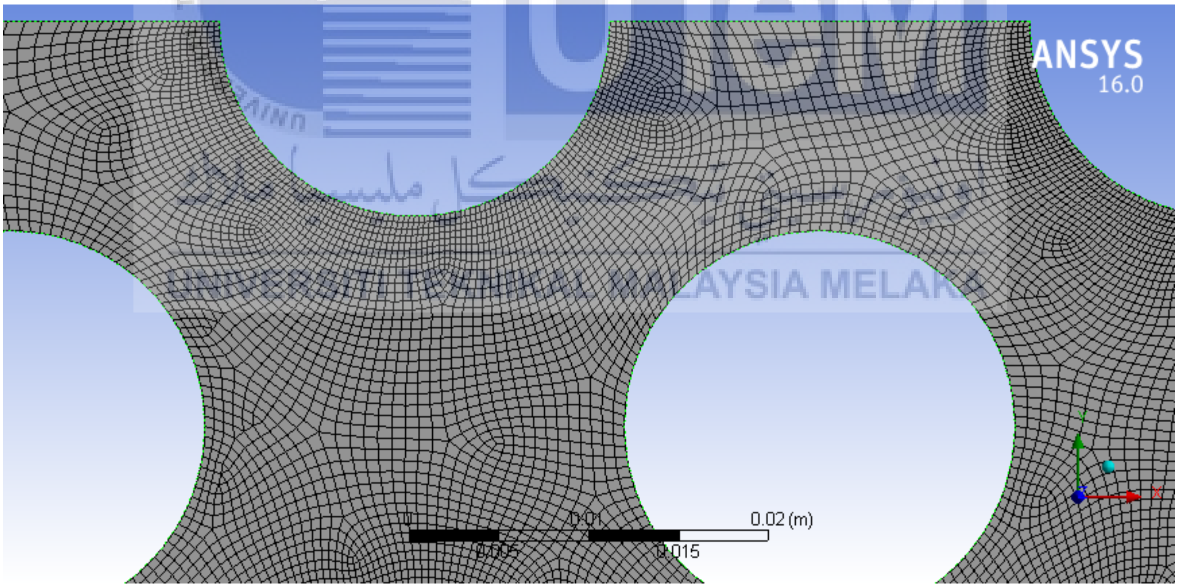

APPENDIX E

Grid no. 6, No of elements: 19170, Relevance centre: fine, smoothing: high, number of division: 50, behavior: hard, face refinement: 2

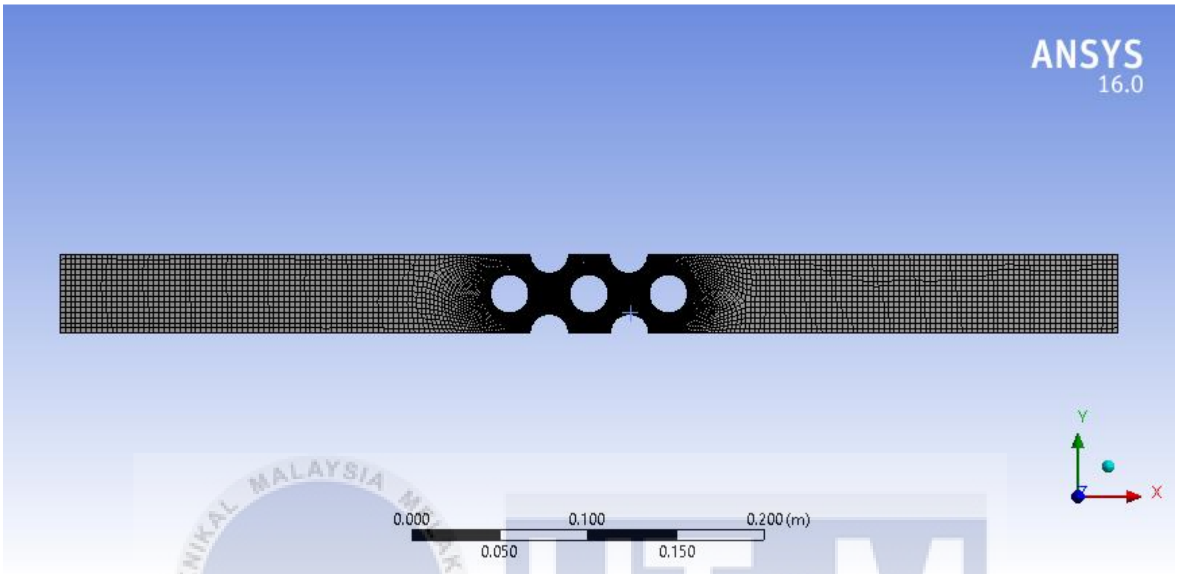

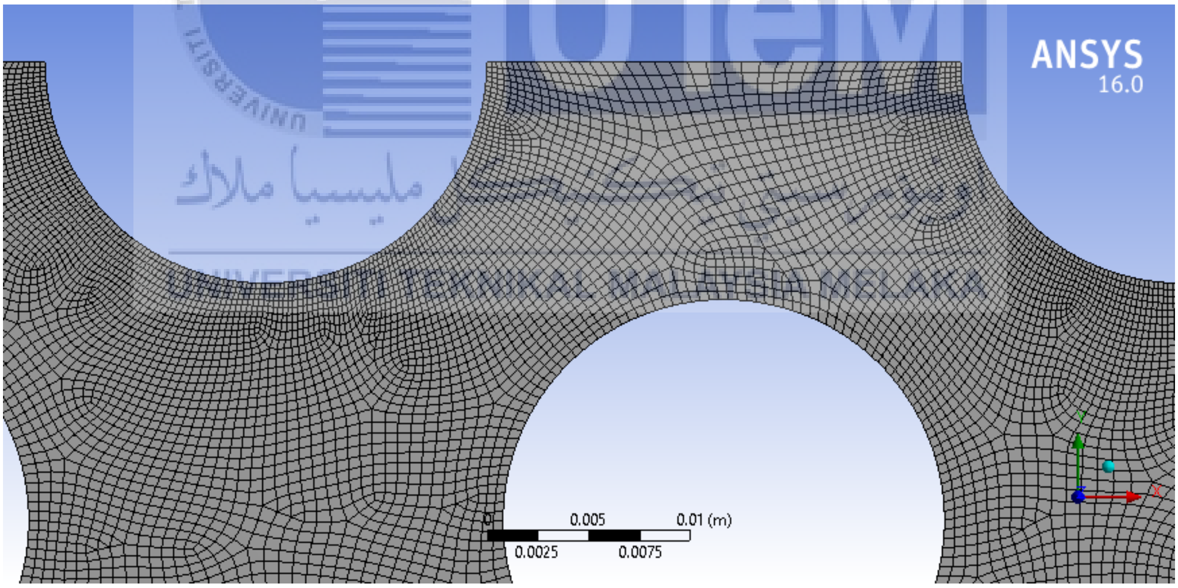

APPENDIX F

Grid no. 7, No of elements: 49675, Relevance centre: fine, smoothing: high, number of division: 50, behavior: hard, face refinement: 2, inflation at tube_wall edges: smooth transition, 10 layers, 1.2 growth rate

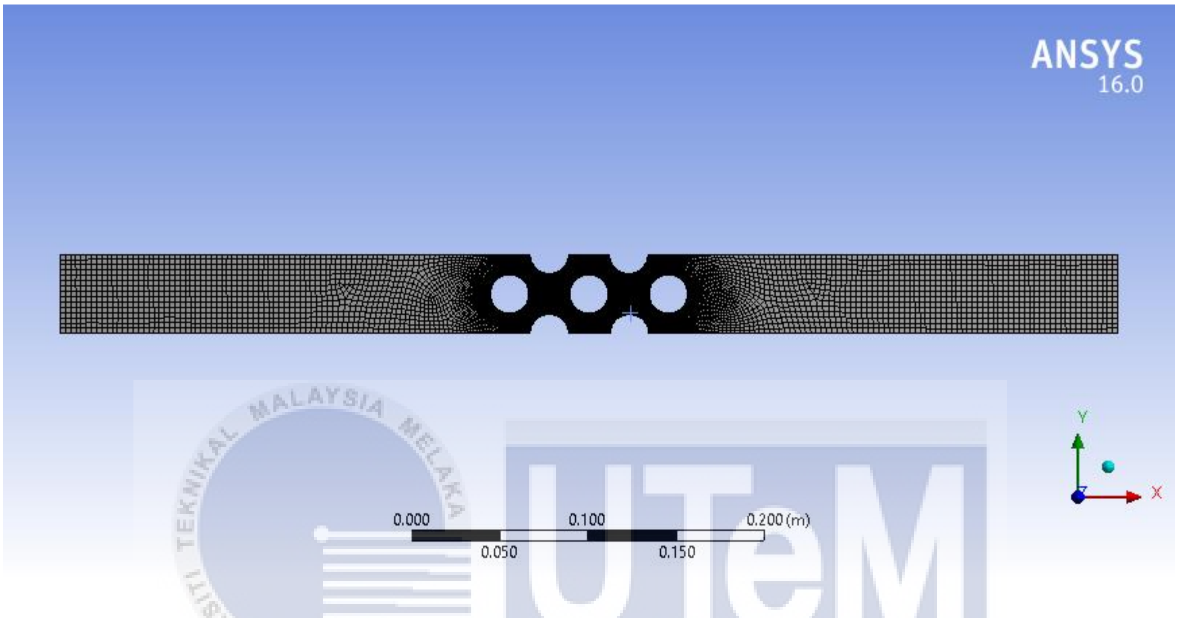

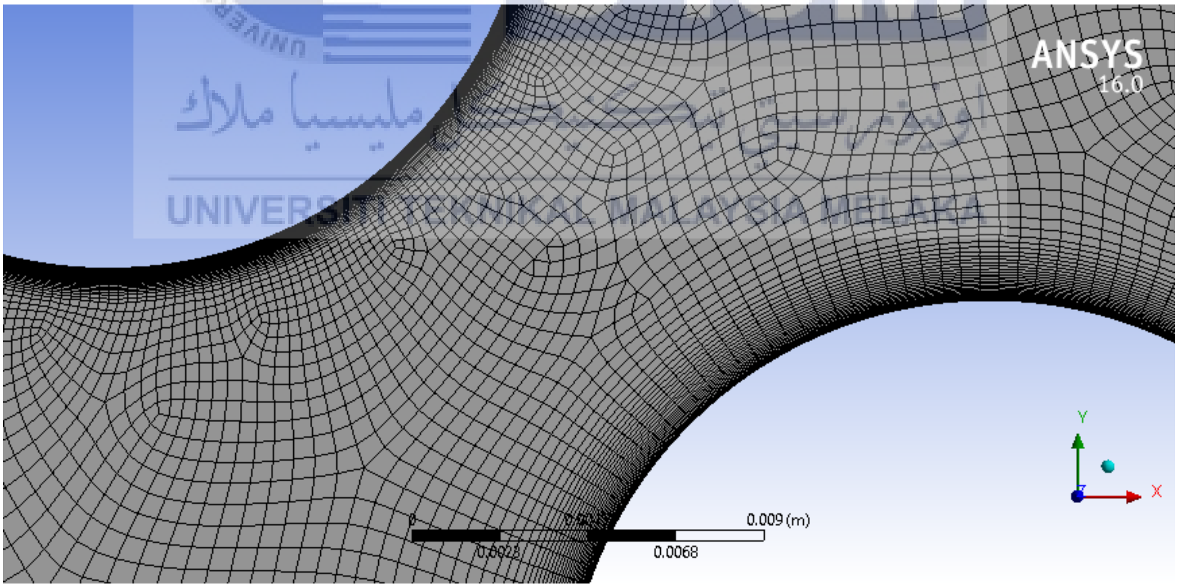

APPENDIX G

Grid no. 8, No of elements: 86892, Relevance centre: fine, smoothing: high, number of division: 50, behavior: hard, face refinement: 3, inflation at tube_wall edges: smooth transition, 10 layers, 1.2 growth rate

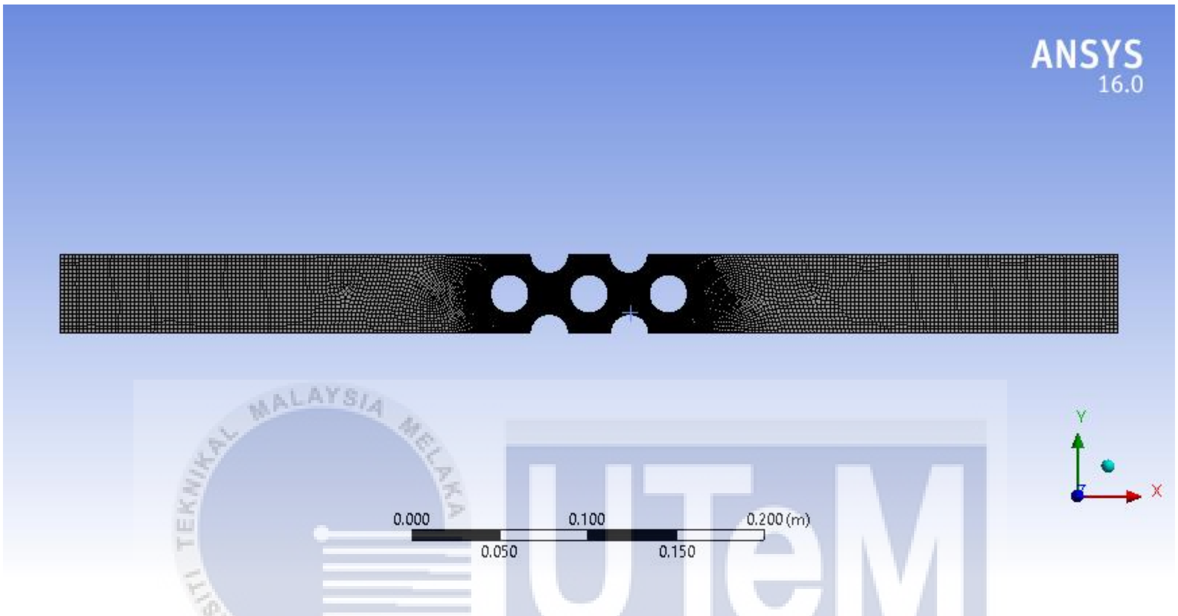

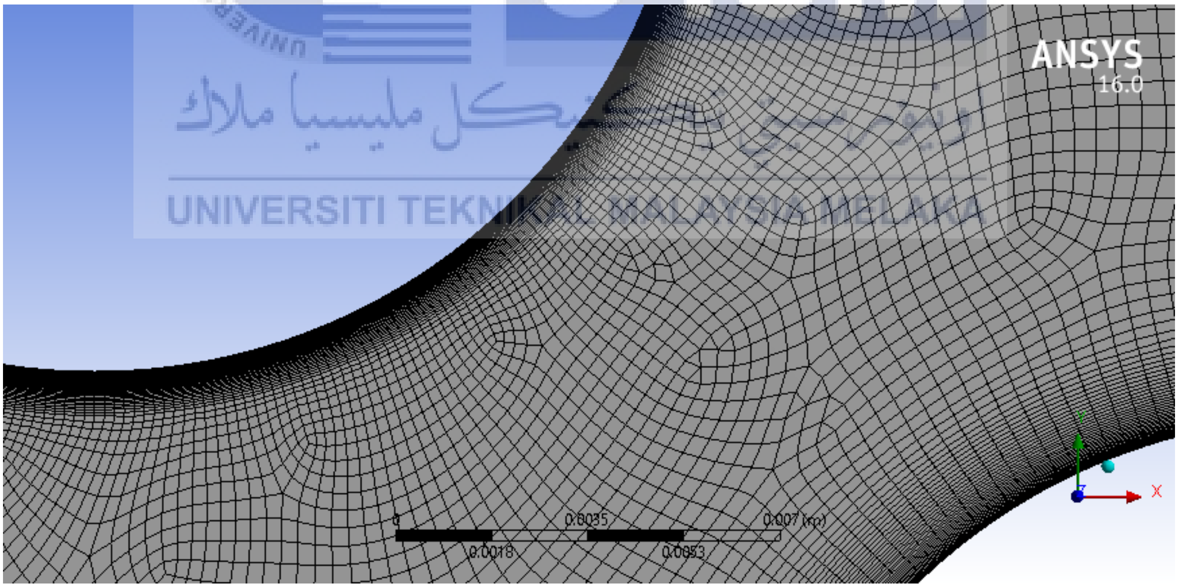

APPENDIX H

Gantt Chart for FYP I

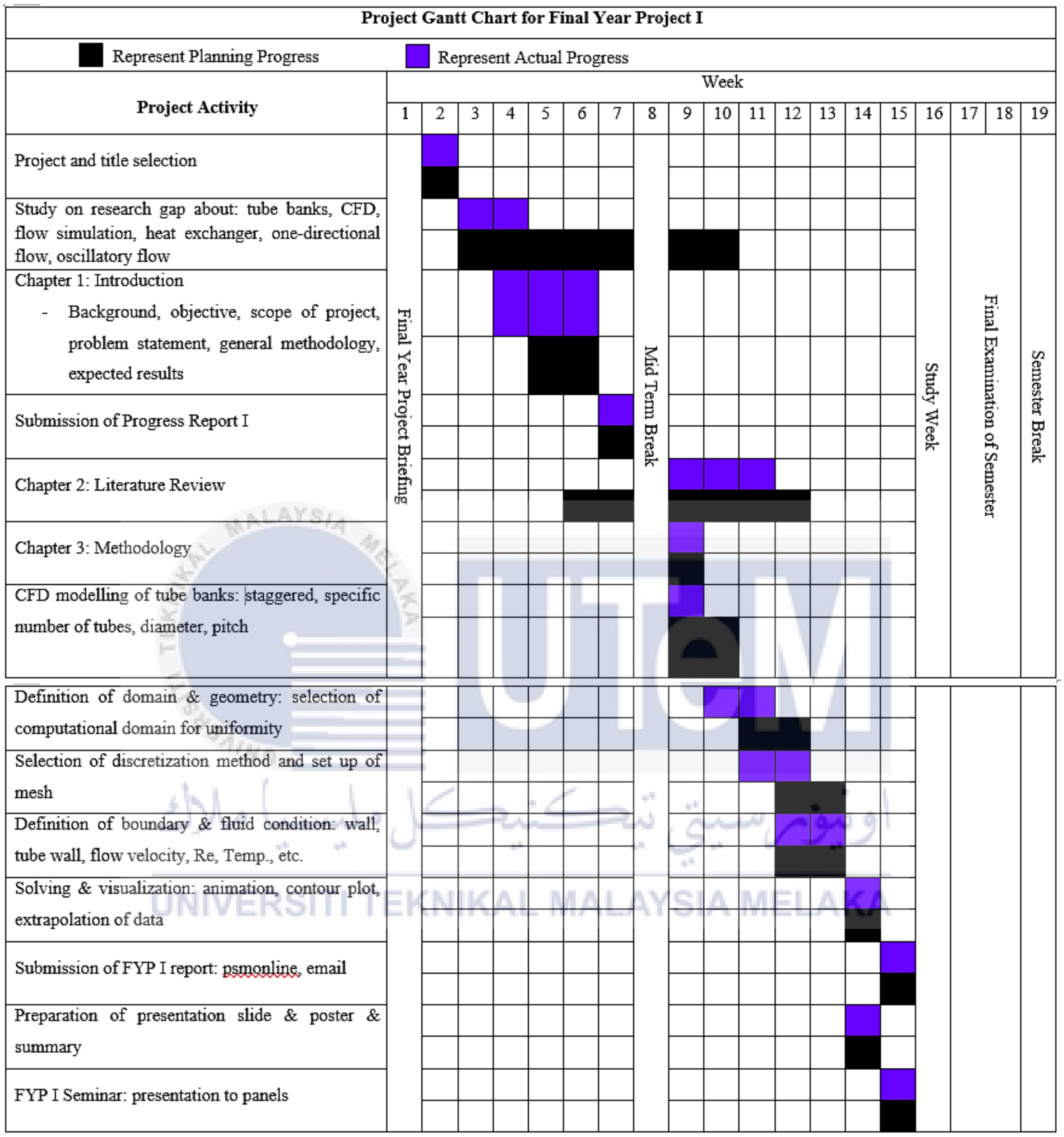

APPENDIX I

Gantt chart for FYP II